2008

On-line cascading event tracking and avoidance decision support tool

Siddhartha Kumar Khaitan
Iowa State University

On-line cascading event tracking and avoidance decision support tool

by

Siddhartha Kumar Khaitan

A dissertation submitted to the graduate faculty

in partial fulfillment of the requirements for the degree of

DOCTOR OF PHILOSOPHY

Major: Electrical Engineering

Program of Study Committee:
James D. McCalley, Major Professor
Venkataramana Ajjarapu
Umesh Vaidya
Hailiang Liu
Srinivas Aluru

Iowa State University

Ames, Iowa

2008

Dedicated to

Sri Krishna Caitanya Mahaprabhu and His Pure Associates

TABLE OF CONTENTS

List of Tables……..vi
List of Figures……..viii

1 Introduction……. 1
1.1 Motivation for Present Research……. 1
1.2 Nature of the Problem……. 2
1.3 Attributes of Blackout……. 3
1.4 Simulator Attributes……. 5
1.5 Research Problem Statement……. 7
1.6 Thesis organization……. 8
2 N-k Contingency Selection……. 10
2.1 System Topology and Primary Multiple Contingencies……. 11
2.2 Graph Theoretic Representations of Power System Topology……. 14
2.3 High-order Contingencies due to inadvertent tripping……. 19
2.3.1 Generalized form for Inadvertent Tripping Contingency……. 23
2.3.2 Special Case……. 25
2.4 Probability calculation illustration for the Typical Substation Topologies……. 27
2.4.1 Ring Bus……. 27
2.4.2 Breaker and a Half Bus (B-HB)……. 28
2.4.3 Single Bus Connected with Tie Breaker (SB-TB)……. 29
2.4.4 Single Breaker and Single Bus (SB-SB)……. 31
2.4.5 Double Breaker and Double Bus (DB-DB)……. 32
2.5 Test System……. 34
2.6 Summary……. 36
3 Numerical methods – Direct methods……. 38
3.1 Formulation of Dynamic Algebraic Equations……. 39
3.2 Solution Strategy……. 42
3.3 Integration Scheme for DAE……. 43
3.3.1 Nonlinear Equation Solution……. 45
3.3.2 Linear equation Solver……. 46
3.3.3 Frontal method……. 47
3.3.4 Multifrontal method……. 50
3.3.5 Time Step……. 61
3.3.6 Jacobian Building……. 61
3.4 Test System……. 62
3.5 Performance Comparison……. 62
3.5.1 Modified Newton Method……. 62
3.5.2 Validation……. 63
3.5.3 Results and Discussion……. 63
4 Numerical methods – Iterative methods……. 68
4.1 Introduction……. 68
4.2 Basic Solution Methodology……. 70
4.2.1 GMRES……. 71
4.2.2 Other Methods……. 72
4.2.3 Restarted method……. 73
4.2.4 Preconditioning……. 74
4.2.5 Preconditioning for the unsymmetric matrices……. 77
4.2.6 The Effect of Ordering……. 79

4.3 Performance Comparison 80
4.3.1 Validation 80
4.3.2 Results and Discussion 81
5 Modeling and protection 88
5.1 Component Modeling and Formulation of Dynamic Algebraic Equations 88
5.1.1 Exciter Model 88
5.1.2 Governor Model 89
5.1.3 AGC Model 89
5.1.4 Over-excitation Limiter Model 90
5.1.5 Load Model 91
5.1.6 Formulation of Dynamic Algebraic Equations 91
5.2 Generator Protection 91
5.2.1 Importance of Generator Protection 91
5.3 Historical Evidence/Perspective 92
5.3.1 Northeast Blackout November 9-10, 1965 92
5.3.2 June 5, 1967, PJM Disturbance 93
5.3.3 North American Northeast Blackouts of 1977 93
5.3.4 French Blackout December 19, 1978 94
5.3.5 Tennessee Disturbance August 22, 1987 94
5.3.6 The Tokyo Blackout 1987 94
5.3.7 PECO Disturbance February 21, 1995 94
5.3.8 Western System July 2, 1996 94
5.3.9 Western System August 10, 1996 95
5.3.10 Chilean Blackout May 1997 95
5.3.11 North American Northeast Blackouts of August 14, 2003 95
5.3.12 Blackout in Southern Sweden and Eastern Denmark – September 23, 2003 95
5.3.13 Italian Blackout September 28, 2003 96
5.3.14 Greece July 12, 2004 96
5.3.15 Australian Blackout Friday August 13, 2004 96
5.3.16 Central-South System Collapse of the Peninsular Malaysia Grid System January 13, 2005 96
5.3.17 Blackout in the Swiss Railway Electricity Supply System June 22, 2005 97
5.3.18 UCTE Major Disturbance of 4 November, 2006 97
5.4 Generator Protection Types and Strategies 97
5.4.1 Overexcitation (Volt per Hertz protection) Device 24 98
5.4.2 Overcurrent 104
5.4.3 Overvoltage 105
5.4.4 Undervoltage 106
5.4.5 Overfrequency 107
5.4.6 Underfrequency 108
5.4.7 Out of Step 112
5.5 Automatic Island Detection and Simulation 116
6 Results and discussion 118
6.1 Validation of the Dynamic Simulation Tool 118
6.2 Decision Event Tree Generation 120
6.2.1 Test Scenario 120
6.2.2 Contingency Event Branch 121
6.2.3 Decision Event Branch Set and Decision Identification 121
6.3 Results Analysis 122
6.3.1 Without Generation Protection 122
6.3.2 With Generation Protection 124

7 Conclusions 133
8 Future Recommendations Based on Discussion with the Industry 136
APPENDIX A: Rare Event Approximation 137
APPENDIX B: Pseudo Code for Graph Search Algorithm for Functional Group Decomposition 138
APPENDIX C: Pseudo Code for Graph Search Algorithm for Inadvertent Tripping Contingency 139
APPENDIX D: One-Line Diagram of Test System 140
APPENDIX E: Test System Data 141
APPENDIX F: IEEE-RTS 24 Bus Test System 143
APPENDIX G: Preconditioned GMRESR Algorithm 144
APPENDIX H: Optimization Code for Redispatch and Load Shedding (from [4]) 145
Acknowledgments 151
List of Publications 153
References 154

LIST OF TABLES

Table 1: Summary on disturbances caused by protection system failures..... 13
Table 2: List of vertex components of the power system diagram in Fig. 5..... 15
Table 3: List of edge components for the power system in Fig. 5..... 16
Table 4: List of functional groups and their failure probabilities..... 17
Table 5: Connections for the interfacing components and the functional group (1- connected, 0- not connected)..... 18
Table 6: A US Utility experience with misoperation..... 20
Table 7: Survey of US Utilities on Relay misoperation..... 20
Table 8 The probability of high-order contingency for different substations..... 34
Table 9: Result of N-k contingency selection algorithm on Test System..... 34
Table 10: Result of N-k contingency selection algorithm on IEEE-RTS 24 Bus Test System..... 34
Table 11 Number of contingencies of type N-k resulting from a single fault (Order P) for 21 Bus System..... 35
Table 12 Number of contingencies of type N-k resulting from a fault/breaker failure (order P^2) for 21 Bus System..... 35
Table 13 Number of contingencies of type N-k resulting from ITC (Order P^2) for 21 Bus System..... 35
Table 14 Number of contingencies of type N-k resulting from a single fault (Order P) for IEEE RTS96..... 35
Table 15 Number of contingencies of type N-k resulting from a fault/breaker failure (order P^2) for IEEE RTS96..... 36
Table 16 Number of contingencies of type N-k resulting from ITC (Order P^2) for IEEE RTS96..... 36
Table 17: Sparse Direct Solvers..... 59
Table 18: 6-generator Test System..... 64
Table 19: 32-generator Test System..... 65
Table 20: 6-generator Test System ((Modified Newton)..... 66
Table 21: 32-generator Test System (Modified Newton)..... 67
Table 22 Comparison of ILU preconditioned different iterative solvers..... 85
Table 23 Comparison of multifrontal preconditioned GMRESR solver with other solvers: 6 generator system..... 86
Table 24 Speed up comparison of multifrontal preconditioned GMRESR solver with other solvers: 6 generator system..... 86
Table 25 Comparison of multifrontal preconditioned GMRESR solver with other solvers: 32 generator test System..... 87
Table 26 Speed up comparison of multifrontal preconditioned GMRESR solver with other solvers: 32 generator test system..... 87
Table 27: Overcurrent relay settings..... 104
Table 28: Typical Overvoltage limits..... 106
Table 29: Initial status of generator for Ontario test system..... 118
Table 30: The bus-breaker connection data..... 141

Table 31: Line data for the test system 142
Table 32: Solution for the sample LP problem in Fig. 55 150

LIST OF FIGURES

Fig. 1: Blackout Impact 3
Fig. 2: Nature of Blackout 4
Fig. 3: Time domain simulator 6
Fig. 4: Simulator attributes (in terms of Decision set priority, Computational characteristics, and simulation model complexity) 6
Fig. 5: One-line diagram of actual system illustrating functional groups 14
Fig. 6: Reduced functional group graph for Fig. 5 18
Fig. 7: Ring bus station with B-matrix 27
Fig. 8: Breaker and a half bus 28
Fig. 9: Single bus connected with tie-breaker and it's B-matrix 30
Fig. 10: Single breaker single bus substation and it's B-matrix 31
Fig. 11: Double breaker and double bus and it's B-matrix 32
Fig. 12: Example for frontal method 49
Fig. 13: Example symmetric positive definite matrix and it's Cholesky factor matrix 52
Fig. 14: Elimination tree for matrix *A* 52
Fig. 15: Algorithm for multifrontal Cholesky factorization 56
Fig. 16: Example for unsymmetric multifrontal method 58
Fig. 17 Comparison of simulation plots for Gaussian elimination and for multifrontal method 63
Fig. 18: Performance Comparison for a 6 generator system 64
Fig. 19: Performance Comparison for a 32-generator test system 65
Fig. 20 Comparison of simulation plots for the multifrontal preconditioned GMRESR solver and for the multifrontal solver 81
Fig. 21 The non zero pattern of a typical Jacobian matrix in dynamic simulation 83
Fig. 22 RCM Reordered non zero element distribution for the matrix in Fig. 21 84
Fig. 23 Symamd Reordered non zero element distribution for the matrix in Fig. 21 84
Fig. 24: Block diagram of exciter 88
Fig. 25: Governor 89
Fig. 26: Block diagram of Automatic Generation Controller (AGC) 90
Fig. 27: Over-exciter limiter 90
Fig. 28: System islanding into 5 areas [144] 93
Fig. 29: Steam Turbine Partial or Full-Load Operating Limitations During Abnormal Frequency [176] 110
Fig. 30: Time accumulation based Timers [170] 112
Fig. 31: Loss of field relay Characteristics 113
Fig. 32 Representation of the DFS algorithm 116
Fig. 33 A typical cascading scenario 117
Fig. 34: ETMSP type 30 exciter for Ontario hydro 4-generator 118
Fig. 35: Response of generator after a temporary fault at bus section 5 (ETMSP) 119
Fig. 36: Response of a generator after a temporary fault at bus section 5 (Developed Simulator) 119
Fig. 37: Dynamic event tree template for the test system 120
Fig. 38: System load ramp curve 120

Fig. 39: Branch loading after loss of the largest generator 123
Fig. 40: Line flow response after the loss of the generator G102 123
Fig. 41: Voltage response after the loss of G102 124
Fig. 42: Sequence of events leading to cascading 126
Fig. 43: Maximum line flow in a cascading scenario 126
Fig. 44: Lowest voltage in the system for a cascading scenario 127
Fig. 45: Sequence of events leading to islanding 128
Fig. 46: The two islands resulting from the sequence of events in Fig. 45 128
Fig. 47: Maximum line flow in an islanded scenario 129
Fig. 48 Circuit loading with and without generator protection 130
Fig. 49 Voltage response of system with and without generator protection 130
Fig. 50: A scenario with the initiating contingency as generator trip 131
Fig. 51: Maximum line flow with corrective actions to prevent generator trip and relieve line overloading 132
Fig. 52: Lowest voltage in the system with corrective actions to prevent generator trip and relieve line overloading 132
Fig. 53: One line diagram of a test system 140
Fig. 54: IEEE RTS-24 bus test system substation diagram 143
Fig. 55: Example system for linear programming illustration 149

CHAPTER 1 INTRODUCTION

1.1 Motivation for Present Research

Steady state and time domain simulation tools are an integral part in the design, optimization, and operation of large interconnected power system. The purpose of simulation is online monitoring, tracking, and devising preventive or correcting action strategies for mitigating the frequency and impact of high consequence events. Common to both steady state and dynamic simulation is the processing of data from power system SCADA (Supervisory Control and Data Acquisition). It collects data from various sensors at a factory, plant, or in other remote locations, and then sends this data to a central computer which then manages and controls the data. The data is primarily used for topology processing, state estimation for steady state power flow solutions, contingency selection and assessment of power system security. Most control centers around the world perform steady state contingency analysis because of speed requirements for online security assessment. Online dynamic simulation still remains a goal to achieve for most control centers. The power system response to disturbances is decided not only by fast dynamics of its machines, but also by the action of slow processes such as tap changers and load dynamics. They often cause voltage problems and/or thermal loading problems after an extended period. Thus, extended term (1-2 hours) time domain simulator is the preferred tool to unearth the power system's ability to withstand large disturbances over extended periods of time. This would provide operators with a capability enhancement tool to deal with unforeseen initiating events/severe disturbances and complex unfolding of sequence of events, which can lead to cascading. Such information is not available today in control centers with dynamic simulation tools.

A common perspective today is that a key to cascading outage defense is the level of situational awareness held by grid operators, and limitations are associated with the limited monitoring and data exchange capabilities beyond the control areas [1]. Yet, modern power system operators are supervising one of the most complex systems of the society and are expected to take apt, correct and alert actions to ensure operational reliability and security of the power system. Under normal conditions they are able to sufficiently control the power

system with sufficient automatic control support. Severe disturbances and complex unfolding of post disturbance phenomena, including interdependent events, demand critical actions to be taken on the part of the operators which make them even more dependent on decision support and automatic controls at different levels [2, 3].

The market liberalization and push to operate the power system close to operational limits with less redundancy due to constraints placed by economical and environmental factors have made the operation more complex and exposed the power system to greater vulnerability to a disturbance, especially severe disturbances. There is indication in other industries (e.g., airline, nuclear, process control) that they employ a computational capability which provides operators with ways to predict system response and identify corrective actions. We think that power system operators should have a similar capability. The evolving power system demands ongoing and online operator training and capability enhancement tool to deal with any unforeseen initiating event/severe disturbance and unpredictable unfolding sequence of events.

On line dynamic simulation of power systems will have significant impact on their future design and operation. It will enhance power system security and reliability and hence customer satisfaction and utility profits, and will promote secure power grid expansion. To meet this challenging task of proper operator response and training, the attributes of an on-line mid-term simulator are proposed. This simulator will be used on-line to prepare the operators against extreme contingencies. It is expected to be a generalized event based corrective control/decision support for the operators. This motivates the research.

1.2 Nature of the Problem

To get an idea about the size of the problem which the big control centers deal with in practice, we can consider the example of Midwest ISO (MISO) and PJM ISO. MISO is responsible for monitoring and control of a large portion of the eastern US interconnection spanning 15 states and part of Canada, where the model represents approximately 33,000 buses and 120,000 branches. PJM model has 2500 generators, and 13,500 buses. The magnitude of the problem is in terms of tens of thousands of differential algebraic equations.

This chapter outlines the need for an extended term time domain simulator as an on-line cascading event tracking & avoidance decision support tool. At the outset, it discusses the

blackout attributes, derived from a study of blackouts around the world over the past 40 years. This forms the foundation for the desirable simulator attributes. The chapter concludes with a summary of the simulator attributes.

1.3 Attributes of Blackout

We performed an extensive study of the blackouts around the world in the past 40 years (see www.ece.cmu.edu/cascadingfailures). A condensed version of this study is summarized in Fig. 1 and Fig. 2. We summarize our observations as follows:

- three of the 4 largest blackouts occurred in last 10 years
- the number of blackouts greater than 1000 MW doubles every 10 years
- 50% of them involved generation and 90% involved transmission
- 40% involved proper protection action
- 50% were slow (more than 3 minutes)
- 60% involved number of dependent events
- 50% had significant time between initiating and pre-collapse events

IMPACT

Location	Date	MW Lost	Duration	People affected	Approximate cost
US-NE	11/9/1965	20000	13 hours	30 million	
US-NE	7/13/1977	6000	22 hours	3 million	300 million
France	12/19/1978	30000	10 hours		
West Coast	12/22/1982	12350		5 million	
Sweden	12/27/1983	> 7000	5.5 hours	4.5 million	
Brazil	4/18/1984	15762			
Brazil	8/18/1985	7793			
Hydro Quebec	4/18/1988	18500			
US-West	1/17/1994	7500			
Brazil	12/13/1994	8630			
US-West	12/14/1994	9336		1.5 million	
Brazil	3/26/1996	5746			
US-West	7/2/1996	11743		1.5 million	
US-West	7/3/1996	1200		small number	
US-West	8/10/1996	30489		7.5 million	1 billion dollars
MAPP, NW Ontario	6/25/1998	950	19 hours	0.152 million	
San Francisco	12/8/1998	1200	8 hours	1 million	
Brazil	3/11/1999	25000	4 hours	75 million	
Brazil	5/16/1999	2000			
India	1/2/2001	12000	13 hours	220 million	107 million
Rome	6/26/2003	2150		7.3 million	
US-NE	8/14/2003	62000	1-2 days	50 million	4-6 billion
Denmark/Sweden	9/23/2003	6300	6.5 hours	5 million	
Italy	9/28/2003	27000	19.5 hours	57 million	
Croatia	12/1/2003	1270 mwh			2.5 million
Greece	7/12/2004	9000	3 hours	5 million	
Moscow/Russia	5/24-25/2005	2500	>6 hours	4 million	
European Blackout	11/412006	6400	1 Hour	15 million	

Fig. 1: Blackout Impact

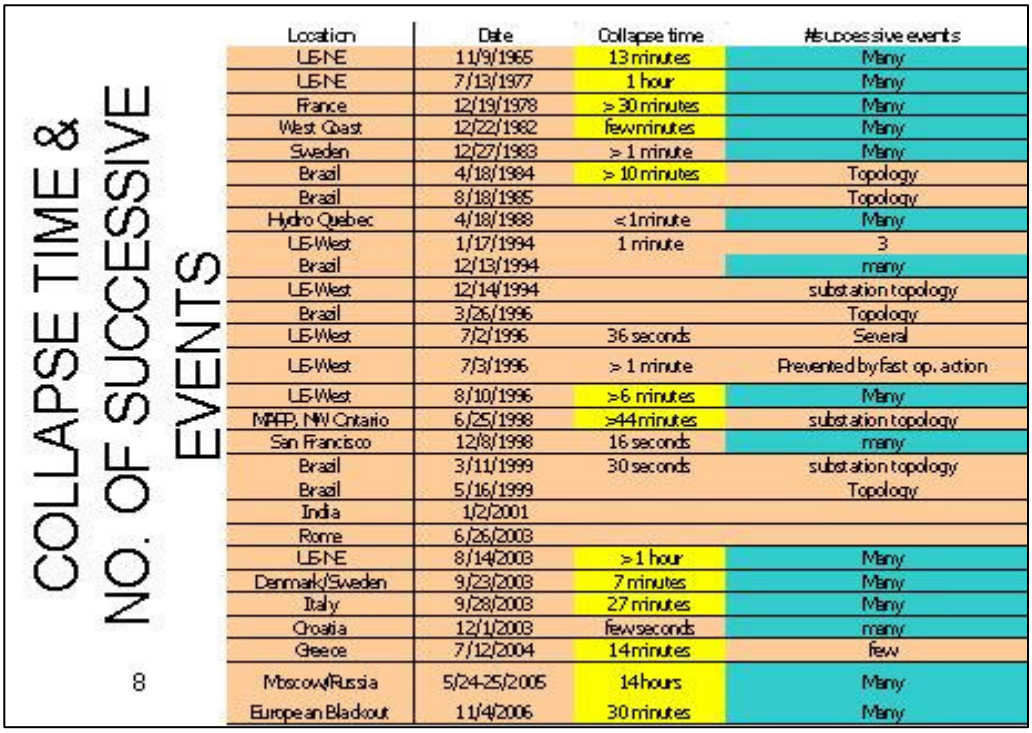

Location	Date	Collapse time	#successive events
US-NE	11/9/1965	13 minutes	Many
US-NE	7/13/1977	1 hour	Many
France	12/19/1978	> 30 minutes	Many
West Coast	12/22/1982	few minutes	Many
Sweden	12/27/1983	> 1 minute	Many
Brazil	4/18/1984	> 10 minutes	Topology
Brazil	8/18/1985		Topology
Hydro Quebec	4/18/1988	< 1 minute	Many
US-West	1/17/1994	1 minute	3
Brazil	12/13/1994		many
US-West	12/14/1994		substation topology
Brazil	3/26/1996		Topology
US-West	7/2/1996	36 seconds	Several
US-West	7/3/1996	> 1 minute	Prevented by fast op. action
US-West	8/10/1996	>6 minutes	Many
MAPP, NW Ontario	6/25/1998	>44 minutes	substation topology
San Francisco	12/8/1998	16 seconds	many
Brazil	3/11/1999	30 seconds	substation topology
Brazil	5/16/1999		Topology
India	1/2/2001		
Rome	6/26/2003		
US-NE	8/14/2003	> 1 hour	Many
Denmark/Sweden	9/23/2003	7 minutes	Many
Italy	9/28/2003	27 minutes	Many
Croatia	12/1/2003	few seconds	many
Greece	7/12/2004	14 minutes	few
Moscow/Russia	5/24-25/2005	14 hours	Many
European Blackout	11/4/2006	30 minutes	Many

Fig. 2: Nature of Blackout

This study indicates that the nature of the blackouts with respect to time may be roughly classified as either fast (less than 3 minutes) or slow. And when they are slow, they always involve a cascading sequence. It is for the slow types that we propose a simulator as a decision support tool for the operators. There are four typical stages of such cascading sequences [4].

1. Initiating contingency;
2. Steady-state progression (slow succession);
    - System becomes stressed with heavy loading on lines, transformers, and generator;
    - Successive events occur, typically the trip of other components with fairly large inter-event time intervals.
3. Transient progression (fast succession);
    - System goes under-frequency and/or under-voltage;
    - Large number of components begins tripping quickly.
4. Uncontrolled islanding and blackout.

An important attribute of the events in stage two is that they are almost always dependent events in that their occurrence depends on the occurrence of one or more earlier events. It is recognized that the probability of occurrence of successive events increases dramatically following the occurrence of a contingency. The time interval between an initiating event and successive events varies greatly. For example, the time between a fault and an inadvertent relay trip can be less than a second. However, if a fault followed by line clearing causes line overload and/or generator over-excitation, subsequent tripping may follow minutes or even hours later. The time interval may be long enough for an operator to initiate actions to mitigate the undesirable trend.

1.4 Simulator Attributes

The methodology discussed in Chapter 2 forms the foundation for continuous tracking of the system topology to generate high risk extended contingencies list for online security assessment. The proposed simulator should have the following features [5]:

- Intelligently select triggering events based on substation topology using switch-breaker data already existing in topology processor (chapter 2)
- Simulate conditions in the mid-term time frame (hours) very fast (chapter 3)
- Have detailed protective relaying and control system modeling (chapter 4)
- Provide decision support in the face of unfolding events (chapter 5)
- Provide “blackout avoidance” training tool for operators (chapter 5)
- Continuously identify catastrophic event sequences together with actions operators can take to mitigate them (chapter 5)
- Use current or forecasted conditions
- Store results for fast retrieval should an event occur

In keeping with the above a time domain simulator is the preferred analysis tool. However, it must be specialized to perform extended-term (several hours) of simulation ***very fast***, as suggested by the second bullet above. This means it must model both fast and slow dynamics and be capable of lengthening time steps when fast dynamics are inactive. In addition, it must have the necessary intelligence to recognize when failure conditions are encountered, retrieve earlier conditions, and determine appropriate actions; it must also have

modeling capability for a wide range of protection devices. Fig. 3 illustrates a typical output from the proposed time domain simulator with desired capabilities of fast, long term, adaptive time step dynamic simulation of slow and fast dynamics and appropriate control action determination to arrest unfolding cascading event. The philosophy is to prepare and revise, track and defend.

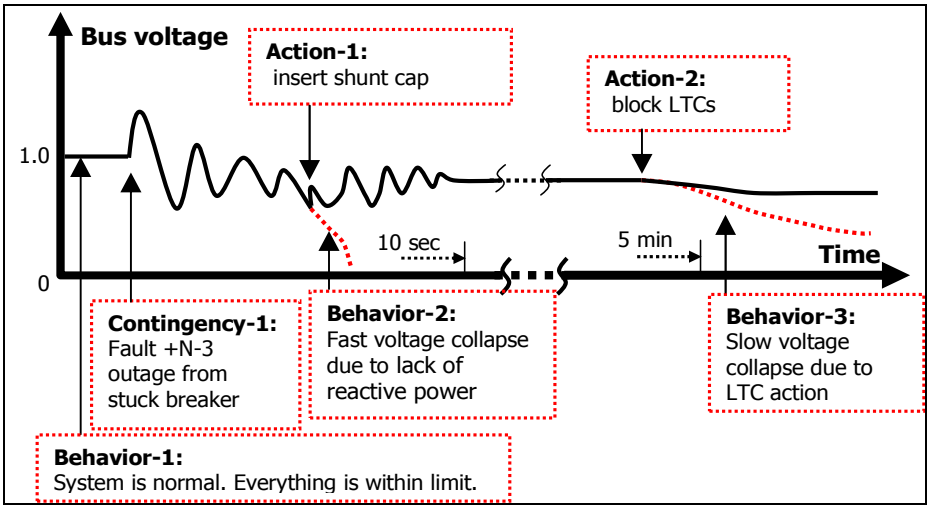

Fig. 3: Time domain simulator

Finally, in order to combine it with contingency identification and apply it online, it should be able to integrate with system real time information seamlessly, including switch-breaker data for automatic initiating event identification. Fig. 4 captures the proposed simulator's desired attributes in three dimensions of versatility namely: 1) Simulation model complexity 2) Computational characteristics 3) Decision Set Priority

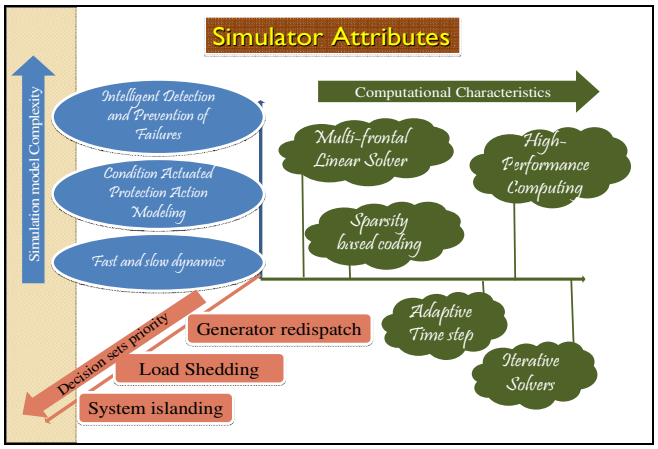

Fig. 4: Simulator attributes (in terms of Decision set priority, Computational characteristics, and simulation model complexity)

In this research, all the aspects of the proposed simulator's desired attributes have been addressed with the exception of its deploying to multiple CPUs, a task which is being pursued in a follow up PSerc project.

1.5 Research Problem Statement

The research problem statement is "*to provide operators with a **very fast** (online) computational capability to predict system response and identify corrective actions through analytical modeling and **fast** numerical simulation studies for low probability, high-consequence catastrophic events by exploiting the state of the art in software and hardware*". This is accomplished in terms of the following intermediate goals:

i) Development of a systematic methodology for the identification of high order *N-k* protection related inadvertent tripping contingencies from substation topology and switch/breaker status and verify against test systems.

ii) Establishing the importance of generator protection modeling in dynamic simulation and implementation of generator protection models for generator protection under abnormal conditions.

iii) Development of Depth First Search based algorithms to simulate cascading phenomena in the face of evolution of multiple islands. Island detection is done through graph search algorithms based on Breadth First Search techniques to check the connectivity of the components.

iv) Implementation and development of efficient numerical techniques to gain high computational efficiency

   a. Implementation of available multifrontal algorithms for the solution of sparse linear system in time domain simulation.
   b. Optimization of multifrontal algorithms for power systems to achieve high speed.
   c. Implementation of other sparse solvers available in Matlab and comparison with multifrontal methods.
   d. Development of new preconditioned iterative algorithms for power

system time domain simulation.

1.6 Thesis organization

The dissertation is divided into eight chapters and its outline is described as given below.

- **Chapter One: Introduction.**

  Importance and Impact of dynamic simulation, blackout attributes, simulator attributes, objectives of the research and outline of the thesis.

- **Chapter Two: N-k Contingency Selection.**

  This chapter describes a topological graph search algorithm to identify inadvertent tripping contingencies and their associated probability magnitudes, given an initial outage. The computed probability magnitudes serve to identify critical protection systems in the network. We use them to extend the conventional contingency list to include these high risk multi-element contingencies. The developed methodology is illustrated through five substation configurations including single breaker-single bus, ring bus, double breaker-double bus, single-bus connected with bus tie, and breaker and a half. Results of its validation and application to test systems are also reported.

- **Chapter Three: Numerical methods – Direct methods**

  In this chapter the nature and the uniqueness of the differential-algebraic equations (DAE), and potential targets for enhancing computational efficiency is discussed. This chapter proposes the application of Unsymmetric Multifrontal method to solve the linear equations formed as a result of the solution of the DAE encountered in the power system dynamic simulation. The frontal and multifrontal methods and the advantages of multifrontal methods are identified. The proposed method is compared with the full Gaussian Elimination solver and other sparse solvers and the results are reported.

- **Chapter Four: Numerical methods – Iterative methods**

  Multifrontal based preconditioner is developed for iterative methods for the solution of the linear equations. It is compared with ILU preconditioner based other iterative methods and multifrontal based direct methods.

- **Chapter Five: Modeling and protection.**

This chapter describes the modeling of the power system components and generator protection adopted for this research. Importance of generator protection with reference to past 40 years of blackouts is presented. Detailed explanation of generator protection modeling used in this research is given. DFS based algorithms are developed for graph traversal in the case of a cascading event leading to the formation of multiple islands.

- **Chapter Six: Results and discussion.**

  Validation of the simulator developed. Results and discussion of the implementation of the above described component modeling and generator protection and graph search based island detection and simulation are illustrated on a test system.

- **Chapter Seven: Conclusions.**

- **Chapter Eight: Future Recommendations.**

CHAPTER 2 *N-k* CONTINGENCY SELECTION

There is a growing need to provide operators with enhanced on-line information regarding system security levels, their influencing factors, and associated corrective actions. Amongst several causes of cascading [6] one of the major contributions comes from high order initiating contingencies—removal of several power system components in a relatively very short time, typically within seconds. We refer to such events as *N-k* events where it is implicit that $k>1$. Contingency set identification is an essential step in monitoring the power system security level [6]. Generally, various screening methods are used for selecting and ranking contingencies using an appropriate severity index from a presumed N-1 credible set [7, 8] on contingency selection emphasizes screening methods to select contingencies from a presumed $N-1$ contingency set plus a limited number of high order contingencies, ranking them using an appropriate severity index.

Although some exceptions [9,10,11] include studies on the effect of multiple component contingencies caused by substation and protection failures, the research on systematic selection of high order contingencies is limited. [12] and [13] proposed the on-line detection of hidden failure in protection device to prevent cascading failure. These proposed methods require extensive information on the logic of protection devices installed in power systems, which makes their implementation difficult.

It can be argued that most of these contingencies are so low in probability that they do not warrant attention. However, $N-k$ events do occur, and when they do, consequences can be severe. In addition, different *N-k* events have different probabilities, some commensurate with *N*-1 events. These very practical facts motivate identification of inadvertent tripping contingencies (ITC) for on-line security assessment. ITC comprises almost 59% of the protection related *N-k* contingencies. Reference [14] has described a method for identifying the remaining 41% of the protection related high order *N-k* contingencies which include breaker failure and protection failure to trip. The composition of these two sets can be added to the standard contingency list used by the energy management system (EMS) for transmission security assessment.

The purpose of this chapter is to illustrate a systematic analytical methodology for automatic identification of ITC together with their probabilities. A graph search algorithm for automatic identification of ITC from topology data is developed to gain computational efficiency over the analytical method for identification of the ITC. A systematic method to calculate the probabilities of *N-k* inadvertent contingencies for online security assessment is proposed and validated.

The developed methodology is illustrated through five substation configurations including single breaker-single bus, ring bus, double breaker-double bus, single-bus connected with bus tie, and breaker and a half. The difference between these five configurations lies in their robustness to *N-k* contingencies as illustrated in the probability calculation. The developed algorithms are implemented in Visual C++ and tested on a test system and IEEE-RTS 24 bus test system given in Appendix D and Appendix F.

Section 2.1 identifies the causes and types of high order N-*k* contingencies as a result of topological variation, presents an analysis of the database provided by the (NERC) Disturbance Analysis Working Group (DAWG) on large disturbances that have occurred in the bulk transmission systems in North America from 1984-2002. Section 2.2 uses an example to describe the graph theoretic representation of the power system in terms of edges, vertices, and a corresponding incidence matrix. Section 2.3 develops equations for computing probability of inadvertent tripping contingency and generalizes the equations developed in section 2.3 and presents a method to calculate the probability of inadvertent tripping or protection system misoperation following an initial event. Section 2.4 illustrates the method using five basic substation topological configurations. Section 2.5 further illustrates using two test systems, and Section 2.6 concludes.

2.1 System Topology and Primary Multiple Contingencies

Transmission substations are normally designed to ensure that a single fault results in at most the loss of a single circuit. However, the actual substation topology, at any given moment, may differ from the designed configuration, as the topological configuration of a substation, in terms of the connectivity of the elements through the switching devices (switches and breakers), may change. Variations in substation topology can occur as a result

of operator action for purposes of facility maintenance and for purposes of mitigating undesirable operating conditions such as high circuit loading or out-of-limit voltages. To a lesser extent, topological variation may also occur as a result of forced outages.

Substation topological variation may, in some instances, result in situations where the operation of the protective systems, in response to the occurrence of a fault in the network, removes two or more elements when clearing the fault. Such topologies significantly increase the risk-level of the network, as it exposes the system to a multi-outage contingency as a result of a single fault, whose probability is equivalent to that of an *N*-1 contingency. As *N-k* contingencies are inherently more severe than *N*-1 contingencies, an *N-k* contingency having a probability of the same order of magnitude as an *N*-1 contingency may cause a very high amount of risk, since risk associated with a specific contingency is the expected value of the contingency consequence [15].

We will classify event probabilities by their *probability order* [16, 17, 18] which is best described by an example. If the probability of an event, say a fault at a particular location, occurring in the next hour, is 10^{-5}, then the probability of two independent faults occurring in the next time hour is 10^{-10}, and three independent faults 10^{-15}, and so on. We say, then, that any event (or event combination, independent or not) with probability having order of magnitude -5 is an *order* 1 event, any event with probability having order of magnitude -10 is an *order* 2 event, any event with probability having order of magnitude -15 is an *order* 3 event, and so on. A detailed discussion on probability precision based on rare event approximation and *probability orders* is given in Appendix A.

An operator may not be aware of increased *N-k* likelihood that results from switching actions. In this case, automated detection is critical. Even if the operator is aware of the increased likelihood, the question remains as to its severity and therefore its risk. A search algorithm and the associated code have been developed to detect these situations and the pseudo code is given in Appendix B. It is discussed in detail in [4]. The inputs required for the algorithm include the breaker-switch status data obtained from the SCADA system. As this data is also used for EMS topology processing, it is available in most control centers.

Another cause of *N-k* events is the failure of a breaker to open or protection failure to trip under a faulted condition. Such an event is of lower probability than that of an *N-1* outage, as

it is comprised of a fault and a protection system failure. Because these are two independent events, it is of *order* 2. Yet, the severity, in terms of number of outaged elements, may be extreme, and therefore the risk may not be negligible. The graph-search algorithm given in Appendix B also detects this situation. This is also discussed in detail in [4].A systematic methodology for the probability calculation of inadvertent tripping or protection system misoperation leading to *N-k* events is developed in the current research and illustrated through five substation topologies [19]. This is an *order* 2 or higher *order* contingency.

The NERC Disturbance Analysis Working Group (DAWG) provides a database on large disturbances that have occurred in the bulk transmission systems in North America since 1984 [20]. The analysis of this information has resulted in a classification of three types among those related to protection failures: (1) inadvertent tripping, (2) protection relay fail to trip, and (3) breaker failure. A summary of the DAWG database in terms of this classification is given in Table 1. The approach developed in this work identifies the highest probability occurrence of the first category of these three different kinds of protection failure events.

Table 1: Summary on disturbances caused by protection system failures

Year	Inadvertent Tripping	Protection fails to trip	Breaker Failure	Total No. protection malfunction
1984	4	0	1	5
1985	2	0	5	7
1986	1	1	2	4
1987	2	0	0	2
1988	6	0	0	6
1989	6	0	0	6
1990	0	2	1	3
1991	3	1	1	5
1992	1	1	2	4
1993	1	0	3	4
1994	2	0	3	5
1995	5	1	1	7
1996	2	0	1	3
1997	1	0	2	3
1998	0	0	0	0
1999	0	1	0	1
2000	2	0	2	4
2001	4	1	0	5
2002	5	0	1	6
Total	47	8	25	80
Percentage	58.75%	10%	31.25%	100%

2.2 Graph Theoretic Representations of Power System Topology

The one-line diagram in Fig. 5 shows part of a real power system with bus bar segment BS-7 out for maintenance. Every component is tagged with a unique ID. Each of the components other than a bus section connects two different bus sections. In reality not all non-bus-section components (line, breaker, capacitor, generator, and switches) are joined by two bus bars. In this case a bus section is inserted between two non-bus-section components. This ensures that the data format for the topology of the power system is the same as those in EMS. A bus section is connected by one or more other types of components. If we take all the breakers and open switches (which form a cut set) away from the diagram, the whole diagram is decomposed into seven isolated parts. Each of the isolated parts is contained within a dashed circle. The components contained in each dashed circle of form a *functional group* (Fig. 5) A functional group does not include any circuit breaker and open switch, which forms the interface between two different functional groups. Generally, there is only one interfacing component, a breaker or a switch, connecting two functional groups.

The functional groups are identified with dashed circles as in the one-line diagram in Fig. 5, and each one is assigned a label $FG-i$. The interfacing components between each functional group are indicated with a grey ellipse, i.e., components BR-1, BR-2, BR-3, SW-2, and SW-3.

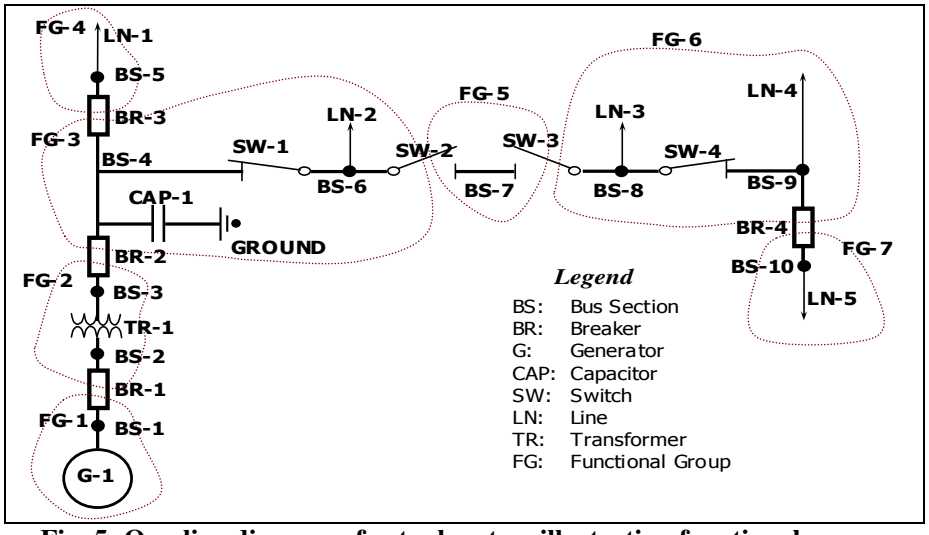

Fig. 5: One-line diagram of actual system illustrating functional groups

The expressions P_{FT}^{i}, P_{FL}^{i} and P_{PD}^{i} are three different reliability indices defined for power system components. P_{FT}^{i} is the probability that component has a ground fault contingency and P_{FL}^{i} means the probability that the component fails and has to be forced out from operation. Since fault contingency is only one of the different modes of failure, P_{FL}^{i} must be greater than or equal to P_{FT}^{i}. P_{PD}^{i} is called *per demand fail probability*, i.e. the conditional probability that the component fails to perform an action when the component is demanded to perform that action. Not all components require all three reliability indices. Both P_{FT}^{i} and P_{FL}^{i} are defined for non bus-section and non switching-components (line, capacitor and generator) because these components have many failure modes in addition to ground fault. Since these components are static devices that do not receive any command from control and perform any action, they do not have an P_{FD}^{i} index. Only P_{FL}^{i} is defined for bus sections since they are static and fault is virtually the only possible failure mode for them. Only P_{PD}^{i} is defined for switching components (breakers and switches) as they receive command from protection relay to connect or disconnect actions. Although it is possible for a switch component to have ground fault or other mode of failure, this probability is transferred to that of the two components the switch component connects by increasing the P_{FT}^{i} and P_{FL}^{i}. The value of P_{PD}^{i} depends on the switching status of the component. If the component is already in OPEN (or OFF) state, then P_{PD}^{i} is zero, otherwise, it is the conditional probability that the component fails to open when required.

The previous discussion is summarized in Table 2 and Table 3, for the specific sample system of Fig. 5. All the components treated as vertices are listed in Table 2, and all the components treated as edges are listed in Table 3. Each component is assigned a number I.D. in addition to the name I.D.

Table 2: List of vertex components of the power system diagram in Fig. 5

Name I.D.	BS-1	BS-2	BS-3	BS-4	BS-5	BS-6	BS-7	BS-8	BS-9	BS-10
Number	17	18	19	20	21	22	23	24	25	26
Fault Prob.	P_{FT}^{17}	P_{FT}^{18}	P_{FT}^{19}	P_{FT}^{20}	P_{FT}^{21}	P_{FT}^{22}	P_{FT}^{23}	P_{FT}^{24}	P_{FT}^{25}	P_{FT}^{26}

Since each functional group is tripped by protection relays as a whole entity, any fault or failure of a component within the group will cause the whole group to be tripped. The probability a functional group is tripped can be calculated as $\sum_{i \in S_i} P_{FL}^{i}$, where the elements of S_i are the indices of all the components in functional group i. The probability that a functional group is tripped due to fault can be calculated as $\sum_{i \in S_i} P_{FT}^{i}$ in the same way.

Table 3: List of edge components for the power system in Fig. 5

Name I.D.	No I.D.	Connected Bus Sections		Status	Probability		
		From	To		Fault	Fail	Per Demand
G-1	1	BS-1	Ground	Online	P_{FT}^{1}	P_{FL}^{1}	—
LN-1	2	BS-5	other system	Online	P_{FT}^{2}	P_{FL}^{2}	—
LN-2	3	BS-6	other system	Online	P_{FT}^{3}	P_{FL}^{3}	—
LN-3	4	BS-8	other system	Online	P_{FT}^{4}	P_{FL}^{4}	—
LN-4	5	BS-9	other system	Online	P_{FT}^{5}	P_{FL}^{5}	—
LN-5	6	BS-10	other system	Online	P_{FT}^{5}	P_{FL}^{5}	—
TR-1	7	BS-2	BS-3	Online	P_{FT}^{6}	P_{FL}^{6}	—
CAP-1	8	BS-4	Ground	Online	P_{FT}^{7}	P_{FL}^{7}	—
BR-1	9	BS-1	BS-2	On	0	0	P_{PD}^{9}
BR-2	10	BS-3	BS-4	On	0	0	P_{PD}^{10}
BR-3	11	BS-4	BS-5	On	0	0	P_{PD}^{11}
BR-4	12	BS-9	BS-10	On	0	0	P_{PD}^{12}
SW-1	13	BS-4	BS-6	On	0	0	P_{PD}^{13}
SW-2	14	BS-6	BS-7	Off	0	0	P_{PD}^{14}
SW-3	15	BS-7	BS-8	Off	0	0	P_{PD}^{15}
SW-4	16	BS-8	BS-9	On	0	0	P_{PD}^{16}

We assume the availability of the connection data for each power substation and the components within and between them, as summarized in the 3rd and 4th columns of Table 3. The equations for each individual group are summarized in the last two columns of Table 4. We perform a graph search using this information to identify the functional groups. The results of this search for this example are provided in the first four columns of Table 4.

Table 4: List of functional groups and their failure probabilities

Functional Group FG-i	Interfacing Components (breaker or Open switch)	Per Demand Fail Prob. Of Interfacing Components	Non-interfacing Components S_i =	Fault/Failure Prob. Of Functional groups	
				Fault: $P_{FG_i}^{FT}$	Failure: $P_{FG_i}^{FL}$
FG-1	BR-1	P_{PD}^{9}	S_1 = {1,17}	$\sum_{i\in\{1,17\}} P_{FT}^{i}$	$\sum_{i\in\{1,17\}} P_{FL}^{i}$
FG-2	BR-1, BR-2	P_{PD}^{9}, P_{PD}^{10}	S_2 = {7,18,19}	$\sum_{i\in\{7,18,19\}} P_{FT}^{i}$	$\sum_{i\in\{7,18,19\}} P_{FL}^{i}$
FG-3	BR-2, BR-3, SW-2	P_{PD}^{10}, P_{PD}^{11}	S_3 = {8, 20, 13, 22, 3}	$\sum_{i\in\{8,\,20,\,13,\,22,\,3\}} P_{FT}^{i}$	$\sum_{i\in\{8,\,20,\,13,\,22,\,3\}} P_{FL}^{i}$
FG-4	BR-3	P_{PD}^{11}	S_4 = {2, 21}	$\sum_{i\in\{2,\,21\}} P_{FT}^{i}$	$\sum_{i\in\{2,\,21\}} P_{FL}^{i}$
FG-5	SW-2, SW-3	P_{PD}^{14}, P_{PD}^{15}	S_5 = {23}	$\sum_{i\in\{23\}} P_{FT}^{i}$	$\sum_{i\in\{23\}} P_{FL}^{i}$
FG-6	SW-3, BR-4	P_{PD}^{15}, P_{PD}^{12}	S_6 = {24, 4, 16, 25, 5}	$\sum_{i\in\{24,\,4,\,16,\,25,\,5\}} P_{FT}^{i}$	$\sum_{i\in\{24,\,4,\,16,\,25,\,5\}} P_{FL}^{i}$
FG-7	BR-4	P_{PD}^{12}	S_7 = {26, 6}	$\sum_{i\in\{26,\,6\}} P_{FT}^{i}$	$\sum_{i\in\{26,\,6\}} P_{FL}^{i}$

The fifth column of Table 4 provides the failure probabilities of the functional groups, which are the summation of the failure probabilities of the non-interfacing components comprising the functional group.

If we take each functional group as a graph theoretic vertex, and any component (a breaker or an open switch) between two functional groups as an edge then Fig. 5 can be reduced as in Fig. 6. If we define $(FG\text{-}i,\ FG\text{-}j)$ to be the component joining $FG\text{-}i$ and $FG\text{-}j$, the new graph can be expressed by $G=(X,\ E)$

where $X = \{FG\text{-}1,\ FG\text{-}2,\ FG\text{-}3,\ FG\text{-}4,\ FG\text{-}5,\ FG\text{-}7,\ FG\text{-}7\}$

and $E = \{(FG\text{-}1,\ FG\text{-}2),\ (FG\text{-}2,\ FG\text{-}3),\ (FG\text{-}3,\ FG\text{-}4),\ (FG\text{-}3,\ FG\text{-}5),$

$(FG\text{-}5, FG\text{-}6),\ (FG\text{-}6,\ FG\text{-}7)\}$

$= \{BR\text{-}1,\ BR\text{-}2,\ BR\text{-}3,\ SW\text{-}2,\ SW\text{-}3,\ BR\text{-}4\}$

Fig. 6 shows the graph defined by $G=(X,\ E)$. Since the graph is an undirected graph, the pairs in E are defined as exchangeable, i.e. $(FG\text{-}i,\ FG\text{-}j)=(FG\text{-}j,\ FG\text{-}i)$.

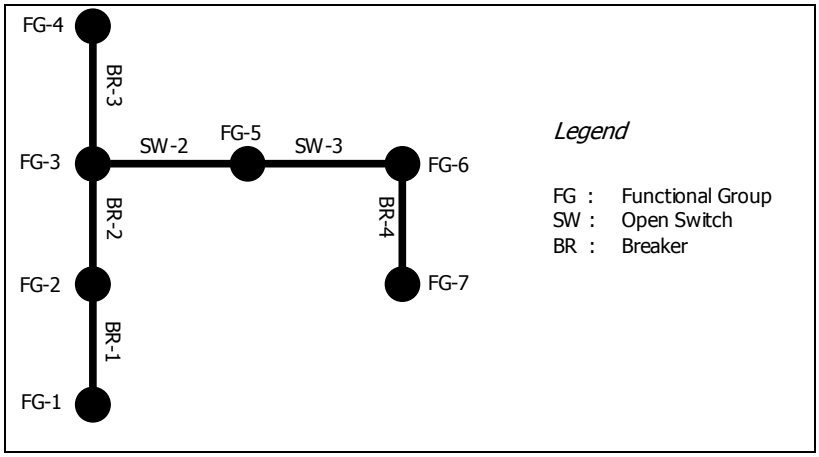

Fig. 6: Reduced functional group graph for Fig. 5

The results of the graph search also enable identification of the interconnections between functional groups, as summarized in Table 5. Each column in the table corresponds to a functional group, while each row corresponds to an interfacing component. There are two ones in each row, which indicate the interfacing component joint the two corresponding functional groups. The rest of the elements are all zeros. The array of elements in Table 3 can be represented via a matrix B in (1) where each row of B corresponds to an interfacing component, and each column corresponds to a functional group. This matrix is also called incidence matrix in graph theory [21].

Table 5: Connections for the interfacing components and the functional group (1- connected, 0- not connected)

—	FG-1	FG-2	FG-3	FG-4	FG-5	FG-6	FG-7
BR-1	1	1	0	0	0	0	0
BR-2	0	1	1	0	0	0	0
BR-3	0	0	1	1	0	0	0
SW-2	0	0	1	0	1	0	0
SW-3	0	0	0	0	1	1	0
BR-4	0	0	0	0	0	1	1

$$B = \begin{pmatrix} 1 & 1 & 0 & 0 & 0 & 0 & 0 \\ 0 & 1 & 1 & 0 & 0 & 0 & 0 \\ 0 & 0 & 1 & 1 & 0 & 0 & 0 \\ 0 & 0 & 1 & 0 & 1 & 0 & 0 \\ 0 & 0 & 0 & 0 & 1 & 1 & 0 \\ 0 & 0 & 0 & 0 & 0 & 1 & 1 \end{pmatrix} \quad (1)$$

2.3 High-order Contingencies due to inadvertent tripping

Inadvertent tripping after an initial fault or failure often leads to higher order contingencies. Inadvertent tripping generally occurs in the vicinity of the initial fault. Inadvertent tripping contingency forms the major part (about 55%) of the large system disturbances due to protection related cascading as given in Table 1. From practical experience it is seen that CT saturation causes misoperation of differential relays during external faults and delayed operation during internal faults. Inadvertent tripping often occurs at off-nominal frequency and due to outdated settings, human errors or overlapping zones of protection. The Northeast blackout on November 9, 1965, resulted in the loss of over 20,000 MW of load and affected 30 million people. It was a result of a faulty relay setting resulting in the tripping of one of five heavily loaded 230-kV transmission lines and the system cascaded in 2.5 seconds. On December 14, 1995, a fault occurred on a 345 kV line in southern Idaho, which tripped correctly, followed by an incorrect trip of a parallel line and a third line tripped on overloading. System instability resulted in the formation of four islands, with system frequency dropping to 58.75 Hz and 3,000 MW of load curtailed by under frequency load shedding. The blackout of West Coast on July 2, 1996 resulted in the loss of 11,850 MW of load and affected 2 million. Again it was a result of incorrect tripping of a parallel line after the initial contingency of a line sagging into a tree and resulted in the formation of five islands. In all the above cascading events inadvertent tripping played an important role. The table below summarizes an US utility experience with inadvertent tripping, and Table 7 summarizes the survey result conducted by Working Group I17 Transmission System Relay Performance Comparison on misoperation [22]. The percentage misoperations are calculated via the misoperation formula given below

$$\%\ misoperation = \frac{All\ misoperations}{Total\#\ of\ events + K} * 100 \tag{2}$$

Table 6: A US Utility experience with misoperation

Utility: **Time Period:** Jan. - Dec. 2004

Voltage:	Dependability			Security		System Restoration	Total Misoperations
138 kV	Failure to Trip	Failure to Interrupt	Slow Trip	Unnecessary Trip During Fault	Unnecessary Trip Other Than Fault	Failure to Reclose	
Relay System	2	0	19	18	5	7	51
Circuit Breaker	1	1	0	0	3	2	7
Total Protective System	3	1	19	18	8	9	58
Percent Incorrect Operation Relay System	0.5%	0.0%	4.7%	4.5%	1.2%	1.7%	12.7%
Percent Incorrect Operation Circuit Breaker	0.3%	0.3%	0.0%	0.0%	0.8%	0.5%	1.8%
Percent Incorrect Operation Protective System	0.7%	0.2%	4.7%	4.5%	2.0%	2.2%	14.4%

138 kV

Relay K =	5
Breaker K =	0
Total Operations:	397

Table 7: Survey of US Utilities on Relay misoperation

% INCORRECT OPERATIONS, YEAR 2003

Company	Total Events	K Factor	Relay Misoperations		Voltage	Failure to Trip	Failure to Interrupt	Slow Trip	Unnecessary Trip During Fault	Unnecessary Trip Other Than Fault	Failure to Reclose	Total Misoperations
A					Above 400							
B												
C	3	0	1			0.0%	0.0%	0.0%	0.0%	33.3%	0.0%	33.3%
D												
E												
F												
H												
I												
A	23	0	4		301 - 400	0.0%	0.0%	0.0%	8.7%	8.7%	0.0%	17.4%
B	136	2	20			0.7%	0.0%	1.4%	5.1%	2.2%	5.1%	14.5%
C	22	1	13			0.0%	0.0%	0.0%	13.0%	39.1%	4.3%	56.5%
D												
E	16	4	7			0.0%	0.0%	0.0%	0.0%	0.0%	35.0%	35.0%
F	1	0	0			0.0%	0.0%	0.0%	0.0%	0.0%	0.0%	0.0%
H												
I	9	0	3			0.0%	0.0%	0.0%	0.0%	0.0%	33.3%	33.3%
A					201 - 300							
B												
C	9	1	2			0.0%	0.0%	0.0%	0.0%	20.0%	0.0%	20.0%
D												
E	1	0	0			0.0%	0.0%	0.0%	0.0%	0.0%	0.0%	0.0%
F												
H												
I												
A	72	0	22		101 - 200	1.4%	0.0%	1.4%	19.4%	8.3%	0.0%	30.6%
B	303	9	46			0.0%	0.0%	2.9%	6.7%	0.6%	4.5%	14.7%
C	128	0	29			0.0%	0.0%	0.0%	7.8%	7.0%	7.8%	22.7%
D												
E	115	3	23			0.8%	0.0%	0.0%	14.4%	4.2%	0.0%	19.5%
F	15	1	10			0.0%	0.0%	0.0%	50.0%	12.5%	0.0%	62.5%
H												
I	10	6	11			6.3%	0.0%	0.0%	18.8%	6.3%	37.5%	68.8%
A	105	0	7		51 - 100	1.0%	0.0%	0.0%	4.8%	0.0%	1.0%	6.7%
B	697	1	12			0.0%	0.0%	0.0%	1.1%	0.0%	0.6%	1.7%
C	397	1	24			0.3%	0.0%	0.0%	2.8%	0.8%	2.3%	6.0%
D												
E	291	5	30			0.7%	0.0%	0.3%	6.4%	1.0%	1.7%	10.1%
F												
H												
I	47	0	6			0.0%	0.0%	2.1%	4.3%	4.3%	2.1%	12.8%

It is assumed that only line or functional group connected to the initial contingent functional group or line will suffer inadvertent tripping. This assumption for the derivation of Inadvertent Tripping Contingency is based on the zones of protection in the real system. The bases of this assumption are:

1. Anecdotal evidence suggests that inadvertent tripping of an element is more likely with the size of transients experienced by the element, and the further the element is from the disturbance; the less likely will be the inadvertent trip.
2. We have no information of more than one simultaneous inadvertent tripping from the open literature.

If there is more than one functional group that can suffer inadvertent tripping than it is assumed that only one of them can suffer inadvertent tripping at a time. However, one can extend the equations developed below to account for exceptions in case the situation demands.

A systematic methodology for the probability calculation of inadvertent tripping is developed and illustrated through the five substation topologies discussed above.

The total probability of an inadvertent tripping contingency (ITC) k involving line i and line j can be calculated by

$$\begin{aligned} P_{ITC_k} &= \Pr(line\ j\ trips | line\ i\ trips) + \Pr(line\ i\ trips | line\ j\ trips) \\ &= \Pr(line\ j\ trips \cap line\ i\ trips) / \Pr(line\ i\ trips) \\ &+ \Pr(line\ i\ trips \cap line\ j\ trips) / \Pr(line\ j\ trips) \\ &= \Pr(line\ j\ trips \cap line\ i\ trips) * \\ &\left[(\Pr(line\ i\ trips) + \Pr(line\ j\ trips)) / (\Pr(line\ i\ trips) * \Pr(line\ j\ trips))\right] \end{aligned} \tag{3}$$

assuming that the probability of failure/fault to be same for each line. Let

p_{lf}^{i} : fault probability of line i. It is assumed to be the same (denoted as p_l) for all transmission lines;

Therefore,

$$\begin{aligned} P_{ITC_k} &= \Pr(line\ j\ trips \cap line\ i\ trips)[(2 * p_l)/(p_l^2)] \\ &= \Pr(line\ j\ trips \cap line\ i\ trips) * 2 * (1/p_l) \end{aligned} \tag{4}$$

The result generalizes in terms of the functional group concept discussed earlier. Let us consider two functional groups represented by FG-*i* and FG-*j*. The probability that a

functional group FG-i is tripped due to failure of a component can be calculated as $\sum_{i \in S_i} P_{FL}^{j}$, where the elements of S_i are the indices of all the components in functional group i. The probability that a functional group is tripped due to fault can be calculated as $\sum_{i \in S_i} P_{FT}^{j}$ in the same way.

The probability of an ITC k due to failure that involved FG- i and FG- j can be calculated by

$$\begin{aligned} &P_{ITC_k} = \Pr(FG-j\,trips \mid FG-i\,trips) + \Pr(FG-i\,trips \mid FG-j\,trips) \\ &where \\ &\Pr(FG-j\,trips \mid FG-i\,trips) = \Pr(FG-j\,trips \cap FG-i\,trips) / \Pr(FG-i\,trips) \end{aligned} \tag{5}$$

$$\begin{aligned} P_{ITC_k} &= \Pr(FG-j\ trips \cap FG-i\ trips) / \Pr(FG-i\ trips) \\ &\quad + \Pr(FG-i\ trips \cap Fg-j\ trips) / \Pr(FG-j\ trips) \\ &= \Pr(FG-j\ trips \cap FG-i\ trips) * \\ &\quad \left[(\Pr(FG-i\ trips) + \Pr(FG-j\ trips)) / (\Pr(FG-i\ trips) * \Pr(FG-j\ trips)\right] \\ &= \Pr(FG-j\ trips \cap FG-i\ trips) \left[\sum_{i \in S_i} P_{FL}^{i} + \sum_{i \in S_i} P_{FL}^{j} \right] / \left[\left(\sum_{i \in S_i} P_{FL}^{i} \right) * \left(\sum_{i \in S_i} P_{FL}^{j} \right) \right] \end{aligned}$$

Similarly the probability of an ITC k due to fault that involved FG- i and FG- j can be calculated by

$$P_{ITC_k} = \Pr(FG-j\ trips \cap FG-i\ trips) \left[\sum_{i \in S_i} P_{FT}^{i} + \sum_{i \in S_i} P_{FT}^{j} \right] / \left[\left(\sum_{i \in S_i} P_{FT}^{i} \right) * \left(\sum_{i \in S_i} P_{FT}^{j} \right) \right] \tag{6}$$

In the above case it was considered that there is a possibility of only one additional functional group suffering inadvertent tripping. When there are more functional groups which can trip inadvertently then one can similarly find an expression of the total probability by conditioning on each functional group sequentially and adding their probabilities. For example when the failure of one can initiate inadvertent tripping of either of the two then the expression for total ITC probability will look like

$$P_{ITC_i} = \Pr(FG-i\,trips\,or\,FG-j\,trips \mid FG-k\ trips) + \Pr(FG-i\,trips\,or\,FG-k\,trips \mid FG-\ j\ trips) + \Pr(FG-j\,trips\,or\,FG-k\,trips \mid FG-i\ trips) \quad (7)$$

2.3.1 Generalized form for Inadvertent Tripping Contingency

In this section a generalized method from the system topology to find the total probability of ITC after an initial contingency is developed. As it was discussed above, the power system can be represented as an undirected graph with functional groups as the vertices and the interfacing elements as the edges. The graph search algorithm developed enables identification of the interconnections between functional groups. The methodology will be illustrated with the example of the power system shown in Fig. 5 and the result generalized. For the power system shown in Fig. 5, the result of the graph search is summarized in Table 5. Each column in the table corresponds to a functional group, while each row corresponds to an interfacing component. There are two ones in each row, which indicate the interfacing component joining the two corresponding functional groups. The rest of the elements are all zeros. This is represented as the incidence matrix in (1) which is reproduced below

$$B = \begin{pmatrix} 1 & 1 & 0 & 0 & 0 & 0 & 0 \\ 0 & 1 & 1 & 0 & 0 & 0 & 0 \\ 0 & 0 & 1 & 1 & 0 & 0 & 0 \\ 0 & 0 & 1 & 0 & 1 & 0 & 0 \\ 0 & 0 & 0 & 0 & 1 & 1 & 0 \\ 0 & 0 & 0 & 0 & 0 & 1 & 1 \end{pmatrix} \quad (8)$$

The new matrix B^T in (9) is obtained by taking the transpose of the matrix B in (1)

$$B^T = \begin{pmatrix} 1 & 0 & 0 & 0 & 0 & 0 \\ 1 & 1 & 0 & 0 & 0 & 0 \\ 0 & 1 & 1 & 1 & 0 & 0 \\ 0 & 0 & 1 & 0 & 0 & 0 \\ 0 & 0 & 0 & 1 & 1 & 0 \\ 0 & 0 & 0 & 0 & 1 & 1 \\ 0 & 0 & 0 & 0 & 0 & 1 \end{pmatrix} \quad (9)$$

Each column in (9) corresponds to an interfacing component, while each row corresponds to a functional group.

$$X = \{FG\text{-}1,\ FG\text{-}2,\ FG\text{-}3,\ FG\text{-}4,\ FG\text{-}5,\ FG\text{-}6,\ FG\text{-}7\} \tag{10}$$

$$K = \bigcap P(B * diag(X)) \tag{11}$$

$$D = diag(K) \tag{12}$$

$$C(1) = (1\ 1\ 1\ ....) \tag{13}$$

where C(1) is the unit column matrix of order (1*7), $\bigcap P$ is the joint probability of failure of the functional groups in each row of the matrix $B * diag(X)$ which can be approximately calculated from the outage data base available in the utilities for past many years.

Then all the equations in (5) and (6) can be summarized in the matrix form as

$$P_{IFG}^{FT} = (1/P_{FG_1}^{FT}, 1/P_{FG_2}^{FT}, 1/P_{FG_3}^{FT}, 1/P_{FG_4}^{FT}, 1/P_{FG_5}^{FT}, 1/P_{FG_6}^{FT}, 1/P_{FG_7}^{FT})^T \tag{14}$$

$$P_{ITC} = [(B^T * D)^T * diag(P_{IFG}^{FT})]^T * C(1) \tag{15}$$

$$P_{ITC} = \begin{pmatrix} P_{FG_1}^{ITC} \\ P_{FG_2}^{ITC} \\ P_{FG_3}^{ITC} \\ P_{FG_4}^{ITC} \\ P_{FG_5}^{ITC} \\ P_{FG_6}^{ITC} \\ P_{FG_7}^{ITC} \end{pmatrix} \tag{16}$$

and $P_{FG_1}^{ITC}$ is the total probability of ITC given the fault/ failure in functional group 1. It is assumed that $P_{FG_i}^{FT}$ is not identically equal to zero. In other words it is not a bus section. The case where FG_i is a bus section is discussed as a special case below.

Equation (16) is the general formula for any power system whose topology is known in terms of the switching elements and components of the functional group. So for the power

system example in Fig. 5, the ITC probability for each functional group can be calculated as below.

$$\begin{pmatrix} P_{FG_1}^{ITC} \\ P_{FG_2}^{ITC} \\ P_{FG_3}^{ITC} \\ P_{FG_4}^{ITC} \\ P_{FG_5}^{ITC} \\ P_{FG_6}^{ITC} \\ P_{FG_7}^{ITC} \end{pmatrix} = [A * diag(P_{IFG}^{FT})]^T * C(1) \tag{17}$$

where $A = \left[\begin{pmatrix} 1&0&0&0&0&0 \\ 1&1&0&0&0&0 \\ 0&1&1&1&0&0 \\ 0&0&1&0&0&0 \\ 0&0&0&1&1&0 \\ 0&0&0&0&1&1 \\ 0&0&0&0&0&1 \end{pmatrix} * \begin{pmatrix} P(FG_1 \cap FG_2) & 0 & 0 & 0 & 0 & 0 \\ 0 & P(FG_2 \cap FG_3) & 0 & 0 & 0 & 0 \\ 0 & 0 & P(FG_3 \cap FG_4) & 0 & 0 & 0 \\ 0 & 0 & 0 & P(FG_3 \cap FG_5) & 0 & 0 \\ 0 & 0 & 0 & 0 & P(FG_5 \cap FG_6) & 0 \\ 0 & 0 & 0 & 0 & 0 & P(FG_6 \cap FG_7) \end{pmatrix} \right]^T$

In the same way the ITC can be found for any power system once the functional groups are identified. With the changing topology of the power system the functional groups can be identified in an updating mode and continuous tracking of increased ITC probability can be very useful in real time operations.

2.3.2 Special Case

When all the functional group(s) connected by the interfacing element(s) of the failed or faulted functional group contains/contain only bus sections as their components then all the functional groups connected to these bus sections will have equal probability to suffer inadvertent tripping. This special case is incorporated by modifying the matrix B. The

modified matrix is obtained by subtracting the column corresponding to the faulted functional group from the sum of the columns of the functional groups connected to the faulted functional group through the interfacing elements of the faulted functional group. In the next step the columns corresponding to the functional groups connected to the faulted functional group are made zero. To find the ITC corresponding to this special case only the transpose of the column corresponding to the faulted functional group in the B^T matrix is needed. This gives the ITC probability of the functional group which is connected only to the bus section through all interfacing elements. From practical experience the probability of a fault in a bus section is once in a lifetime and is 'almost zero' compared to other components fault probability. Thus the probability of bus fault is assumed to be zero. Similarly the probability of simultaneous outage of two functional groups where one of the functional group is a bus section is zero. Hence the ITC probability for an initial contingency on a bus section is zero and is not calculated.

The analytical equations developed above give a concise mathematical form to identify ITC from the system point of view and calculate their probabilities. They form the foundation for the ITC probability calculation for any power system. However with the size of the system, the size of B becomes very large and sparsity technology has to be used to handle it efficiently. Other matrix operations as in the case of the special case discussed above are also memory intensive.

Therefore based on the analytical foundation, a computer based graph search algorithm is also developed to search for functional groups, its components, the interfacing elements, and to get the ITCs without formulating the B matrix. Once the ITC's are identified their probabilities are calculated as discussed in equations (5) and (6).

In the next section, the probability calculation for the typical substation topologies are illustrated directly from the topology and with the help of the formula developed. This will illustrate the effectiveness of the concise formula developed for a large system where it is not easy to enumerate all the different possibilities easily. A systematic method is indispensable for a large system.

2.4 Probability calculation illustration for the Typical Substation Topologies

2.4.1 Ring Bus

This configuration is simple and straightforward. From Fig. 7, there are a total of four functional groups and four breakers. In this simple configuration from the topology it is evident that a fault on a single line can trigger inadvertent tripping on either of the two lines connected to the same bus through an electrical distance of one breaker. For illustration purposes it is assumed that the fault occurs on line 3 or FG-3 and is tripped correctly.

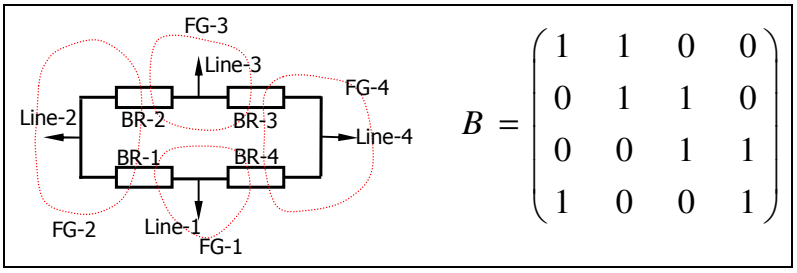

Fig. 7: Ring bus station with B-matrix

Now one of the two functional groups FG-2 or FG-4 can trip inadvertently. The functional group fault probability is calculated as in (12), and assuming the failure probability of bus $p_{bf} \simeq 0$. So the probability of ITC when FG-3 trips is

$$P_{ITC_1} = \Pr(FG-2 \ trips \ or \ FG-4 trips \,|\, FG-3 trips) \tag{18}$$

Since the inadvertent tripping of any of the functional groups is independent of each other and assuming they are disjoint the above expression becomes.

$$\begin{aligned} P_{ITC_1} &= \Pr(FG-2 \ trips \,|\, FG-3 \ trips) + \Pr(FG-4 trips \,|\, FG-3 \ trips) \\ &= [P(FG_2 \cap FG_3) + P(FG_3 \cap FG_4)]\left(1/P_{FG_3}^{FT}\right) \end{aligned} \tag{19}$$

The ITC probability calculations using equations (10)-(16) are also shown below.

$$P_{IFG}^{FT} = (1/P_{FG_1}^{FT}, 1/P_{FG_2}^{FT}, 1/P_{FG_3}^{FT}, 1/P_{FG_4}^{FT})^T \tag{20}$$

$$P_{ITC} = [(B^T * D)^T * diag(P_{IFG}^{FT})]^T * C(1) \tag{21}$$

$$\begin{pmatrix} P_{FG_1}^{ITC} \\ P_{FG_2}^{ITC} \\ P_{FG_3}^{ITC} \\ P_{FG_4}^{ITC} \end{pmatrix} = \left[\left\{ \begin{pmatrix} 1 & 0 & 0 & 1 \\ 1 & 1 & 0 & 0 \\ 0 & 1 & 1 & 0 \\ 0 & 0 & 1 & 1 \end{pmatrix} * \begin{pmatrix} P(FG_1 \cap FG_2) & 0 & 0 & 0 \\ 0 & P(FG_2 \cap FG_3) & 0 & 0 \\ 0 & 0 & P(FG_3 \cap FG_4) & 0 \\ 0 & 0 & 0 & P(FG_1 \cap FG_4) \end{pmatrix} \right\}^T * diag(P_{IFG}^{FT}) \right]^T * \begin{pmatrix} 1 \\ 1 \\ 1 \\ 1 \end{pmatrix}$$

$$\begin{pmatrix} P_{FG_1}^{ITC} \\ P_{FG_2}^{ITC} \\ P_{FG_3}^{ITC} \\ P_{FG_4}^{ITC} \end{pmatrix} = \begin{pmatrix} .. \\ .. \\ [P(FG_2 \cap FG_3) + P(FG_3 \cap FG_4)](1/P_{FG_3}^{FT}) \\ .. \end{pmatrix} \tag{22}$$

which is same as obtained from the topology in (19).

2.4.2 Breaker and a Half Bus (B-HB)

The configuration of B-HB is shown in Fig. 8, having a total of six functional groups and six breakers. In this simple bus configuration a fault on a single line can trigger inadvertent tripping on only lines connected between the same pair of buses through an electrical distance of one breaker and on the same side. For illustration purposes it is assumed that the fault occurs on line 3 or FG-4.

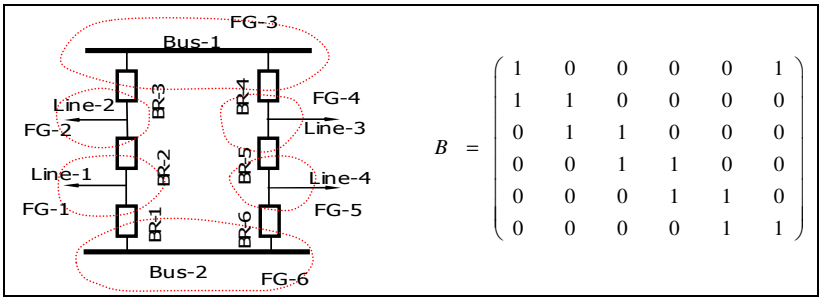

$$B = \begin{pmatrix} 1 & 0 & 0 & 0 & 0 & 1 \\ 1 & 1 & 0 & 0 & 0 & 0 \\ 0 & 1 & 1 & 0 & 0 & 0 \\ 0 & 0 & 1 & 1 & 0 & 0 \\ 0 & 0 & 0 & 1 & 1 & 0 \\ 0 & 0 & 0 & 0 & 1 & 1 \end{pmatrix}$$

Fig. 8: Breaker and a half bus

Now only FG-5 can trip inadvertently which is on the same side as FG-4 and between the same pair of buses. The functional group fault probabilities are calculated, assuming the failure probability of bus $p_{bf} \simeq 0$. So the probability of ITC contingency when FG-4 trips

$$P_{ITC_2} = \Pr(FG-5\ trips \mid FG-4 trips) \tag{23}$$

$$= [P(FG_5 \cap FG_4)]\left(1/P_{FG_4}^{FT}\right)$$

Now from equations (10)-(16) the corresponding equations for a breaker and half are as follows

$$P_{IFG}^{FT} = (1/P_{FG_1}^{FT}, 1/P_{FG_2}^{FT}, 1/P_{FG_3}^{FT}, 1/P_{FG_4}^{FT}, 1/P_{FG_5}^{FT}, 1/P_{FG_6}^{FT})^T \tag{24}$$

where $P_{FG_3}^{FT}$ and $P_{FG_6}^{FT}$ are zero. But all the terms of the form $P(FG_j \cap FG_i) * \left(1/P_{FG_i}^{FT}\right)$ are zero where i = 3, 6 $j \neq i$.

$$P_{ITC} = [(B^T * D)^T * diag(P_{IFG}^{FT})]^T * C(1) \tag{25}$$

$$\begin{pmatrix} P_{FG_1}^{ITC} \\ P_{FG_2}^{ITC} \\ P_{FG_4}^{ITC} \\ P_{FG_6}^{ITC} \end{pmatrix} = \begin{pmatrix} .. \\ .. \\ [P(FG_5 \cap FG_4)]\left(1/P_{FG_4}^{FT}\right) \\ .. \end{pmatrix} \tag{26}$$

which is same as calculated from the topology. In the final expression the terms $P_{FG_3}^{ITC}$ and $P_{FG_6}^{ITC}$ are not included because they are bus sections and ITC corresponding to them is zero as explained earlier.

2.4.3 Single Bus Connected with Tie Breaker (SB-TB)

This configuration SB-TB in Fig. 9 is adapted from SB-SB by splitting the bus and adding a tie-breaker between the two buses. From the topology it is evident that a fault on a single line can trigger inadvertent tripping on only lines connected to the same bus through an electrical distance of one breaker and on the same side of the tie breaker. For illustration purposes it is assumed that the fault occurs on line 1 or FG-1.

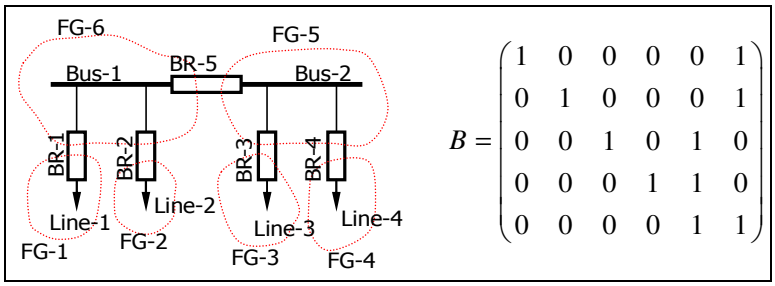

$$B = \begin{pmatrix} 1 & 0 & 0 & 0 & 0 & 1 \\ 0 & 1 & 0 & 0 & 0 & 1 \\ 0 & 0 & 1 & 0 & 1 & 0 \\ 0 & 0 & 0 & 1 & 1 & 0 \\ 0 & 0 & 0 & 0 & 1 & 1 \end{pmatrix}$$

Fig. 9: Single bus connected with tie-breaker and it's B-matrix

So now only FG-2 can trip inadvertently. The functional group fault probability is calculated assuming the failure probability of the bus $p_{bf} \simeq 0$. So the probability of ITC contingency when FG-1 trips is

$$P_{ITC_3} = \Pr(FG-2 \ \ trips | FG-1 trips) \tag{27}$$

$$= [P(FG_2 \cap FG_1)]\left(1/P_{FG_1}^{FT}\right)$$

Now from equations (10)-(16) the corresponding equations for this configuration are as follows

$$P_{IFG}^{FT} = (1/P_{FG_1}^{FT}, 1/P_{FG_2}^{FT}, 1/P_{FG_3}^{FT}, 1/P_{FG_4}^{FT}, 1/P_{FG_5}^{FT}, 1/P_{FG_6}^{FT})^T \tag{28}$$

where $P_{FG_5}^{FT}$ and $P_{FG_6}^{FT}$ are zero. But all the terms of the form $P(FG_j \cap FG_i) * \left(1/P_{FG_i}^{FT}\right)$ are zero where i = 5, 6 $j \neq i$.

$$P_{ITC} = [(B^T * D)^T * diag(P_{IFG}^{FT})]^T * C(1) \tag{29}$$

$$\begin{pmatrix} P_{FG_1}^{ITC} \\ P_{FG_2}^{ITC} \\ P_{FG_3}^{ITC} \\ P_{FG_4}^{ITC} \end{pmatrix} = \begin{pmatrix} [P(FG_2 \cap FG_1)]\left(1/P_{FG_1}^{FT}\right) \\ \vdots \\ \vdots \\ \vdots \end{pmatrix} \tag{30}$$

which is same as calculated from the topology. In the final expression the terms $P_{FG_5}^{ITC}$ and $P_{FG_6}^{ITC}$ are not included because they are bus sections and ITC corresponding to them is zero as explained earlier

2.4.4 Single Breaker and Single Bus (SB-SB)

In the simple configuration in Fig. 10, a fault on a single line can trigger inadvertent tripping on any one of the remaining three lines since all are connected to the same bus through an electrical distance of one breaker. For illustration purposes it is assumed that the fault occurs on line 3 or FG-3.

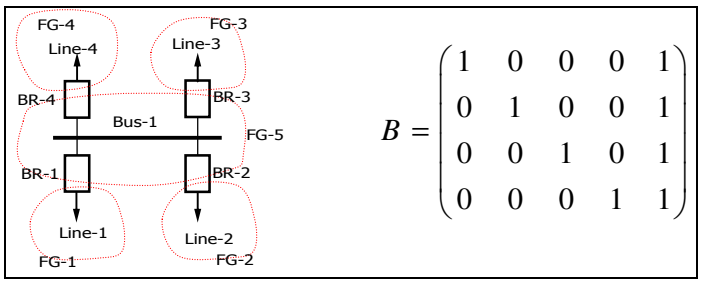

$$B = \begin{pmatrix} 1 & 0 & 0 & 0 & 1 \\ 0 & 1 & 0 & 0 & 1 \\ 0 & 0 & 1 & 0 & 1 \\ 0 & 0 & 0 & 1 & 1 \end{pmatrix}$$

Fig. 10: Single breaker single bus substation and it's B-matrix

Now one or more of the remaining functional groups can trip inadvertently. The functional group fault probability, which is the summation of the fault probability of each component in the functional group, is calculated assuming the failure probability of the bus $p_{bf} \simeq 0$. So the probability of ITC when FG-3 trips is

$$P_{ITC_4} = \Pr(FG-1 \ trips \, or \, FG-2 \ trips \ or \ FG-4 trips \,|\, FG-3 \, trips) \tag{31}$$

Since the inadvertent tripping of any of the functional groups is independent of each other and assuming they are disjoint the above expression becomes.

$$\begin{aligned} P_{ITC_4} &= \Pr(FG-1 \ trips \,|\, FG-3 trips) + \Pr(FG-2 \ trips \,|\, FG-3 \, trips) \\ &\quad + \Pr(FG-4 trips \,|\, FG-3 \, trips) \end{aligned} \tag{32}$$

$$= [P(FG_1 \cap FG_3) + P(FG_2 \cap FG_3) + P(FG_4 \cap FG_3)]\left(1/P_{FG_3}^{FT}\right) \tag{33}$$

This configuration falls under the category of special case where the faulted functional group is connected only to a bus section. So to calculate its ITC probability through (10)-(16) the matrix B is modified as explained earlier. So in this case the B matrix for ITC probability of FG-3 becomes

$$B' = \begin{pmatrix} 1 & 0 & 1 & 0 & 0 \\ 0 & 1 & 1 & 0 & 0 \\ 0 & 0 & 0 & 0 & 0 \\ 0 & 0 & 1 & 1 & 0 \end{pmatrix} \tag{34}$$

$$B^{T'} = (1 \quad 1 \quad 0 \quad 1) \text{ row corresponding to FG-3} \tag{35}$$

$$P_{IFG}^{FT} = (1/P_{FG_1}^{FT}, 1/P_{FG_2}^{FT}, 1/P_{FG_3}^{FT}, 1/P_{FG_4}^{FT}, 1/P_{FG_5}^{FT})^T \tag{36}$$

where $P_{FG_5}^{FT}$ **is** zero. But all the terms of the form $P(FG_j \cap FG_i) * \left(1/P_{FG_i}^{FT}\right)$ are zero where i = 5 and $j \neq i$.

$$P_{ITC} = [(B^T * D)^T * diag(P_{IFG}^{FT})]^T * C(1) \tag{37}$$

$$P_{FG_3}^{ITC} = [P(FG_1 \cap FG_3) + P(FG_2 \cap FG_3) + P(FG_4 \cap FG_3)]\left(1/P_{FG_3}^{FT}\right) \tag{38}$$

which is same as calculated from the topology. In this configuration all the non bus section functional groups are connected only to the bus section and ITC is calculated similarly for each of them.

2.4.5 Double Breaker and Double Bus (DB-DB)

The configuration of DB-DB is shown in Fig. 11, and there are a total of six functional groups and eight breakers, much more than other types of substations. In this configuration a fault on a single line can trigger inadvertent tripping on any one of the remaining three lines since all are connected to the same bus through an electrical distance of one breaker. For illustration purposes it is assumed that the fault occurs on line 1 or FG-1. The functional group fault probabilities are calculated assuming the failure probability of the bus $p_{bf} \simeq 0$.

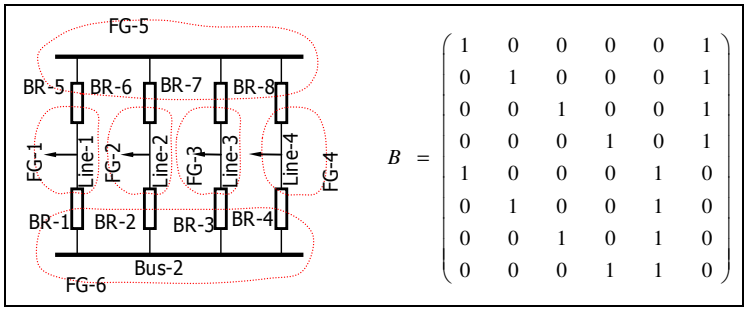

Fig. 11: Double breaker and double bus and it's B-matrix

So the probability of ITC contingency when FG-1 trips is

$$P_{ITC_5} = \Pr(FG-2\ trips\, or\, FG-3\ trips\ or\ FG-4\ trips \mid FG-1\ trips) \tag{39}$$

Since the inadvertent tripping of any of the functional groups is independent of each other and assuming they are disjoint the above expression becomes.

$$\begin{aligned} P_{ITC_5} &= \Pr(FG-2\ trips \mid FG-1 trips) + \Pr(FG-3\ trips \mid FG-1\ trips) \\ &\quad + \Pr(FG-4 trips \mid FG-1\ trips) \end{aligned} \tag{40}$$

$$= [P(FG_1 \cap FG_2) + P(FG_1 \cap FG_3) + P(FG_1 \cap FG_4)]\left(1/P_{FG_1}^{FT}\right) \tag{41}$$

This configuration is similar to SB-SB in that the faulted functional groups are connected only to functional groups containing a bus section. So to calculate its ITC probability the matrix B is modified as explained earlier. So in this case the B matrix for ITC probability of FG-1 becomes

$$B' = \begin{pmatrix} 0 & 0 & 0 & 0 & 0 & 0 \\ 1 & 1 & 0 & 0 & 0 & 0 \\ 1 & 0 & 1 & 0 & 0 & 0 \\ 1 & 0 & 0 & 1 & 0 & 0 \\ 0 & 0 & 0 & 0 & 0 & 0 \\ 1 & 1 & 0 & 0 & 0 & 0 \\ 1 & 0 & 1 & 0 & 0 & 0 \\ 1 & 0 & 0 & 1 & 0 & 0 \end{pmatrix} \tag{42}$$

$$B^{T'} = (0\ 1\ 1\ 1\ 0\ 1\ 1\ 1) \text{ row corresponding to FG-1} \tag{43}$$

$$P_{IFG}^{FT} = (1/P_{FG_1}^{FT}, 1/P_{FG_2}^{FT}, 1/P_{FG_3}^{FT}, 1/P_{FG_4}^{FT}, 1/P_{FG_5}^{FT}, 1/P_{FG_6}^{FT})^T \tag{44}$$

where $P_{FG_5}^{FT}$ and $P_{FG_6}^{FT}$ are zero. But all the terms of the form $P(FG_j \cap FG_i) * \left(1/P_{FG_i}^{FT}\right)$ are zero where i = 5, 6 and $j \neq i$.

$$P_{ITC} = [(B^T * D)^T * diag(P_{IFG}^{FT})]^T * C(1) \tag{45}$$

$$P_{FG_1}^{ITC} = 2 * [P(FG_1 \cap FG_2) + P(FG_1 \cap FG_3) + P(FG_1 \cap FG_4)]\left(1/P_{FG_1}^{FT}\right) \tag{46}$$

This is twice as calculated from the topology. This makes sense because both the functional groups connected to the faulted functional group are in turn connected to same set of functional groups. And with large number of breakers, relays and overlapping zones of protection, along with advantages comes disadvantages of higher likelihood of misoperation

or inadvertent tripping. So ITC probability after an initial contingency is higher than expected. Similarly the ITC probabilities for other non bus section functional groups are computed. Table 8 gives a summary of the topological analysis results for higher order stuck breaker and inadvertent tripping contingencies. In Table 8, the smallest ITC probability ($P_{ITC_2} = k$) is much smaller than the smallest stuck breaker contingency probability ($4 \times p_{sb} \times p_{lb}$).

Table 8 The probability of high-order contingency for different substations

Type	Prob (Fault plus stuck breaker)	Prob (Fault plus ITC)
SB-SB	$4 \times p_{sb} \times p_{lb}$	$3*k$
Ring	$8 \times p_{sb} \times p_{lb}$	$2*k$
SB-TL	$4 \times p_{sb} \times p_{lb}$	k
DB-DB	$8 \times p_{sb} \times p_{lb}$	$3*k$
B-HB	$8 \times p_{sb} \times p_{lb}$	k

2.5 Test System

The developed methodology is implemented in Visual C++ computer language. The program includes the algorithms to calculate the probabilities of functional group and stuck breaker contingencies developed in [14]. Results for the probabilities of these contingencies are the same as in [14].

The approach is tested on a test system given in Appendix D with 12 substations, 6 generators, 10 transformers, 119 bus section nodes and 39 line nodes. The test system data are given in Table 30 and Table 31 (APPENDIX E), and the result for the test system is summarized below in Table 9. The algorithm is also tested on IEEE-RTS 24 bus test system given in Appendix F. The results for the IEEE-RTS system are summarized in Table 10. In both the cases the full run of the program takes less than a second.

Table 9: Result of N-k contingency selection algorithm on Test System

Type	Functional Group	Stuck Breaker	Inadvertent Tripping
Number	71	126	125

Table 10: Result of N-k contingency selection algorithm on IEEE-RTS 24 Bus Test System

Type	Functional Group	Stuck Breaker	Inadvertent Tripping
Number	117	196	147

In both the above cases the results found by the program are the same as those found by inspection. For example, one observes in the 21 bus test system that a fault on line L107 could result in an ITC at bus section 12 removing line L108. The program found this ITC and computed its probability to be 10^{-7}.

Statistics of all the *N-k, k≥1* contingencies for both the systems are shown in Table 1 to Table 16. In each of the following tables the first line in this table shows the number of components lost in a contingency; the second line indicates the number of such contingencies identified. Table 11 and Table 14 show the statistics on contingencies caused by faults (order P) for the 21 bus system and the IEEE RTS96 systems respectively. Table 12 and Table 15 show the statistics on contingencies caused fault followed by breaker failure (order P^2) for the 21 bus system and the IEEE RTS96 systems respectively. Similarly Table 13 and Table 16 show the statistics on contingencies caused by an initial fault followed by an ITC (order P^2) for the 21 bus system and the IEEE RTS96 systems respectively. We only count lines, transformers, generators, and shunts. Loads, switches, breakers, and bus sections are not counted.

From Table 11-Table 16, we observe there are some *N-k (k>1)* events that have probabilities on the order of *N-1* events. Such events are extremely high-risk events. Similarly, there are some *N-k (k>2)* events that have probabilities on the order of *N-2* events. These events are high-risk events.

Table 11 Number of contingencies of type N-k resulting from a single fault (Order P) for 21 Bus System

k	1	2
No.	42	6

Table 12 Number of contingencies of type N-k resulting from a fault/breaker failure (order P^2) for 21 Bus System

k	1	2
No.	59	67

Table 13 Number of contingencies of type N-k resulting from ITC (Order P^2) for 21 Bus System

k	2	3
No.	86	39

Table 14 Number of contingencies of type N-k resulting from a single fault (Order P) for IEEE RTS96

k	1	2
No.	63	4

Table 15 Number of contingencies of type N-k resulting from a fault/breaker failure (order P^2) for IEEE RTS96

k	1	2	3	4
No.	82	88	1	3

Table 16 Number of contingencies of type N-k resulting from ITC (Order P^2) for IEEE RTS96

k	2	3	4
No.	137	5	5

Thus, the developed methodology is powerful yet simple to implement and has immense value in on line tracking of the system's exposure to vulnerability via changes in the system topology.

The topology of the power system is continuously changing and hence the approach can be used in an updating mode, taking into consideration of the changes in the status of the switch-breaker which would normally result in the formation of one or more new functional groups or merging into smaller number of functional groups. This makes the process very computationally efficient

2.6 Summary

This chapter documents systematic method for computing probability *order* of inadvertent tripping contingencies as a function of the switch-breaker data commonly available within the EMS. In many decision problems, knowledge of the "*probability order*" of the significant events is sufficient to distinguish between alternatives because probability order is a reasonable measure of event's probability. Rare event approximations (Appendix A) underpin the selection of high order contingencies for online security assessment. This makes sense because the probability of a compound event is dominated by the lowest order terms.

Five substation configurations, including single-bus connected with bus tie, ring bus, double breaker-double bus, single breaker-single bus, and breaker and a half are used in the illustrations of the probability calculation approach developed for *N-k* ($k \geq 2$ implied) contingencies, and the results are summarized in Table 8.

The methodology developed for probability calculation is simple and needs no extra information other that switch-breaker data which is available in most control centers. The approach can be used in an updating mode with the changes in the topology of the system, taking into consideration changes in the status of the switches and breakers which normally results in formation of one or more new functional groups or merging into smaller number of functional groups. Thus continuous tracking of system topology generates the higher order contingencies based on probability *order* for online security assessment.

CHAPTER 3 NUMERICAL METHODS – DIRECT METHODS

The long-term dynamic simulation of a power system is of interest in this research because it enables the evaluation and analysis of events which may lead to cascading outages. However, in order for such simulation to be of value in an operational context, it must be able to perform simulations very fast. This chapter is motivated by the desire to make algorithmic improvements to power system time domain simulation methods that will enhance computational efficiency.

Power system response to disturbances is decided not only by fast dynamics of its machines, but also by the action of slow processes, such as tap changers and the load dynamics. They often cause voltage problems and/or thermal loading problems after an extended period. Over the decades there has been intense intellectual labor and resulting technological advancement in speed of computers and numerical algorithms. The availability of these sophisticated numerical integration algorithms with variable time steps has made large simulation time steps possible. Commercial programs such as EUROSTAG, GE's EXSTAB, and Powertech's TSAT have successfully implemented the so called "A-stable" implicit method of performing numerical integration [23].

In general, there are two broad categories of numerical methods - the explicit and the implicit. In the explicit methods, the next step calculation uses only the solution information known; whereas the implicit methods use the unknown solution information of next-step(s). Iterative methods, such as Newton method are needed to solve the implicit non-linear equations. One attractive feature of implicit methods lies in the fact that they allow very large time steps. Reference [24] reports the usage of 20 seconds in EXSTAB and [23] reports the usage of 10 seconds time step in EUROSTAG without the loss of numerical stability.

Although some companies have implemented on-line transient instability analysis for detection of early-swing problems, we are aware of no company that has implemented long-term simulation capability for on-line purposes. Reasons for this are (a) perceived need and (b) technological capability. We have addressed the operational need for such simulation capability in Chapter 1, with underlying rationale being it will provide ability to prepare for multi-element (*N-k*) events that can result in severe impact. In this chapter, we address one

aspect of the technological capability issue, and that is algorithmic speed. Given the complexity of the interconnected power grid, it is difficult to gain significant scaling in computational speed without exploiting the structure and the nature of the differential equations governing the power system. In this research we employ advanced numerical algorithms which take advantage of the power system governing equations.

This chapter is organized as follows. Section 3.1 presents in summary form the differential-algebraic equations (DAE which will be derived in Chapter 4), and we discuss their nature and uniqueness. Section 3.2 discusses potential targets for enhancing computational efficiency. Section 3.3 focuses on the algorithmic targets of enhancing computational efficiency, including application of unsymmetric multifrontal methods to the linear system solution step of the implicit integration procedure. The frontal and multifrontal methods and the advantages of multifrontal methods are identified. Section 3.4 illustrates the method on a test system, and Section 3.5 provides a quantitative comparison of the multifrontal methods with the Gaussian elimination and other sparse solvers.

3.1 Formulation of Dynamic Algebraic Equations

Chapter 4 discusses in detail the individual power system component modeling and problem formulation for dynamic simulation studies. For the sake of completion, we preempt the derivations here, and present the resulting differential algebraic equations (DAE) developed in Chapter 4. The equations developed are for all the generations including the exciter, the governor, and the AGC models. The two axis model for the generator is used in the present study. For generators, the notation used is the same as in [25]. The limiter for each variable is implemented in program logic, and is not shown in the equations. The set of differential equations are as follows

$$\frac{\partial \delta}{\partial t} = \omega - 1 \tag{47}$$

$$\frac{\partial \omega}{\partial t} = \left[\left(Y \times P_r \right) - Ds\left(\omega - 1 \right) - \left(E_d^{'} I_d + E_q^{'} I_q - \left(X_q^{'} - X_d^{'} \right) I_q I_d \right) \right] \Big/ T_j \tag{48}$$

$$\frac{\partial E_d^{'}}{\partial t} = \left[-E_d^{'} - \left(X_q - X_q^{'} \right) I_q \right] \Big/ T_{q0}^{'} \tag{49}$$

$$\frac{\partial E_q^{'}}{\partial t} = \left[EDF - E_q^{'} + \left(X_d - X_d^{'} \right) I_d \right] \Big/ T_{d0}^{'} \tag{50}$$

$$\frac{\partial Y}{\partial t} = \left[Y - Y_0 \right] / T_{CH} \tag{51}$$

$$\frac{\partial Y_0}{\partial t} = -R \times K_G \times Y_0 + K_G \left[\left(\omega_r - \omega \right) + R \left(L_{ref\,0}^{g} - \delta_c / T_g \right) \right] \Big/ T_{CH} \tag{52}$$

$$\frac{\partial \Delta E_f}{\partial t} = \left[-\Delta E_f + E_q^{'} + K_a \left(V_{ref} - V_t \right) I_d \right] \Big/ T_e \tag{53}$$

The set of algebraic equations are as follows, where i is the index of the generator, and j is the index of the generator bus.

$$\begin{pmatrix} V_q^i \\ V_d^i \end{pmatrix} - \begin{pmatrix} E_q^{'i} \\ E_d^{'i} \end{pmatrix} + \begin{pmatrix} r^i & -X_d^i \\ X_d^i & r^i \end{pmatrix} \begin{pmatrix} I_q^i \\ I_d^i \end{pmatrix} = 0 \tag{54}$$

for each generator;

$$\begin{pmatrix} V_x^j \\ V_y^j \end{pmatrix} - \begin{pmatrix} \cos\delta^j, & -\sin\delta^j \\ \sin\delta^j, & \cos\delta^j \end{pmatrix} \begin{pmatrix} V_q^j \\ V_d^j \end{pmatrix} = 0 \tag{55}$$

for each generator bus;

$$\begin{pmatrix} I_x^j \\ I_y^j \end{pmatrix} - \begin{pmatrix} \cos\delta^j, & -\sin\delta^j \\ \sin\delta^j, & \cos\delta^j \end{pmatrix} \begin{pmatrix} I_q^j \\ I_d^j \end{pmatrix} = 0 \tag{56}$$

for each generator bus;

$$Y_{bus} \times \begin{pmatrix} V_x^1 \\ V_y^1 \\ \vdots \\ V_x^n \\ V_y^n \end{pmatrix} - \begin{pmatrix} I_x^1 \\ I_y^1 \\ \vdots \\ I_x^n \\ I_y^n \end{pmatrix} = 0 \tag{57}$$

for the whole linear impedance network with n voltage bus (Y_{bus} is the system admittance matrix);

$$\begin{pmatrix} P^i \\ Q^i \end{pmatrix} - \begin{pmatrix} V_x^i & V_y^i \\ V_y^i & -V_x^i \end{pmatrix} \begin{pmatrix} I_x^i \\ I_y^i \end{pmatrix} = 0 \tag{58}$$

for each load bus with constant P and Q. The loads in our test system are modeled as constant active and reactive power injection.

Equations (54) to (56) are for each individual generator. Equations (57) and (58) are for the whole network and each voltage bus respectively. The differential algebraic equation (DAE) developed in (47) through (58) can be summarized as

$$\frac{dx}{dt} = f(x, y) \tag{59}$$

$$0 = g(x, y) \tag{60}$$

where

x is a vector of state variables in (47)~(53)

(59) is the group of equations in (47)~(53)

y is a vector of the additional variables in (54)~(58)

(60) is the group of equations in (54)~(58).

The DAE have been called singular, implicit, differential-algebraic, descriptor, generalized state space, noncanonic, noncausal, degenerate, semistate, constrained, reduced order model, and nonstandard systems depending on the area of application it emerged from.

At this point, we would like to discuss the reasons to consider the equations (83)-(84) in this form, rather than trying to convert it as an ODE to solve. Just like in the present formulation, the formulation of many physical systems takes the form of a DAE depicting a collection of relationships between variables of interest and some of their derivatives. These variables usually have a physical significance. Attempting to covert the DAE to an ODE may result in the loss of their direct meanings and physical significance. Also in many cases it may be time consuming or impossible to obtain an explicit ODE model.

Often parameters are associated with applications like power systems. Changing parameter values can alter the relationships between variables, and may require different explicit models with solution manifolds of different dimensions. If we can solve the DAE

directly, then it becomes easier to study the effect of modeling changes and parametric variations. It also facilitates the interfacing of modeling software with the design software. The change to explicit form can destroy sparsity and prevent the exploitation of system structure, which is one of the major area we take advantage of in this research. All the above advantages and numerical reasons have led to significant research in the development of algorithms for solving DAE. None of the currently available numeric techniques support working with all DAE. Some additional conditions, either on the structure of the DAE and /or the numerical method, need to be satisfied for each case.

In the literature [26], there has been a significant effort to develop A-stable, accurate, and fast numerical integration methods with variable time steps. Although the different numerical integration schemes differ in their convergence, order, stability, and other properties, they do not necessarily offer considerable improvement in computational efficiency. In the next section, we discuss the solution strategy for the integration of DAE which are well suited for power systems.

3.2 Solution Strategy

One of the aims of this research is to obtain high speed to simulate extended time domain simulation for the purpose of online monitoring, tracking, and devising correcting action strategies for mitigating the frequency and impact of high consequence events. Most of the current methods for solving the power system dynamic simulation problems are developed for use on conventional sequential machines. This leads to the natural conclusion that there are two viable options to reduce the wall-clock time to solve a computationally intensive problem like power system time domain simulation. These are i) advanced hardware technology in terms of speed, memory, I/O, architecture and so on, and ii) more efficient algorithm. Although the emphasis is generally on the hardware, nevertheless efficient algorithms can offer great advantage in achieving the desired speed. There exists a symbiotic relationship between the two. We focus on the efficient algorithms to achieve high computational gain.

We can safely divide our simulator software into three parts, namely 1) a user interface 2) DAE solver kernel and 3) the output assembler. The maximum time amounting to almost

90%-95% of the total time is spent on the DAE solver. Any DAE solver requires three categories of numerical analysis techniques:

- Numerical Integration schemes
- Solution of non linear equations
- Solution of linear equations

In the following subsections we discuss the implementation of these numerical techniques.

3.3 Integration Scheme for DAE

As seen in the previous section, the power system is modeled, in summary by a set of thousands of differential and algebraic equations. These have inherent nonlinearities in them and the resulting DAE is highly stiff in nature. Switching events, contingencies, forced outages introduce significant discontinuities in the system variables. The numerical scheme must converge quickly, give desired accuracy, be reliable and stable. The implicit integration scheme called Theta method [27] satisfies all the above requirements and is used in our simulator. It does not have the infamous *Hyper Stability* problem [23], which means that an algorithm will falsely report stability when the physical system is actually unstable. Theta Method is an example of a general approach to designing algorithms in which geometric intuition is replaced by Taylor series expansion. Invariably the implicit function theorem is also used in the design and analysis of the scheme. This method is also known as the weighted method.

Consider $$\frac{dx}{dt} = f(t, y) \tag{61}$$

The theta method can be expressed in the general form as

$$y_{n+1} = y_n + h[\theta f(t_{n+1}, y_{n+1}) + (1-\theta) f(t_n, y_n)] \quad n = 0,1,... \tag{62}$$

where h_n is the time step of integration at time n, n=0,1,2..

$\theta = 0$; Explicit Euler

$\theta = 1$; Implicit Euler

$\theta = ½$; Trapezoidal

The $\theta = 1$ case is very practical. At $\theta = 1$, it is called the ``Backward Euler'' or ``Implicit Euler'' scheme. It is a simple yet robust method for solving stiff ODEs. The difference between the exact solution and the above approximation at $t = t_n$ is

$$\left(\theta - \frac{1}{2}\right) h^2 y^n(t_n) + \left(\frac{1}{2}\theta - \frac{1}{3}\right) h^3 y'''(t_n) + \theta\left(h^4\right) \tag{63}$$

Hence, the method is order 2 for $\theta = ½$ which corresponds to Trapezoidal integration method, and otherwise it is of order 1. The concept of order is based on assumption that error is concentrated on the leading order of the Taylor series expansion (on real computers, h is small, but finite). For example at $\theta = ⅔$, $O\left(h^3\right)$ are removed while retaining $O\left(h^2\right)$. Hence, for different types of $f(t, y)$ one can tune θ to control whether $O\left(h^3\right)$ and higher order terms, or $O\left(h^2\right)$ and higher order terms contribute to the overall error when h is finite. It may be possible to choose θ that generates a more optimal or smaller error.

One can show easily that for $h > 0$ and sufficiently small,

$$\begin{aligned} e_{n+1} &= e_n + \theta h\left[f\left(t_n, y(t_n) + e_n\right) - f\left(t_n, y(t_n)\right)\right] \\ &\quad + (1\text{-}\theta) h\left[f\left(t_{n+1}, y(t_{n+1}) + e_{n+1}\right) - f\left(t_{n+1}, y(t_{n+1})\right)\right] \\ &= \begin{cases} -\frac{1}{12} h^3 y'''(t_n) + O(h^4) & \theta = \frac{1}{2} \\ +(\theta - \frac{1}{2}) h^2 y''(t_n) + O(h^3) & \theta \neq \frac{1}{2} \end{cases} \end{aligned} \tag{64}$$

Similarly, using the implicit function theorem

$$e_{n+1} = \begin{cases} -\frac{1}{12} h^3 y'''(t_n) + O(h^4) & \theta = \frac{1}{2} \\ +(\theta - \frac{1}{2}) h^2 y''(t_n) + O(h^3) & \theta \neq \frac{1}{2} \end{cases} \tag{65}$$

where e_n = error at n^{th} iteration

Both the Euler and Trapezoidal integration scheme fit the equation of the above form. The choice of the Theta method is preferred over the Trapezoidal rule as it avoids the numerical oscillations following the occurrence of switching events, where such oscillations can occur when using the Trapezoidal rule [28].

Discretizing (59) and (60) using Theta-method, we find

$$\left[x_{n+1} - x_n - h\theta \dot{x}_n\right] - (1-\theta) h f\left(x_{n+1}, y_{n+1}\right) = 0 \tag{66}$$

$$g\left(x_{n+1}, y_{n+1}\right) = 0 \tag{67}$$

Note that in (66) and (67), only x_{n+1} and y_{n+1} are unknown variables and the rest are all known. Equations (66) and (67) constitute one set of nonlinear algebraic equations of the form

$$F\left(x_{n+1}, y_{n+1}\right) = 0 \tag{68}$$

The DAE equations now are transformed into a set of purely algebraic equations, which can be solved efficiently by the established Newton-Raphson method. We choose θ = 0.47 for the work reported, as suggested in [23].

3.3.1 Nonlinear Equation Solution

The set of nonlinear equations in (68), are solved at each time step using the Newton-Raphson method where, at the i^{th} iteration, the unknowns are updated as follows:

$$x_{n+1}^{(i)} = x_{n+1}^{i-1} - \gamma\Delta x \tag{69}$$

$$y_{n+1}^{(i)} = x_{n+1}^{i-1} - \gamma\Delta y \tag{70}$$

where Δx and Δy are obtained by solving the set of linear equations:

$$J\begin{bmatrix}\Delta x \\ \Delta y\end{bmatrix} = \begin{bmatrix}R_x \\ R_y\end{bmatrix} \tag{71}$$

which can be represented by

$$Ax = b \tag{72}$$

where:

A=J=Jacobian matrix

R_x=differential equation residual

R_y=algebraic equation residual

$x_{n+1}^{(i)}$, $y_{n+1}^{(i)}$ = state variables and additional variables at the i^{th} iteration

γ=deceleration factor

$$b = \begin{bmatrix}R_x \\ R_y\end{bmatrix}$$

The Newton iterations are stopped when the residual vectors are "smaller" than pre-specified tolerances based on norm and rate of convergence. The computation of the correction vector $[\Delta x, \Delta y]^T$ requires the solution of the set of linear equations given by (96) which is discussed in the next section.

3.3.2 Linear equation Solver

As seen in the previous section the core of any iterative solver like Newton-Raphson is the solution of a system of equations represented by (72). In case of the power system, the Jacobian matrix *A* is highly sparse and the fill-in is very low. This is taken advantage of in the current research to gain high computational efficiency by employing a multifrontal based sparse linear solver. Multifrontal methods have been used earlier in the power system studies in the solution of sparse linear systems arising in the power flow studies. However the matrices in power flow studies have symmetric zero pattern and non zero diagonal elements. On serial platforms the multifrontal methods were used for power flow in references [29] and [30]. Reference [29] implements an older version of multifrontal methods and since then there has been lot of research in the area of multifrontal methods and we have much more advanced algorithms for ordering to reduce fill-in, many new features, higher speed and performance [31, 32, 33, 34, 35]. In reference [30], the main focus of the paper is to promote the FPGA technology for hardware implementation of sparse linear solver as compared to the software solution for multifrontal solver UMFPACK [31]. However from the open literature we have no information of any precedence of the application of multifrontal methods in time domain simulation of power system where the Jacobian is highly unsymmetric and unsymmetric zero pattern.

Steady state and dynamic simulation tools are an integral part in the design, optimization, and operation of large interconnected power system. Advances in numerical methods, sophisticated algorithms for exploiting sparsity and high performance computational resources have made real time tracking of cascading events a conceivable and achievable goal for the power industry.

In the solution of the DAE arising out of the dynamic modeling of the power system, the most vital and computationally intensive steps are the Jacobian building and the solution of the sparse system of linear equations. However the purpose of Jacobian is to provide

adequate convergence and as long as it is achieved, one can use the same partial derivatives [23]. Thus the key computational step amounting to 80%-90% of the machine cycle is the solution of the sparse linear system of equations.

In the solution of the linear equations, the Jacobian matrices do not have any of the desirable structural or numerical properties such as symmetry, positive definiteness, diagonal dominance, and bandedness, which are generally associated with sparse matrices, to exploit in developing efficient algorithms for linear direct solvers. In general, the algorithms for sparse matrices are more complicated than for dense matrices. The complexity is mainly attributed to the need to efficiently handle the fill-in in the factor matrices. A typical sparse solver consists of four distinct steps as opposed to two in the dense case:

1. The ordering step minimizes the fill-in, and exploits special structures, such as block triangular form.
2. An analysis step or symbolic factorization determines the nonzero structures of the factors, and creates suitable data structures for the factors.
3. Numerical factorization computes the factor matrices.
4. The solve step performs forward and/or backward substitutions.

This research offers a new dimension into the solution technique of sparse linear systems arising in the power system dynamic simulation through the implementation of multifrontal methods. Multifrontal methods are a generalization of the frontal methods developed primarily for finite element problems [36] for symmetric positive definite system which were extended to unsymmetric systems [37]. These methods were then applied to general class of problems in reference [38]. In the next section, we discuss the fundamentals of the frontal and the multifrontal methods.

3.3.3 Frontal method

Frontal methods were originally developed for solving banded matrices from finite element problems [36]. The motivation was to limit computation on small matrices to solve problems on machines with small core memories. Presently frontal codes are widely used in finite element problem because very efficient dense matrix kernels, particularly Level 3 Basic Linear Algebra Subprograms (BLAS) [39], can be designed over a wide range of

platforms. A frontal matrix is a small dense submatrix that holds one or more pivot rows and their corresponding pivot columns.

The frontal elimination scheme can be summarized as follows:

1. Assemble a row into the frontal matrix.
2. Determine if any columns are fully summed in the frontal matrix. A column is fully summed if it has all of its nonzero elements in the frontal matrix.
3. If there are fully summed columns, then perform partial pivoting in those columns, eliminating the pivot rows and columns and doing an outer-product update on the remaining part of the frontal matrix.
4. Repeat until all the columns have been eliminated and matrix factorization is complete.

The basic idea in frontal methods is to restrict elimination operations to a frontal matrix, on which dense matrix operations are performed using Level 3 BLAS. In frontal scheme, the factorization proceeds as a sequence of partial factorization on frontal matrices, which can be represented as:

$$F = \begin{bmatrix} F_{11} & F_{12} \\ F_{21} & F_{22} \end{bmatrix} \tag{73}$$

Pivots can be chosen from the matrix F_{11} since there are no other entries in these rows and columns in the overall matrix. Subsequently, F_{11} is factorized, multipliers are stored over F_{12}, and the Schur complement $F_{22} - F_{12}^T F_{11}^{-1} F_{12}$ is formed, using full matrix kernels. At the next stage, further entries from the original matrix are assembled with this Schur complement to form another frontal matrix. For example, consider the 6 by 6 matrix shown in Fig. 12(a). The non-zero entries in the matrix are represented by dots. The frontal method to factorize the matrix proceeds as follows:

In this example, the process begins by assembling row 1 into an empty frontal matrix shown in Fig. 12(b). At this point, none of the variables are fully summed. Subsequently, we assemble row 2 to get the matrix in Fig. 12(c). Now variable 4 is fully summed, and hence, column 4 can be eliminated. To eliminate a column, a pivot needs to be selected in that column. Let it be selected from row 2.

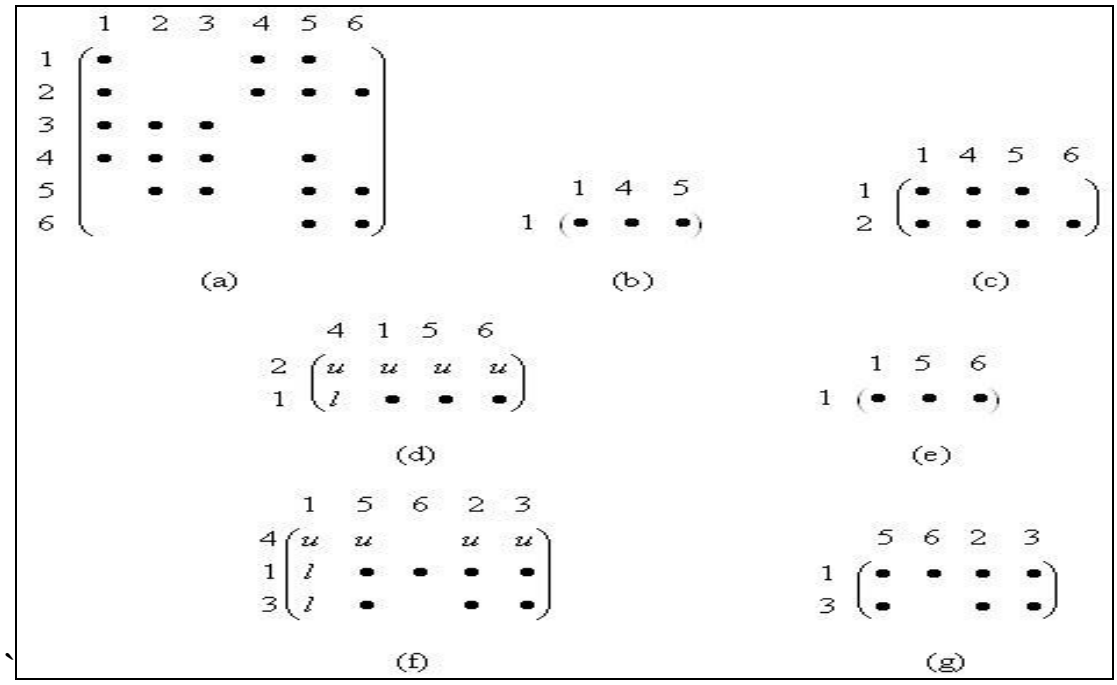

Fig. 12: Example for frontal method

Rearranging the matrix to bring the pivot element (2, 4) to the top left position, we get the matrix in Fig. 12(d). Here, *u* indicates an element of the upper triangular matrix, and *l* denotes an element of the lower triangular matrix. After elimination, the updated frontal matrix would be as shown in Fig. 12(e). In this way, we proceed with assembling rows. Again, when rows 3 and 4 are assembled, variable 1 is fully summed, and hence the column 1 can be eliminated. Choosing the pivot element to be (4, 1), the matrix with pivot element moved to top left corner is shown in Fig. 12(f), and the updated frontal matrix after elimination is shown in Fig. 12(g). In this way, the frontal method continues until matrix factorization is complete.

In the frontal method, the pivot order of the columns is dependent on the row ordering, and the pivot order of the rows can vary only within certain constraints. A row can become pivotal any time between the time it is entered into the frontal matrix and the end of the factorization. Rows are entered into the frontal matrix in a predefined order. The pivot column ordering depends solely on the initial preordering of the rows. Frontal matrix sizes,

and thus the computational performance, depend on row ordering. Thus, there arises a need for a good row ordering to keep the size of the matrix small. There is a vast literature addressing this issue [40].

Frontal methods [41, 42, 43, 44, 45, 46] have demonstrated great potential as a sparse linear equation solver. Although with frontal methods one can achieve large computational gain [47, 48, 49, 50], there are many unnecessary operations on the frontal matrices which are often large and sparse and thus it lowers the overall performance. If we view the factorization in terms of a computational tree where nodes correspond to factorizations of the form as in (97), and edges correspond to the transfer of the Schur complement data, then the computational tree of the method just described would be a chain. Data must be received from the child to complete computation at the parent node. Thus frontal methods offer little scope for parallelism other than that which can be obtained within the higher level BLAS.

These deficiencies can be at least partially overcome through allowing the use of more than one front called multifrontal method [51, 52, 53, 54]. This permits pivot orderings that are better at preserving sparsity and also gives more possibility for exploitation of parallelism through working simultaneously on different fronts

Thus, in our research we have proposed multifrontal methods as a viable solution methodology for large unsymmetric sparse matrices which are common in power system online dynamic simulation. The fundamentals of the multifrontal methods are discussed in the next section.

3.3.4 Multifrontal method

The multifrontal method, is a generalization of the frontal method, and was originally developed for symmetric systems [51]. Subsequently, unsymmetric multifrontal algorithm UMFPACK [31, 32, 33, 34, 35] was developed for general sparse unsymmetric matrices. The advent of multifrontal solvers has greatly increased the efficiency of direct solvers for sparse systems. They make full use of the high performance computer architecture by invoking the level 3 Basic Linear Algebra Subprograms (BLAS) library. Thus memory requirement is greatly reduced and the computing speed is greatly enhanced.

In this section, we give an overview of the multifrontal method for the solution of large sparse matrices. There is a vast literature on the subject. Beginning with its development in

1983 by Duff and Reid [51], it has undergone many developments at different stages of its formulation, and different algorithms perform best for different classes of matrices. Broadly speaking, one can categorize them into following classes: (1) symmetric positive definite matrices [55, 56, 57, 58]; (2) symmetric indefinite matrices [51, 59, 60]; (3) unsymmetric matrices with actual or implied symmetric nonzero pattern [53, 61 , 62 , 63 , 64]; (4) unsymmetric matrices where the unsymmetric nonzero pattern is partially preserved [65]; (5) unsymmetric matrices where the unsymmetric nonzero pattern is fully preserved [31, 66, 67, 68, 69]; and (6) QR factorization of rectangular matrices [70, 71]. There are significant differences amongst the various approaches. In this report, we present the fundamentals of the multifrontal method for symmetric positive definite linear systems, which is easier to understand and forms the foundation for multifrontal approach to other classes of matrices.

The method reorganizes the overall factorization of a sparse matrix into a sequence of subtasks, each of which involves partial factorizations of smaller dense matrices.
Reference [58] forms the foundation for the concepts presented below on the theory of multifrontal methods.

Cholesky factorization of an n by n symmetric positive definite matrix is defined by

$$A = LL^T \tag{74}$$

Depending on the order in which the matrix entries are accessed and/or updated for factorization, the Cholesky factorization can be classified into row, column, or submatrix Cholesky schemes. In row Cholesky, each step computes a factor-row by solving a triangular system, whereas in column Cholesky, the factor matrix is computed column by column with updates from previous column followed by scaling. In submatrix-Cholesky scheme, as each factor column is formed, all its updates to the submatrix remaining to be factored are computed. Based on the above classification, multifrontal method performs Cholesky factorization by submatrices. However, the novel feature of the multifrontal method is that the update contributions from a factor column to the remaining submatrix are computed, but not applied directly to the matrix entries. They are aggregated with contributions from other factor columns before the actual updates are performed.

We will explain the main concepts of the multifrontal method through an example. Consider a sparse symmetric positive definite n by n matrix A and its Cholesky factor as

shown Fig. 13. Each "•" represents an original nonzero in the matrix A, and "o" a fill in for the factor matrix L.

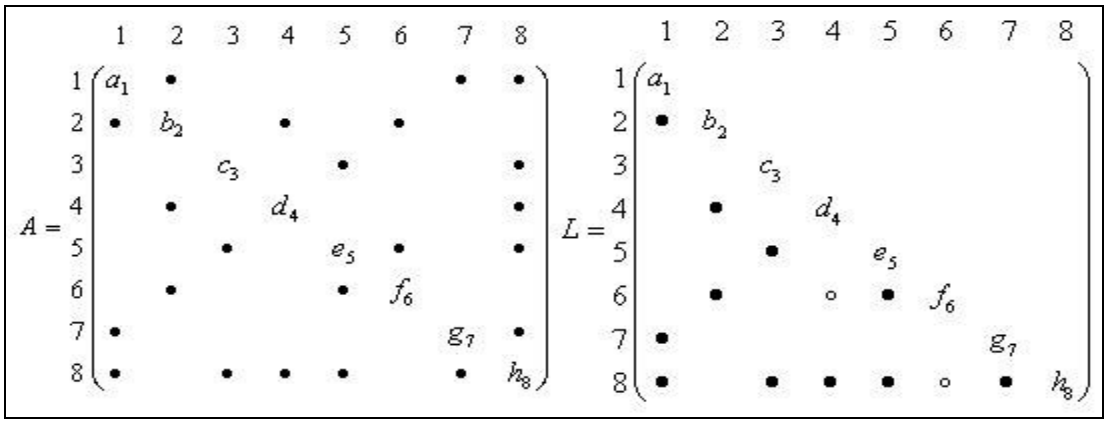

Fig. 13: Example symmetric positive definite matrix and it's Cholesky factor matrix

The elimination tree of the matrix A represented by $T(A)$ is defined to be the structure with n nodes $\{1,...,n\}$ such that node p is the parent of j if and only if

$$p = \min\{i > j \mid l_{ij} \neq 0\} \tag{75}$$

The elimination tree is a tree if A is irreducible, otherwise it will be a forest. For our purposes, we assume it to be tree. There are as many nodes in the tree as there are columns in the matrix or the Cholesky factor. In this example, we have eight nodes. From Fig. 13, we can see that for the fourth node d_4, the parent node is f_6 and for f_6 the parent node is h_8. Similarly for each node we can derive the parent node. Thus, traversing the path for all the nodes, we get the elimination tree shown in Fig. 14 for the example in Fig. 13.

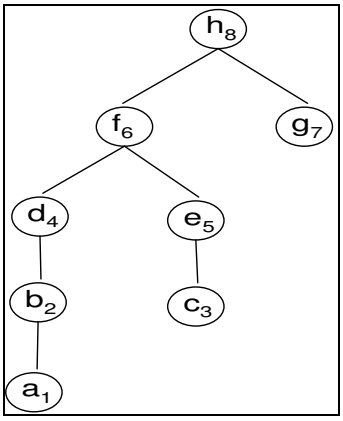

Fig. 14: Elimination tree for matrix A

The most fundamental elements in understanding the multifrontal method are the concepts of frontal matrix, subtree update matrix, and the update matrix. To explain these concepts, we will first introduce the concept of descendents of a node in the elimination tree.

The descendants of the node *j* in the elimination tree *T(A)* contains *j* and the set of nodes in the subtree rooted at the node *j*. The symbol *T*[*j*] is used to represent the set of descendents.

Theorem 1: If node *k* is a descendant of *j* in the elimination tree, then the structure of the vector $(l_{jk} \cdots, l_{jk})^T$ is contained in the structure of $(l_{jj} \cdots, l_{jk})^T$

Theorem 2: If $l_{jk} \neq 0$ 0 and $k < j$, then the node *k* is a descendant of *j* in the elimination tree.

For the above example the descendent of 1 is *T*[1] = {1}, descendents of 2 are *T*[2]={1,2}, descendent of 3 is *T*[3] = {3}, descendents of 4 are *T*[4] = {1,2,4} and of 6 are *T*[6] = {1,2,3,4,5,6}.

Subtree Update Matrix and Frontal Matrix: Let $(i_0, i_1, i_2 \cdots i_r)$ be nonzero row subscripts in the j[th] column of the Cholesky factor, and $i_0 = j$. Then, the subtree update matrix $\bar{U}_j$ at column *j* for the sparse matrix *A* is defined to be

$$\bar{U}_j = -\sum_{k \in T[j]-\{j\}} \begin{pmatrix} l_{j,k} \\ l_{i_1,k} \\ \vdots \\ l_{i_r,k} \end{pmatrix} \begin{pmatrix} l_{j,k} & l_{i_1,k} & \cdots & l_{i_r,k} \end{pmatrix} \tag{75}$$

and the Frontal Matrix F_j is defined to be

$$F_j = \begin{pmatrix} a_{j,j} & a_{j,i_1} & \cdots & a_{j,i_r} \\ a_{i_1,j} & & & \\ \vdots & & 0 & \\ a_{i_r,j} & & & \end{pmatrix} + \bar{U}_j \tag{76}$$

Both F_j and $\bar{U}_j$ have order *r*+1 which is equal to the number of nonzeros in the j^{th} column of the Cholesky factor which includes the diagonal element. From the definition of F_j it is clear that when F_j is computed, the first row/column of F_j has been completely

updated. Therefore, one step of elimination on F_j gives the nonzero entries of the factor column L_{*j}. So F_j can be factorized as

$$F_j = \begin{pmatrix} l_{j,j} & 0 \\ l_{i_1,j} & \\ \vdots & I \\ l_{i_r,j} & \end{pmatrix} \begin{pmatrix} 1 & 0 \\ & \\ 0 & U_j \end{pmatrix} \begin{pmatrix} l_{j,j} & l_{i_1,j} & \cdots & l_{i_r,j} \\ & & & \\ 0 & & I & \end{pmatrix} \tag{77}$$

This gives the Update matrix U_j after one step elimination on F_j. The Update Matrix is a full matrix and is derived from equation to be

$$U_j = -\sum_{k \in T[j]} \begin{pmatrix} l_{i_1,k} \\ \vdots \\ l_{i_r,k} \end{pmatrix} \begin{pmatrix} l_{i_1,k} & \cdots & l_{i_r,k} \end{pmatrix} \tag{78}$$

It is clear from the definition of $\bar{U}_j$ and U_j, that $\bar{U}_j$ is used to form the j^{th} frontal matrix F; whereas U_j is generated from an elimination step with F_j. $\bar{U}_j$ has one more row/column than U_j.

We saw above that the descendent of 1 is $T[1] = \{1\}$, descendents of 2 are $T[2] = \{1,2\}$, descendent of 3 is $T[3] = \{3\}$, descendents of 4 are $T[4] = \{1,2,4\}$ and of 6 are $T[6] = \{1,2,3,4,5,6\}$. So, from the definition of subtree update matrix, we have $\bar{U}_1 = 0$ and therefore F_1 is

$$F_1 = \begin{pmatrix} a_{1,1} & a_{1,2} & a_{1,7} & a_{1,8} \\ a_{2,1} & 0 & 0 & 0 \\ a_{7,1} & 0 & 0 & 0 \\ a_{8,1} & 0 & 0 & 0 \end{pmatrix} + \bar{U}_1 = \begin{pmatrix} a_{1,1} & a_{1,2} & a_{1,7} & a_{1,8} \\ a_{2,1} & 0 & 0 & 0 \\ a_{7,1} & 0 & 0 & 0 \\ a_{8,1} & 0 & 0 & 0 \end{pmatrix} \tag{79}$$

$$\text{Therefore } U_1 = -\begin{pmatrix} l_{2,1}^2 & l_{2,1}l_{7,1} & l_{2,1}l_{8,1} \\ l_{7,1}l_{2,1} & l_{7,1}^2 & l_{7,1}l_{8,1} \\ l_{8,1}l_{2,1} & l_{8,1}l_{7,1} & l_{8,1}^2 \end{pmatrix} \tag{80}$$

Similarly, we can then calculate $\bar{U}_2$, and hence F_2 and the update matrix. The process continues till the entire matrix is factorized. The advantage with multifrontal method is that it is not sequential; rather it has a parallel hierarchy as visible from the elimination tree of the

given example. Formation of the subtree update matrix begins on multiple fronts namely $\bar{U}_1$, $\bar{U}_3$ and $\bar{U}_7$. We can verify that for the above example the subtree update matrices $\bar{U}_1$ to $\bar{U}_4$ are as given below.

$$\begin{aligned}
\bar{U}_1 &= 0 \\
\bar{U}_2 &= -\begin{pmatrix} l_{2,1} \\ 0 \\ 0 \end{pmatrix} \begin{pmatrix} l_{2,1} & 0 & 0 \end{pmatrix} \\
\bar{U}_3 &= 0 \\
\bar{U}_4 &= -\begin{pmatrix} 0 \\ 0 \\ l_{8,1} \end{pmatrix} \begin{pmatrix} 0 & 0 & l_{8,1} \end{pmatrix} - \begin{pmatrix} l_{4,2} \\ l_{6,2} \\ 0 \end{pmatrix} \begin{pmatrix} l_{4,2} & l_{6,2} & 0 \end{pmatrix}
\end{aligned} \tag{81}$$

Matrix extend add operator: Let R be an r by r matrix with $r \le n$ and S be an s by s matrix with $s \le n$. Each row/column of R and S corresponds to a row/column of the given n by n matrix A. Let $i_1 \le i_2 \le \cdots i_r$ be the subscripts of R in A, and $j_1 \le j_2 \le \cdots j_s$ be those of S. Consider the union of the two subscript sets. Let $k_1, k_2, \cdots k_t$ be the resulting union. The matrix R can be extended to conform to the subscript set $(k_1, k_2, \cdots k_t)$, by introducing a number of zero rows and columns. In a similar way, the matrix S can be extended. Here, $R \overset{+}{} S$ is defined to be the t by t matrix T formed by adding the two extended matrices of R and S. The matrix operator "$\overset{+}{}$" is known as the matrix extend-add operator. For example, let

$$R = \begin{pmatrix} p & q \\ u & v \end{pmatrix}, \quad S = \begin{pmatrix} w & x \\ y & z \end{pmatrix} \text{ then} \tag{82}$$

$$R \overset{+}{} S = \begin{pmatrix} p & q & 0 \\ u & v & 0 \\ 0 & 0 & 0 \end{pmatrix} + \begin{pmatrix} w & 0 & x \\ 0 & 0 & 0 \\ y & 0 & z \end{pmatrix} = \begin{pmatrix} p+w & q & x \\ u & v & 0 \\ y & 0 & z \end{pmatrix} \tag{83}$$

Now, in terms of the extend-add operator defined above, we can see that the relationship between the frontal matrices $\{ F_j \}$ and the update matrices $\{ U_j \}$ is

$$F_j = \begin{pmatrix} a_{j,j} & a_{j,i_1} & \cdots & a_{j,i_r} \\ a_{i_1,j} & & & \\ \vdots & & 0 & \\ a_{i_r,j} & & & \end{pmatrix} \dotplus U_{c_1} \dotplus \ldots \dotplus U_{c_s} \tag{84}$$

where $c_1, c_2, \cdots c_s$ are the children of the node j in the elimination tree. Thus $\bar{U}_j = U_{c_1} \dotplus \ldots \dotplus U_{c_s}$, and $T[j]$-$\{j\}$ is the disjoint union of the nodes in the subtree $T[c_1]$,..., $T[c_s]$. Duff and Reid [51] refer to the process of forming the j^{th} frontal matrix F_j from A_{*j} and the update matrices of its tree children as the frontal *matrix assembly* operation, and the tree structure on which the assembly operations are based is called the assembly tree.

We now summarize the essence of the multifrontal methods in the form of an algorithm for multifrontal Cholesky factorization in Fig. 15.

$j = 1$
while $(j \le n)$

i. Let $(i_0, i_1, i_2 \cdots i_r)$ be nonzero row subscripts in the j^{th} column of the Cholesky factor.

ii. Form the update matrix $\bar{U} = U_{c_1} \dotplus \ldots \dotplus U_{c_s}$

iii. $$F_j = \begin{pmatrix} a_{j,j} & a_{j,i_1} & \cdots & a_{j,i_r} \\ a_{i_1,j} & & & \\ \vdots & & 0 & \\ a_{i_r,j} & & & \end{pmatrix} \dotplus \bar{U}$$

iv. Factor F_j into

v. $$F_j = \begin{pmatrix} l_{j,j} & 0 \\ l_{i_1,j} & \\ \vdots & I \\ l_{i_r,j} & \end{pmatrix} \begin{pmatrix} 1 & 0 \\ & \\ 0 & U_j \end{pmatrix} \begin{pmatrix} l_{j,j} & l_{i_1,j} & \cdots & l_{i_r,j} \\ & & & \\ 0 & & I & \end{pmatrix}$$

end

Fig. 15: Algorithm for multifrontal Cholesky factorization

In summary, the multifrontal method reorganizes the numerical computation, and the factorization is performed as a sequence of factorization on multiple fronts. In practice,

structural pre-processing [58] is done to reduce the working storage requirements by restructuring the tree, and finding the optimal post-ordering of the tree. After the pre-processing, the computation of the Cholesky factor matrix by the multifrontal method is done as described in the above algorithm in Fig. 15.

As discussed earlier, there exist many approaches to apply the multifrontal method for different classes of matrices. Broadly, they can be classified into: (1) symmetric positive definite matrices; (2) symmetric indefinite matrices; (3) unsymmetric matrices with actual or implied symmetric nonzero pattern; (4) unsymmetric matrices where the unsymmetric nonzero pattern is partially preserved; (5) unsymmetric matrices where the unsymmetric nonzero pattern is fully preserved; and (6) QR factorization of rectangular matrices.

Below, we give the summary of the discussion on the differences in the multifrontal methods for the above classes of matrices presented in reference [33]. For approaches (1) to (4), the frontal matrices are related to one another by the elimination tree of A, or the elimination tree of $A+A^T$ if A is unsymmetric. The elimination tree has n nodes, each node corresponding to one pivot row and column. A frontal matrix assembles the contribution blocks of each of its children in the assembly tree. The assembly step thus adds the contribution blocks of each child into the current frontal matrix. For symmetric positive definite matrices, all of the pivots originally assigned to a frontal matrix by the symbolic analysis phase are numerically factorized within that frontal matrix. For other matrices, some pivots might not be eliminated, and the contribution block may be larger than predicted. The un-eliminated pivot is delayed, and its elimination is attempted in the parent instead.

In the first three approaches, the frontal matrices are square. The frontal matrix may be rectangular, but the assembly tree is still used. The first four approaches precede the numerical factorization with a symmetric reordering of A or $A+A^T$, typically with a minimum degree or nested-dissection ordering as part of a symbolic analysis phase.

UMFPACK is based on the fifth approach. It does not use a pre-ordering or symbolic analysis phase. Rectangular frontal matrices are constructed during numerical factorization, using an approximate Markowitz ordering.. The frontal matrices are related to one another via a directed acyclic graph (DAG) rather than an elimination tree. The last approach, multifrontal QR factorization [70, 71], is based on the column elimination tree of A.

Now we illustrate with a simple example in Fig. 16, the working of the multifrontal method for the same unsymmetrical matrix in Fig. 12 for which the working of frontal method was illustrated earlier. The frontal matrices here are rectangular and not square.

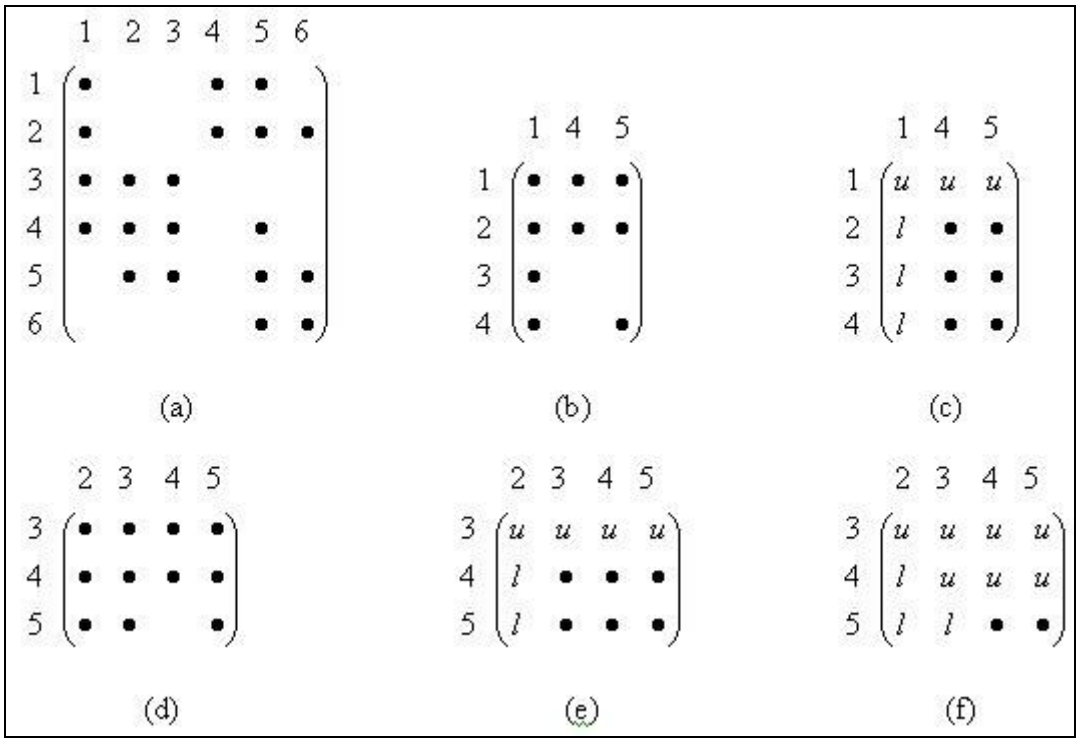

Fig. 16: Example for unsymmetric multifrontal method

Consider the unsymmetrical matrix shown in Fig. 16(a). An initial pivot element is chosen, say element (1, 1). The corresponding first frontal matrix with this pivot row and column and all contributions to them is shown in Fig. 16(b). Subsequently, a pivot operation is performed to eliminate variable 1, which gives the resultant frontal matrix with *u* (upper triangular matrix), *l* (lower triangular matrix), and the non-zero entries in the non-pivot rows and columns corresponding to the contribution block (represented by dots). Further, after the elimination of variable 1, another pivot is selected, say (3, 2). A new frontal matrix is then constructed with row 3 and column 2, with all contributions to them from both the original matrix and the contribution block of the previous frontal matrix. The resulting frontal matrix is shown in Fig. 16(c). After performing a pivot operation to eliminate variable 2, we get the matrix as shown in Fig. 16(d), but here another pivot operation on element (4, 3) can be

performed to eliminate variable 3 as well, since all contributions to row 4 and column 3 can also be assembled into the same matrix. A pivot operation on element (4, 3) reduces the frontal matrix further as shown in Fig. 16(e). In this way, the frontal matrices are continued to be assembled, and pivot operations are performed on them until the matrix is completely factorized. Table 17 below lists the available direct solvers for serial machines [72]

Table 17: Sparse Direct Solvers

Code	Technique	Scope	Contact	Ref.
CHOLMOD	Left-looking	SPD	Davis	[73]
MA57	Multifrontal	Sym	HSL	[51]
MA41	Multifrontal	Sym-pat	HSL	[61]
MA42	Frontal	Unsym	HSL	[49]
MA67	Multifrontal	Sym	HSL	[74]
MA48	Right-looking	Unsym	HSL	[54]
Oblio	Left/right/Multifr.	sym, out-core	Dobrian	[75]
SPARSE	Right-looking	Unsym	Kundert	[76]
SPARSPAK	Left-looking	SPD, Unsym, QR	George et al.	[77]
SPOOLES	Left-looking	Sym, Sym-pat, QR	Ashcraft	[78]
SuperLLT	Left-looking	SPD	Ng	[79]
SuperLU	Left-looking	Unsym	Li	[80]
UMFPACK	Multifrontal	Unsym	Davis	[81]

Abbreviations used in the table:

SPD : symmetric and positive definite

Sym : symmetric and may be indefinite

Sym-pat: symmetric non zero pattern but unsymmetric values

Unsym: unsymmetrical

In the present study, UMFPACK 4.4 [34] is used as the engine for the solution of equations (80) and (81) by multifrontal direct method. UMFPACK consists of a set of ANSI/ISO C routines for solving unsymmetric sparse linear systems using unsymmetric multifrontal method. It requires the unsymmetric, sparse matrix to be input in a sparse triplet (compressed sparse column) format. UMFPACK 4.4 consists of four steps for solving the linear system. In the first step, it reorders the rows and columns such that the factors suffer little fill, or that the matrix has special structure, such as block-triangular form. In the second, it performs symbolic factorization, computing the upper bounds on the non zeros in L and U, the floating point operations required, and the memory usage of the factorization routine. It is an analysis step to determine the nonzero structures of the factors, and to create suitable data

structures for the factors. In the third step, numerical factorization is carried out to compute the *LU* factors. Finally, it solves the linear system using the computed *LU* factors by performing the forward and back substitutions.

Different pre-ordering strategies are used to make the solver more memory efficient. It finds both a row and column pivot ordering as the matrix is factorized. No preordering or partial preordering is used. At the start of the factorization, no frontal matrix exists. It starts a new frontal matrix with a global Markowitz-style pivot search. It combines a column ordering strategy with a right-looking unsymmetric-pattern multifrontal numerical factorization. All pivots with zero Markowitz cost are eliminated first and placed in the *LU* factors. In the analysis phase it selects one of three ordering and pivoting strategies namely unsymmetric, 2-by-2, or symmetric. For symmetric matrices with non zero elements in the diagonal, the symmetric strategy is used to compute a column ordering using approximate minimum degree (AMD). No modification of the column ordering is made during the numerical factorization. A nonzero diagonal entry is selected as a suitable pivot if, in magnitude it is at least *a* times the largest entry in its column. Otherwise, an off-diagonal pivot is selected with magnitude at least *b* times the largest entry in its column. The parameters *a* and *b* are controllable with default values of 0.001 and 0.1, respectively. Thus, strong preference is given to pivoting on diagonal entries. For symmetric indefinite problems with zero entries in the diagonal, the 2 by 2 strategy is selected wherein a row permutation is done, that puts nonzero entries onto the diagonal. Then, the symmetric strategy is applied to the permuted matrix.

It is possible that the built-in ordering schemes may not be the best for the target applications, and one may use an external ordering scheme for better performance. The multifrontal method for the solving sparse systems of linear equations offers a significant performance advantage over more conventional factorization schemes by permitting efficient utilization of parallelism and memory hierarchy. The main concern of the present study is the quantitative comparison of the performance of Newton's method coupled with the multifrontal solver and one with the Gaussian elimination.

3.3.5 Time Step

Reference [23] provides an excellent discussion on the variable time step strategy chosen for the Theta method. In this research also we use the variable time step scheme. However, the criteria used for time step adjustment are more stringent than in reference [23]. The maximum time step used in our simulator is 40 seconds unlike 20 seconds in reference [23]. The minimum time step is 0.0002. The increase in time step depends on both the local truncation error and the number of iterations it takes to converge to the solution for each time step. If the iteration error is less than the tolerance, and the number of iterations it takes to converge to solution is less than a predefined number for 5 consecutive time steps, then the time step is doubled. However, if the number of iterations is more than the maximum number of iterations, or the iteration error is greater than the maximum tolerance, then the integration is repeated with time step reduced to half. On the other hand, if the number of iterations is more than a predefined number of iterations which is 6 in this case, and the iteration error is within the tolerance, then the time step is reduced for the solution of the next time step. Reduction in time step is also by a factor of 2 but is fixed at minimum. Failure to reduce the time step for ascertained number of times will result in stopping the integration.

3.3.6 Jacobian Building

The task of Jacobian building for every iteration within an integration time step is a formidable task in terms of computational resources required. The demand on time increases with the increase in size of the power system. Thus, we use the same Jacobian matrix as long as the convergence is acceptable and fast. Since the terms of the Jacobian involve time step, there is a direct relation between the variation in time step, system condition, and frequency of Jacobian building. Interested readers can see reference [23] for more elaborate discussion on considerations on Jacobian matrix computation. Effective strategy to rebuild Jacobian has resulted in considerable time saving for each simulation. The results are presented in the next section.

3.4 Test System

The proposed method is tested on two systems i) IEEE RTS-96 with 33 generators, and ii) Test system with 6 generators, 21 bus, 21 lines, 9 transformers and 3 tie lines as shown in the Appendix F and Appendix D respectively.

3.5 Performance Comparison

The system is simulated for 3600 seconds on a Pentium 4, 2.8 GHz, and 1 GB RAM. The system is simulated with an initial contingency which belongs to the set of contingencies containing functional group contingency, stuck breaker contingency or inadvertent trip contingency. A 20% load ramping from 900 seconds to 2700 seconds is also implemented.

Performance comparison is performed against Gaussian Elimination methods and sparse solvers which include CHOLMOD [47], a set of ANSI C routines for sparse Cholesky factorization and update/downdate, GPLU [22] QR factorization [48] and a sparse LU factorization routine which utilizes routines from LAPACK. These sparse solvers are also present in the Matlab.

3.5.1 Modified Newton Method

In this formulation we propose to use the same LU factors repeatedly for subsequent iterations till the convergence degrades or in other words takes more than a specified number of iterations to achieve convergence. In the present formulation we used a simple criterion based on number of iterations the multifrontal solver takes for convergence for five consecutive time steps. If it is more than five iterations for each time step than the factors are rebuilt, other wise the same LU factors are reused for all subsequent iterations. The strategy to rebuild the factors can be further improved by more experimentation and combining it with the strategy to rebuild the Jacobian. This results in huge computational gain. This is due to the fact that primarily there are three fundamental steps in the multifrontal solver namely symbolic factorization, numerical factorization and the solution step. The most computationally intensive steps are the symbolic factorization and the numerical factorization which amounts to almost five to ten times the solution step. In the conventional solution method the coefficient matrix is factorized at every step in the solution of the linear equation.

However if we can use the same factors then the solution step is very cheap although it may take more number of iteration to achieve convergence. However the overall computational gain achieved is much more and increase in number of iterations has insignificant impact. We refer this implementation as the modified multifrontal based Newton method or modified Newton method. This is similar to very dishonest Newton method in the literature [82] however its implementation criterion differs from application to application and with different solvers robustness. In the results section we will refer it as modified multifrontal.

3.5.2 Validation

Fig. 17 below shows for the six generator test system the comparison of simulation plots by the full Gaussian Elimination solver and the Multifrontal methods. As seen in the figure, both the methods provided the same solution. This was also found to be true for all the other solvers for both the test systems.

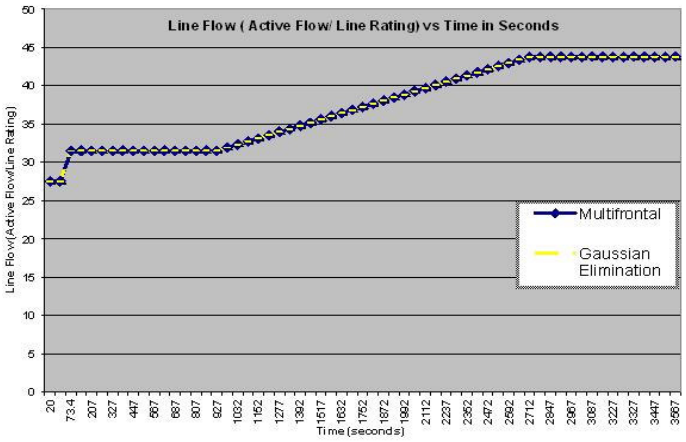

Fig. 17 Comparison of simulation plots for Gaussian elimination and for multifrontal method

3.5.3 Results and Discussion

Table 18 shows the performance comparison for the multifrontal method with the full Gaussian elimination algorithm and the sparse solvers on the 6 generator test system for 6 different critical initiating contingencies on the system. For the sparse solvers only the best results of all the sparse solvers are reported. Column 1 shows the contingency number, columns 2,3 and 4 show the simulation time in seconds with the multifrontal algorithm, Gaussian Elimination and the sparse solvers respectively. Column 5 shows the speed-up using the multifrontal method compared to Gaussian, which varies between 3.75 times to 7 times and Column 6 shows the speed-up with other sparse solvers, varying between 3 to 5.4

times. For this system there are a total of around 300 contingencies including all N-1, contingencies due to breaker failure, protection failure to trip, and due to inadvertent tripping. The time savings for 300 contingencies is provided in columns 7 and 8. The multifrontal method would save around 16 to 22 hours computing time compared to Gaussian Elimination and 11 to 17 hours compared to other sparse solvers.

Table 18: 6-generator Test System

Contingency no.	Multi Frontal (Secs)	Gaussian Elimatn (Secs)	Sparse Solvers (Secs)	Speed up (Col3/ Col2)	Speed up (Col4/ Col2)	Difference in time (saving) for 300 contingencies	
						Gaussian methods	Sparse solvers
						Hrs	Hrs
1	46.138	321.505	250.206	6.968	5.423	22.94725	17.005
2	56.816	261.394	189.31	4.600	3.332	17.04817	11.041
3	44.08	232.613	210.96	5.277	4.786	15.71108	13.907
4	65.624	247.113	205.534	3.765	3.132	15.12408	11.659
5	51.826	287.003	258.197	5.537	4.982	19.59808	17.197
6	69.622	260.988	209.631	3.748	3.011	15.94717	11.667

The Fig. 18 below compares graphically the speed of the multifrontal method to that of the Gaussian algorithm for the 6 generator test system.

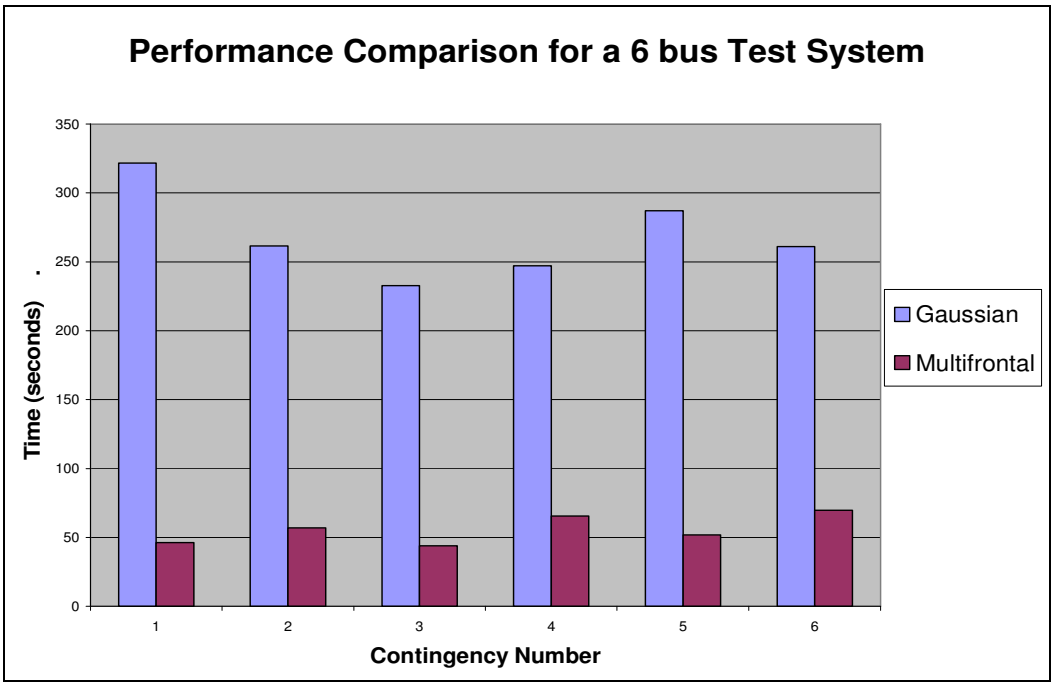

Fig. 18: Performance Comparison for a 6 generator system

Table 19 similarly shows the performance comparison results for the 32 generator RTS system for 3 different critical initiating contingencies on the system. We observe that the speed-up against the Gaussian Elimination varies between 4 times to 6.4 times and against

the other sparse solvers it varies between 3.2 to 4.2 times. Again for this system if we are to analyze 300 contingencies as in the previous case, we can see from columns 7 and 8 that using the multifrontal method saves around 67 to 100 hours computing time compared to Gaussian Elimination and between 49 to 67 hours compared to other commonly available sparse solvers.

Table 19: 32-generator Test System

Contingency no.	Multi Frontal (Secs)	Gaussian Elimatn (Secs)	Sparse Solvers (Secs)	Speed up (Col3/ Col2)	Speed up (Col4/ Col2)	Difference in time (saving) for 300 contingencies	
						Gaussian methods	Sparse solvers
						Hrs	Hrs
1	222.807	1420.789	944.256	6.376	4.238	99.833	60.120
2	356.227	1419.301	1165.931	3.984	3.273	88.585	67.475
3	242.878	1047.513	828.699	4.312	3.412	67.052	48.818

The Fig. 19 below compares graphically the speed of the multifrontal method to that of the Gaussian algorithm for the 32 generator test system.

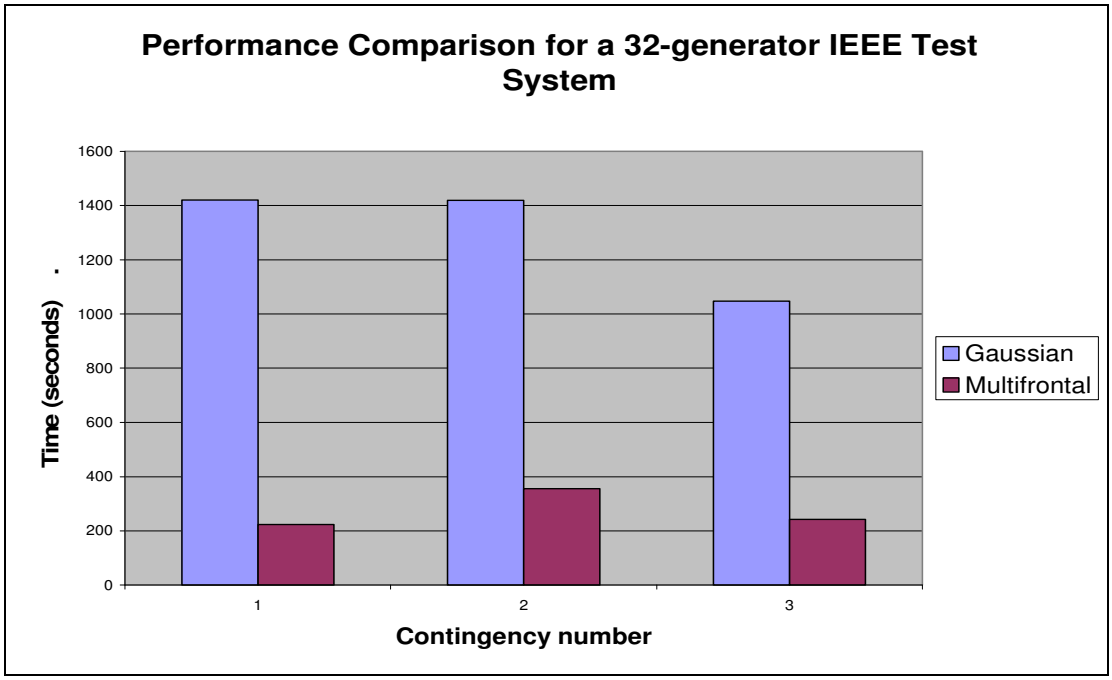

Fig. 19: Performance Comparison for a 32-generator test system

From the numerical results above we observe that the time saving is almost linearly related to the increase in the number of generators in the system and also the speed up increases with the size of the system and hence the size of the Jacobian. In the test system we

had 6 generators and in the RTS system there were 32 generators. There was almost five times increase in the number of generators. From Table 18 and Table 19 we can see that there was a corresponding increase in time savings and speed up. This is because the size of the matrix linearly scales with the number of generators (assuming 10^{th} order ODE per generator) and the algebraic equations corresponding to the network. The gain offered by the multifrontal methods becomes significantly more important with the real time systems. Thus the multifrontal methods may be viewed as a fundamentally important enabling technology.

Table 20 and Table 21 shown below shows the performance comparison results of the modified multifrontal methods with the other sparse solvers. As can be seen from the results in Table 18 and Table 20 that the speed-up which was 3 to 5.4 times in the case of full multifrontal method has increased to 7.55 to 8.3 times in the case of modified multifrontal methods for the 6 generator test system.

Table 20: 6-generator Test System ((Modified Newton)

Contingency no.	Modified Multi Frontal (Secs)	Sparse Solvers (Secs)	Speed up (Col3/ Col2)	Difference in time (saving) for 300 contingencies Hrs Sparse solvers
1	33.119	250.206	7.554	18.091
2	24.897	189.31	7.603	13.701
3	25.780	210.96	8.182	15.431
4	24.978	205.534	8.228	15.046
5	34.030	258.197	7.587	18.680
6	27.210	209.631	7.704	15.202

Similarly we can see from Table 19 and Table 21 that the speed-up which was 3.2 to 4.2 times in the case of full multifrontal method has increased to 24.1 to 28.675 times in the case of modified multifrontal methods for the 32 generator test system. This is huge computational gain as compared to the six generator case. This was expected with the increase in size of the system since the computational cost for the symbolic and the numerical factorization increases nonlinearly with the increase in size of the matrix as compared to the solution step. Thus intelligent reuse of the LU factors can result in orders of magnitude saving in computational time.

Table 21: 32-generator Test System (Modified Newton)

Contingency no.	Modified Multi Frontal (Secs)	Sparse Solvers (Secs)	Speed up (Col3/ Col2)	Difference in time (saving) for 300 contingencies Hrs Sparse solvers
1	32.928	944.256	28.675	75.943
2	44.781	1165.931	26.035	93.429
3	29.252	828.699	28.328	66.620
4	38.524	928.564	24.103	74.170

CHAPTER 4 NUMERICAL METHODS - ITERATIVE METHODS

4.1 Introduction

In the traditional classification, the solution methods to the linear system of equations are divided into two classes namely the direct methods and the iterative methods. However in the present context with the number of ideas and techniques from the sparse direct solvers being effectively applied in the iterative solution paradigm, there is no more a very clear boundary between the direct and the iterative methods. Additionally the field of iterative methods comprises a wide range of techniques, ranging from purely iterative methods, like the classical Jacobi, Gauss–Seidel, and SOR iterations, to Krylov subspace methods, which theoretically converge in a finite number of steps in exact arithmetic, to multilevel methods. The introduction of preconditioners has further made the distinction unclear. The use of the direct solution ideas and techniques has made the iterative methods increasingly more reliable and robust.

For large systems the direct methods are less efficient than iterative methods because of round-off errors. For sparse coefficient matrices the amount of storage space required for iterative solutions on a computer is far less than it is required for direct methods and thus making them more attractive than the direct methods. The scalability of the direct methods is very poor with problem size in terms of operation counts and memory requirements for 3 D problems as those arising in rotating channel in computational fluid dynamics in the solution of the Navier Stokes equations and from the discretizations of PDEs in 3 D space from other applications. Detailed, three-dimensional multi physics simulations carried out as part of the U.S. DOE ASCI program lead to linear systems of the order of billions. Iterative methods are the only viable option for large scale problems of this magnitude. Although iterative methods require less storage and often fewer operations than direct methods (especially in cases where an approximate solution of relatively low accuracy is sought), they often fail to compete with the reliability of direct methods. In many applications, iterative methods fail and preconditioning is necessary, though not always sufficient, to attain convergence in a reasonable amount of time.

A lot of research efforts in the developments for the iterative methods came from the impetus from the nuclear industry where they have been widely used for a long time [83,84,85].

The power of most iterative methods lies in the cheapness with which each iteration step is performed. However this may entail a number of iterations for the solution to converge. This can be reduced by preconditioning the matrix but then the cost of each iteration increases. Most of the current iterative methods use Krylov sequences. In a Krylov-sequence based method, an approximate solution to the problem is computed from the subspaces of increasing dimension usually with some optimality condition over all vectors in the subspace so that the solution will be obtained when the subspace is of sufficient dimension. The two most widely used Krylov subspace methods for the solution of unsymmetric systems are GMRES and BiCGStab. The advantage of the latter is that of limited storage needs, but there are many problems for which this method does not work well. Thus for such problems, GMRES, being robust has become the method of choice, and this has led both to its ample study and to many extensions and variants. In general, there is no one method which is recommended for all problems [86].

Reference [87] presents the state-of-the-art research in applying iterative techniques to power system problems. It concludes that in terms of applicability, iterative methods cannot compete with direct methods because of convergence problems. Alleviating convergence problems requires good choice of preconditioners which do not add to computational complexity. Reliability of iterative solvers depends on the quality of preconditioners, than on the particular Krylov subspace accelerators used. In particular, the Jacobian for the time domain simulation is highly unsymmetric, with non-symmetric nonzero pattern. It was shown in the literature [88] that proper scaling of the Jacobian is important in case of non-symmetric Jacobian matrix to achieve convergence and computational gain with incomplete factorization based preconditioners. This research proposes to develop multifrontal based robust and computationally cheap preconditioners for power systems as compared to incomplete LU factorization preconditioners used in the literature [87].

4.2 Basic Solution Methodology

Let x_0 be an initial approximation to the solution of

$$\text{Ax} = \text{b} \tag{85}$$

$$r_0 = b - Ax_0 \tag{86}$$

be the initial residual and let

$$K_m(A, r_0) = span\{ r_0, Ar_0, A^2 r_0, ..., A^{m-1} r_0 \}$$

be the Krylov subspace of dimension m defined by A and r_0. The short-hand notation K_m is used when the dependence on A and on the specific vector r_0 is clear from the context. Note that these subspaces are nested, i.e., $K_m \subseteq K_{m+1}$. Krylov subspace methods are iterative methods in which at the mth step an approximation to the solution of (85), x_m, is found in $x_0 + K_m$, i.e., this approximation is of the form $x_m = x_0 + q_{m-1}(A)r_0$, where q_{m-1} is a polynomial of degree at most m − 1. If the system is real, q_{m-1} can be chosen to have real coefficients. This natural expression implies that the residual $r_m = b - Ax_m$ is associated with the so-called residual polynomial p_m of degree at most m with $p_m(0) = 1$ since

$$r_m = b - Ax_m = r_0 + q_{m-1}(A)r_0 = p_m(A)r_0 . \tag{87}$$

Analogously, the error satisfies $x_m - x_* = p_m(A)(x_0 - x_*)$ where x_* is the solution of equation (85). Let us denote by P_m the set of all polynomials p of degree at most m such that p(0) = 1. The approximation $x_m \in x_0 + K_m$ (or equivalently, the corresponding polynomial) is often found by requiring x_m to be the minimizer of some functional. Different methods depend on the choice of this functional, on the characteristics of the matrix, and on some implementation details, and thus, each method defines implicitly a different polynomial $p_m \in P_m$ $(or\, q_{m-1})$. For example, in the popular GMRES [89], the approximation x_m is the one minimizing the 2-norm of the residual.

In the process of iteratively constructing a basis of K_m, each method can be implemented so that at each iteration only one or two matrix-vector multiplications with A is required, in the form $z = Av$ (in some methods an additional operation of the form $y = A^T w$ is needed).

This fact drives the practical applicability of these methods. In fact, the matrix itself is not needed, only its action as an operator on a vector is used, usually as a call to a subroutine.

The method starts with an initial vector x_0, with initial residual $r_0 = b - Ax_0$ and at the mth step obtain an element x_m of $x_0 + K_m(A, r_0)$ satisfying a projection or minimizing condition of some kind. Let $r_m = b - Ax_m$ be the residual at the mth step. A general condition is the minimum residual condition:

$$\|r_m\| = \min_{x \in x_0 + K_m} \|b - Ax\| \tag{88}$$

We note that the nested property of the Krylov subspaces, imply that any method for which the above condition holds will, in exact arithmetic, terminate in at most n steps. Of course, in practice one wants the methods to produce a good approximation to the solution of (85) in many fewer than n iterations.

4.2.1 GMRES

The Krylov subspace method GMRES (Generalized Minimal Residual), was first proposed by Saad and Schultz [89]. The projection condition is to minimize the residual over all possible vectors in the Krylov subspace $K_m(A, r_0)$. That is, one obtains x_m such that

$$\|r_m\| = \|b - Ax_m\| = \min_{x \in x_0 + K_m} \|b - Ax\| \tag{89}$$

.For GMRES, usually the 2-norm is used. The solution of the least squares problem (89) is unique as long as A has full rank [90]. The key to GMRES is the implementation of the solution of the least squares problem (89) using an orthonormal basis of the Krylov subspace produced by the Arnoldi procedure. We write the GMRES approximation at the mth step as

$$x_m = V_m y_m \tag{90}$$

for some $y_m \in R^m$.

The sequence of residual norms $\|r_m\|$ generated by GMRES, like for all methods satisfying the minimum residual condition (88) on nested subspaces, is non-increasing. The main disadvantage of GMRES is that as the iterations proceed, i.e., as m grows, the storage requirements grow accordingly. One needs mn storage locations to store the matrix V_m. There

are several alternatives to alleviate this, using, e.g., restarted or truncated methods. In this research we use the restarted approach to control m.

4.2.2 Other Methods

Bi Conjugate Gradient (BiCG) is a different implementation of the Lanczos method, and in exact arithmetic, the approximation x_m is the same as that of the Lanczos method, The problems of the unsymmetric Lanczos method are present in BiCG, and in addition, the method may break down if the LU factorization without pivoting does not exist, whence this is called a pivot breakdown. In reference [91] a procedure, called QMR (Quasi-Minimum Residual) is proposed, that replaces the Lanczos solution iterates with a new sequence of approximate solutions such that the associated residuals satisfy a quasi-optimal minimization condition. In addition to overcoming the possible erratic behavior of the BiCG residual, the proposed approach also avoids pivot breakdown. QMR methods overcome this difficulty by solving the least squares problem instead of implicitly solving the m × m linear system. There are several reasons why Lanczos or BiCG are not much used nowadays. In addition to the possible breakdown of two-sided Lanczos and the need to have access to both operators A and A^T, the Lanczos method is not very stable [92], and the residual norms may have large oscillations, sometimes referred to as irregular (or erratic) convergence. In fact, unlike the minimum residual methods, the residual norms for these methods are not necessarily non increasing. This should not be a problem as long as there is a downward trend, but it is preferred to have a smooth decreasing curve, and this fact has led to several suggestions on how to achieve some smoothing. However, smoothing the residual does not improve the numerical properties of the short-term Lanczos recurrence.

BiCG stabilized (Bi-CGStab) is not very effective when the spectrum has large imaginary components, as is the case, e.g., for matrices stemming from advection dominated PDEs; [93,94] and often in power systems.

We mention though the following well-known comparison between the norm of the QMR residual, and that of GMRES, denoted by r_m^Q and r_m^G, respectively

$$\left\| r_m^Q \right\| \le k(W_{m+1} \left\| r_m^G \right\| \tag{91}$$

which was first obtained by Nachtigal [95]. Since $r_m^G \le r_m^Q$, if $W_{m+1}^T W_{m+1} = I_{m+1}$ then it must hold $\left\|r_m^Q\right\| = \left\|r_m^G\right\|$. In general, the bound suggests that the QMR residual norm may be very far from the optimal GMRES norm when the chosen basis is ill conditioned. However, it was recently shown in [96] that this type of bound may considerably underestimate the actual behavior of quasi-optimal methods, in this case that of QMR. In particular, as long as the basis vectors remain linearly independent, convergence is not significantly different. We point out that in (91) the comparison of the two methods is done at the same iteration. An alternative measure of delay is obtained by monitoring the number of iterations required for the two methods to reach the same accuracy.

4.2.3 Restarted method

The iterative methods based on the full Arnoldi recurrence methodology for unsymmetric matrices are in general very expensive in terms of storage requirements. This is because a large number of iterations may be required to achieve a sufficiently accuracy, and meanwhile the Arnoldi matrix becomes unacceptably large to be stored and kept orthonormal. The general practice is to restart the method after a maximum subspace dimension is reached. In other words if iterations are restarted after m iteration then the current solution and the residual approximations become the initial quantities for the next recursion executed for at most m iterations and this process is repeated till the desired accuracy is reached. The advantage of a restarted procedure is that at most m iterations of the Arnoldi method are carried out, so that both computational costs and memory allocations per cycle are under control. But this comes at the cost of losing the optimality properties of the process after the first restart as in GMRES. As a result, the overall process may not converge. In the case of GMRES, for instance, the outer recurrence may stagnate with $\left\|r_m^{i+1}\right\| \le \left\|r_m^i\right\|$ for all i. Note that in GMRES the residual norm cannot increase in the outer iteration, since the optimality of the inner GMRES step ensures that $\left\|r_m^i\right\| \le \left\|r_0^i\right\|$ for all i. If stagnation occurs, a simple cure is to enlarge the maximum allowed subspace dimension, m, to enrich the subspace information. However enlarging the subspace dimension does not always ensure faster convergence [97,98]. Sometimes however it may not be possible to choose a larger m for large problems due to storage and other constraints. Good choice of m can be advantageous [99]. Other

schemes can be coupled with GMRES at restart time, resulting in better restarting strategies than restarted GMRES [100].

4.2.4 Preconditioning

Preconditioning is the most important and critical factor in the development of efficient iterative solvers that can compete with direct solvers in terms of reliability and robustness. Thus there have been more research efforts on preconditioners than on the direct and Krylov subspace methods put together. Trefethen and Bau in [101, p. 319] states emphatically:

"*In ending this book with the subject of preconditioners, we find ourselves at the philosophical center of the scientific computing of the future.... Nothing will be more central to computational science in the next century than the art of transforming a problem that appears intractable into another whose solution can be approximated rapidly. For Krylov subspace matrix iterations, this is preconditioning.*"

Preconditioning refers to transforming the linear system (85) into another system to improve the spectral properties of the coefficient matrix for iterative solution.

If M is a nonsingular matrix that approximates A (in some sense), then the linear system

$$M^{-1}Ax = M^{-1}b \tag{92}$$

has the same solution as (85) but may be easier to solve. Here M is the preconditioner. In cases where M^{-1} is explicitly known (as with polynomial preconditioners or sparse approximate inverses), the preconditioner is M^{-1} rather than M.

System (2) is preconditioned from the left, but one can also precondition from the right:

$$AM^{-1}y = b, x = M^{-1}y \tag{93}$$

When Krylov subspace methods are used, it is not necessary to form the preconditioned matrices $M^{-1}A$ or AM^{-1} explicitly (this would be too expensive, and we would lose sparsity). Instead, matrix–vector products with A and solutions of linear systems of the form $Mz = r$ are performed (or matrix–vector products with M^{-1} if this is explicitly known).

In addition, *split preconditioning* is also possible, i.e.,

$$M_1^{-1}AM_2^{-1}y = M_1^{-1}b, x = M_2^{-1}y \tag{94}$$

where the preconditioner is now $M = M_1M_2$. The type of preconditioning used depends on the choice of the iterative method, problem characteristics, and so forth.

For symmetric positive definite (SPD) problems, distribution of the eigenvalues of the coefficient matrix governs the rate of convergence of the iterative methods like the conjugate gradient method. The preconditioned system aims to have a smaller spectral condition number, and/or eigenvalues clustered around 1. ***For unsymmetric (non normal) problems the situation is more complicated, and the eigenvalues may not describe the convergence of unsymmetric matrix iterations like GMRES*** **[102].** Nevertheless, a clustered spectrum (away from 0) often results in rapid convergence, particularly when the preconditioned matrix is close to normal For example, with residual minimizing methods, like GMRES, right preconditioning is often used. In the non normal case, solvers like GMRES can behave very differently depending on whether a given preconditioner is applied on the left or on the right [103, p. 255,104, p. 66]. In general, a good preconditioner *M* should meet the following requirements: 1) the preconditioned system should be easy to solve, 2) The preconditioner should be cheap to construct and apply, 3) their inverse should be cheaply applicable, 4) their use should entail low memory requirements, 5) the transformed problem should converge faster (less computational time) than the original problem.

The first, third and the fifth properties require fast convergence properties of the preconditioned iteration, while the rest ensures that each iteration step is not too expensive. It is important to strike a balance between the two requirements as they are competing with each other. With a good preconditioner, the computing time for the preconditioned iteration is usually significantly reduced compared to the unpreconditioned one. One of the important goals is to construct good quality preconditioners which can be reused in the solution of linear systems with same or slowly changing or similar coefficient matrices and different right hand side. This justifies spending computational cost on the construction of such preconditioners. This is often the case when solving the system of linear equations arising out of the solution of the non linear equations by Newton's method. The Jacobian matrix evolves slowly and thus the factors of the preconditioners can be reused till the convergence degrades with disturbances in terms of the contingencies or the changing load and other changes in the system when the preconditioners need to be rebuilt.

In general there are two approaches to construct preconditioners, namely problem specific or for a narrow class of problems and the other a generalized preconditioner.

Problem specific or specialized algorithms can be very optimal, effective and successful for a narrow class of problems. This however requires complete knowledge of the problem at hand, including the model and the equations governing the system, the domain of integration, the boundary conditions, details of the discretizations, and so forth. For example in [105], the method of diffusion synthetic acceleration (DSA) [106,107,108], which is widely used in the transport community, can be regarded as a physics-based preconditioner for the transport equation.

The problem-specific approach may not always be feasible or even desirable. The complete knowledge of the problem to be solved, or the information may not be available, too difficult to comprehend for the software developer to use or too difficult to obtain. Furthermore these approaches are in general very ***sensitive to the details of the problem***, ***and even slight changes in the problem can compromise the effectiveness of the solver***. For example in the power system application for the time domain solution, changes in the system topology due to breaker status changes or contingencies, load changes from very light load to heavy load, and other system condition changes might degrade the quality of the preconditioner to the extent of worse performance than the unpreconditioned system. Also different power systems would require different preconditioners to be developed. For these reasons, there is a need for general purpose preconditioning techniques that are applicable over a wide range of problems and are robust. The current research is motivated by this fact and we attempt to develop such preconditioners which would be applicable for a wide range of problems including power systems. These are multifrontal based preconditioners which are very robust and cheap and can be applicable to problems from different fields of applications.

These general purpose preconditioner techniques are efficient over a wide spectrum of problems and achieve good efficiency and can be further optimized for specific problems Algebraic methods are often easier to develop and to use and are particularly well suited for irregular problems such as may arise in power system dynamic simulation and from discretizations of PDEs in the solution of Navier Stokes equations The resulting general purpose preconditioners can be competitive with optimal, less versatile problem-specific

techniques. Finally, algebraic methods are often used as basic components in more sophisticated, problem-specific solvers [109].

4.2.5 Preconditioning for the unsymmetric matrices.

In the unsymmetric case, incomplete factorizations are widely used. But even in the simplest cases, the amount of success often depends on the ability to tune the fill-in and threshold parameters [88]. Unfortunately, these algebraic approaches do not work well in all cases. As discussed earlier ***part of the difficulty in the unsymmetric case is due to the fact that the convergence of the Krylov subspace methods does not depend only on the eigenvalues and their relative position on the complex plane i.e clustering,, especially in the non-normal case, but also there is often a lack of diagonal dominance which strongly influences the stability of the incomplete factorization based preconditioners.***

In fact in the unsymmetric cases even the existence of a stable *complete* factorization without pivoting is not guaranteed. Even if the incomplete factorization process can be completed without breakdowns, there is no guarantee in general that it will result in a useful preconditioner. Especially for unsymmetric problems, the incomplete factors L and U may happen to be very ill conditioned, even for a well-conditioned A. Application of the preconditioner, which involves a forward substitution for L and a back substitution for U, may introduce large errors that can destroy the effectiveness of the preconditioner. ***In a nutshell, instability in the ILU factors is related to lack of diagonal dominance.*** The two types of instability (zero or small pivots and unstable triangular solves) can occur independently of one another, although they are frequently observed together in matrices that are strongly unsymmetric and far from diagonally dominant as is the case arising in power system dynamic analysis and those arising in the solution of the Navier–Stokes equations. The quality of an incomplete factorization $A \approx LU$ can be gauged, at least in principle, by its ***accuracy*** **and** ***stability***. **Accuracy** refers to how close the incomplete factors of A are to the exact ones and can be measured by $N_1 = \|A - LU\|_F$. For some classes of problems, including symmetric M-matrices, it can be shown [110,111] that the number of preconditioned CG iterations is almost directly related to N_1, so that improving the accuracy of the incomplete factorization by allowing additional fill will result in a decrease of the number of iterations to converge. However, for more general problems (and especially for highly unsymmetric and

indefinite matrices) this is not necessarily the case, and N_1 alone may be a poor indicator of the quality of the preconditioner. **Stability** refers to how close the preconditioned matrix $(LU)^{-1}A$ is to the identity matrix I and is measured by $N_2 = \left\| I - (LU)^{-1}A \right\|_F$ or by $N_2 = \left\| I - A(LU)^{-1} \right\|_F$ for right preconditioning system. Let $R = LU - A$, the residual matrix, we get $I - (LU)^{-1}A = (LU)^{-1}A$ and it becomes clear that an incomplete factorization can be accurate (small N_1) but unstable (large N_2). Indeed, if either L^{-1} or U^{-1} has very large entries (unstable, or ill-conditioned triangular solves), then N^2 can be many orders of magnitude larger than N^1. In this case, failure of the preconditioned iteration is to be expected [112,113]. Thus, for general matrices N^2 is a more telling measure of preconditioning quality than N^1. Although it is not practical to compute N^2, even a rough estimate can be quite useful. As recommended in [94], an inexpensive way of detecting ill conditioning in the ILU factors is to compute $\left\| (LU)^{-1}e \right\|_\infty$, where e denotes the n-vector with all entries equal to 1. Note that this amounts to solving a linear system with the factored coefficient matrix LU and e as the right-hand side. This is, of course, only a lower bound for $\left\| (LU)^{-1} \right\|_\infty$, but it has been found to be quite useful in practice. A very large value of this quantity will reveal an ill conditioning and therefore a not so useful preconditioner and will indicate the need to compute a better one.

Instabilities in the preconditioner construction and application can often be avoided by suitably preprocessing the coefficient matrix A. These preprocessings consist of a combination of symmetric permutations, nonsymmetric ones, and scalings aimed at improving the conditioning, diagonal dominance, and structure of the coefficient matrix.

Finally, *a priori* information on the nature of the problem need to be incorporated into a **general-purpose preconditioner like ILU** to obtain a stable and effective preconditioner. For example in [114], good results were obtained in the solution of complex symmetric indefinite systems arising from the Helmholtz equation using variants of incomplete factorization methods that make clever use of available knowledge of the spectrum of the discrete Helmholtz operator. This shows that purely algebraic methods, such as ILU preconditioners, can be made more competitive by exploiting available information about a particular class of problems. Still their successful and effective application for unsymmetric

matrices as those arising in power system remains a challenge. This motivates the development of very robust and efficient multifrontal based preconditioners for the power system.

4.2.6 The Effect of Ordering

Incomplete factorization preconditioners are sensitive to the ordering of unknowns and equations. Reorderings have been used to reduce fill-in (as with sparse direct solvers), to introduce parallelism in the construction and application of ILU preconditioners, and to improve the stability of the incomplete factorization. In most cases, reorderings tend to affect the rate of convergence of preconditioned Krylov subspace methods.

The effects of reorderings on the convergence of preconditioned Krylov subspace methods have been studied by a number of authors, mostly experimentally, and are still the subject of some debate [115,116,117,118,119,120,121,122,123,124,125,126,127] . In general, the ordering used and the corresponding preconditioned iteration interact in rather complex and not-well understood ways.

Sparse matrix reorderings have been in use for a long time in connection with direct solution methods [128]. Classical ordering strategies include bandwidth- and profile reducing orderings, such as reverse Cuthill–McKee (RCM) [129], Sloan's ordering [130], and the Gibbs–Poole–Stockmeyer ordering [131]; variants of the minimum degree ordering [132, 133]; and (generalized) nested dissection [134,135]. These orderings are based solely on the structure (graph) of the matrix and not on the numerical values of the matrix entries. For direct solvers based on complete matrix factorizations this is justified, particularly in the SPD case, where pivoting for numerical stability is unnecessary. However, for incomplete factorizations, the effectiveness of which is strongly affected by the size of the dropped entries, orderings based on graph information only may result in poor preconditioners. Thus, it is not surprising that some of the best orderings for direct solvers, such as minimum degree or nested dissection, often perform poorly when used with incomplete factorizations.

This phenomenon has been pointed out, for SPD matrices arising from diffusion-type problems in 2D [136]. It is shown that when a minimum degree ordering of the grid points was used, the rate of convergence of conjugate gradients preconditioned with a no-fill incomplete Cholesky factorization was significantly worse than when a natural

(lexicographical) ordering was used. The reason for this is that even though fewer nonzeros are likely to be dropped with a minimum-degree ordering (which is known to result in very sparse complete factors), the average size of the fill-ins is much larger, so that the norm of the remainder matrix $R = A - LL^T$ ends up being larger with minimum-degree than with the natural ordering [137, pp. 465–466]. However, fill-reducing orderings fare much better if some amount of fill-in is allowed in the incomplete factors. As shown in [136], minimum degree performs no worse than the natural ordering with a drop tolerance based Incomplete Cholesky (IC). Similar remarks apply to other orderings, such as nested dissection and red–black; RCM was found to be equivalent or slightly better than the natural ordering, depending on whether a level-of-fill or a drop tolerance approach was used. Hence, at least for this class of problems, there is little to be gained with the use of sparse matrix orderings. For finite element matrices, where a "natural" ordering of the unknowns may not exist, the authors of [136] recommend the use of RCM. In [138,139] variants of RCM were shown to be beneficial in IC preconditioning of strongly anisotropic problems arising in oil reservoir simulations. An intuitive explanation of the good performance of RCM with IC preconditioning has been recently proposed [140]. It should be mentioned that minimum degree may be beneficial for difficult problems requiring a fairly accurate incomplete factorization and thus large amounts of fill [141].

However we found that for the unsymmetric case of the power system dynamic simulation the effect of the ordering was to worsen the performance of the incomplete factorization based preconditioners. In most cases the solution did not converge for cases where the L and U factors were computed after the ordering of the coefficient matrix. In other cases there was stagnation of the solution vector.

4.3 Performance Comparison

4.3.1 Validation

The Fig. 20 below shows for the six generator test system the comparison of simulation plots by the multifrontal preconditioner based GMRESR iterative solver and the direct methods based multifrontal LU solver. As seen in the figure, both the methods provided the same solution.

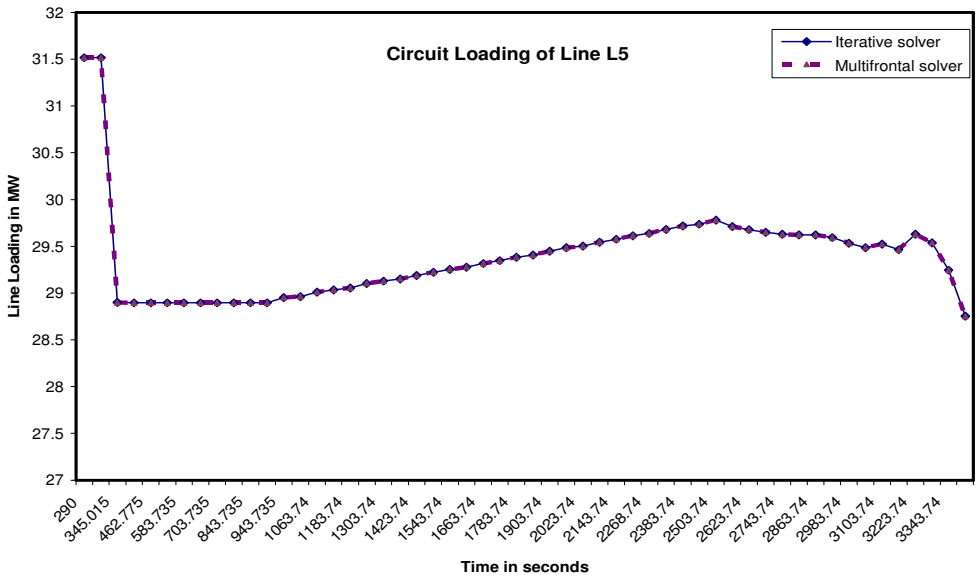

Fig. 20 Comparison of simulation plots for the multifrontal preconditioned GMRESR solver and for the multifrontal solver

4.3.2 Results and Discussion

In this study, an efficient and robust variant of GMRES known as restarted GMRES (GMRESR) [142] was used. The GMRESR algorithm with preconditioning for solving the linear system of equations (85) is given in the Appendix G. In this algorithm, two iterative loops are performed – the inner loop and an outer loop, both based on GMRES algorithm. An internal preconditioning operation is applied using GMRES in the inner loop using few steps

A good preconditioner is essential to accelerate the convergence of iterative methods. In the GMRESR algorithm given in Appendix G an external multifrontal based preconditioner is applied in addition to the internal GMRES preconditioning operation. This is crucial for accelerating its convergence. The other incomplete factorization based preconditioners like ILU were used with iterative methods like GMRES, BiCGStab, QMR for the purpose of performance comparison and showing the effectiveness and robustness of the multifrontal preconditioned GMRESR method and ineffectiveness of other preconditioners for the power system dynamic simulation problem. The ILU preconditioned GMRES and its variants were used in the literature but it was concluded that the fill in factor and the threshold to restart are highly problem specific and in general a large fill was required and the Jacobian had to the preprocessed with scaling to achieve good convergence. With the power system in a flux and the corresponding Jacobian matrix changing, it would require repeated preprocessing of the

Jacobian and evaluation of the proper scaling factor, fill-in factor and threshold value to achieve computational gain over direct methods. This would become a very challenging task especially for large power system and changing topology where the even order of the Jacobian varies. Thus ILU preconditioners are not so effective for the linear system of equations arising in power system. This motivates the development of highly robust and general purpose multifrontal preconditioners which are cheap to obtain and facilitates fast convergence.

The *LU* factors obtained from the multifrontal solver are used to obtain the preconditioner. In the Newton's iterations, the left hand side matrix is the Jacobian $\left(\underset{\approx}{J}\right)$, which is intelligently updated as discussed in the last chapter. The first iteration is solved using the multifrontal solver and the *LU* factors are stored in the memory. During subsequent iterations, equation (85) is solved using the GMRES iteration. The *LU* factors stored for the initial Jacobian $\underset{\approx}{J}^{(0)}$ are used as preconditioner in the subsequent iterations and time steps till the convergence degrades. Then the factors are recalculated. Since the *LU* factors are already stored, the preconditioning step is relatively inexpensive.

There is a significant reduction in the time taken by subsequent iterations of the GMRES solver as compared to the iteration where the LU factors are computed. This is due to the fact that the GMRES solver uses the previous *LU* factors. This accumulates to give the overall computational efficiency.

Another important advantage of using the multifrontal preconditioner with GMRESR is that the Newton's quadratic convergence is obtained in less computational time. However with the ILU preconditioners this is not true because the approximate LU factors used in the iterative steps increase the number of iterations for convergence and often it is much slower. In unsymmetric cases they may not converge at all without high degree of fill in which is computationally very costly. This is true in the case of power system dynamic simulations where the Jacobian matrices obtained are highly unsymmetric and with zero entries in the diagonal. This causes very poor performance of the ILU preconditioners. In other words the preconditioners actually worsen the convergence rate. To overcome this limitation, the ILU preconditioners can be applied with segregated algorithms in combination with other

techniques to handle the diagonal zero introducing component. This however would lose the quadratic convergence property of Newton's method. Thus, GMRES with multifrontal based preconditioner provides a good alternative to highly unsymmetric problems and can be a viable option for 3D Navier Stokes equations.

As discussed earlier, reordering with the ILU preconditioners in the present problem degraded the convergence characteristic drastically and in most cases the solution did not converge or took lot of iterations to converge. We implemented RCM, symamd, colamd, symmmd orderings available in Matlab, with the GMRESR, BiCGstab, and QMR. The results are not reported because of no convergence in most cases. This was due to the fact that although the LU factors were computed faster due to reordering schemes in some cases but the LU factors in themselves were not so accurate and stable. This led to the failure in the iteration step.

The figure below Fig. 21 shows the non zero element distribution of the Jacobian matrix obtained from the dynamic simulation of the 6 generator test system.

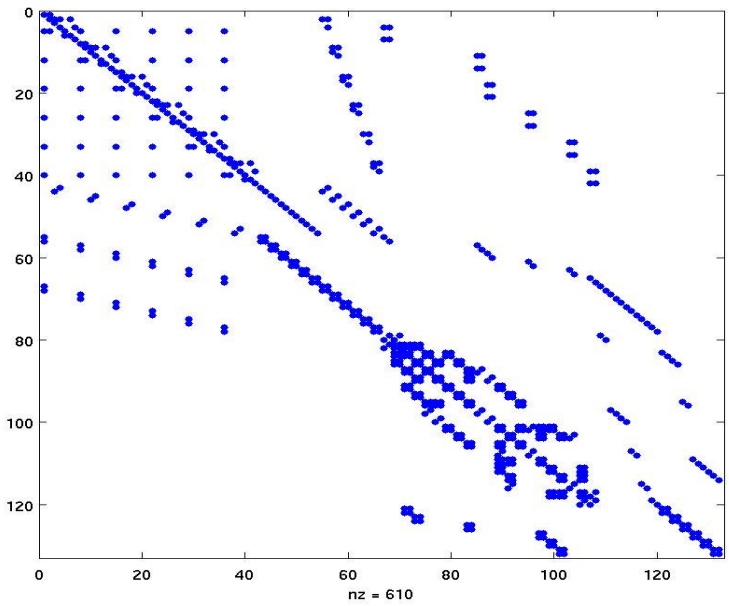

Fig. 21 The non zero pattern of a typical Jacobian matrix in dynamic simulation

The Figure below show the RCM reordered non zero element distribution for the matrix in Fig. 21

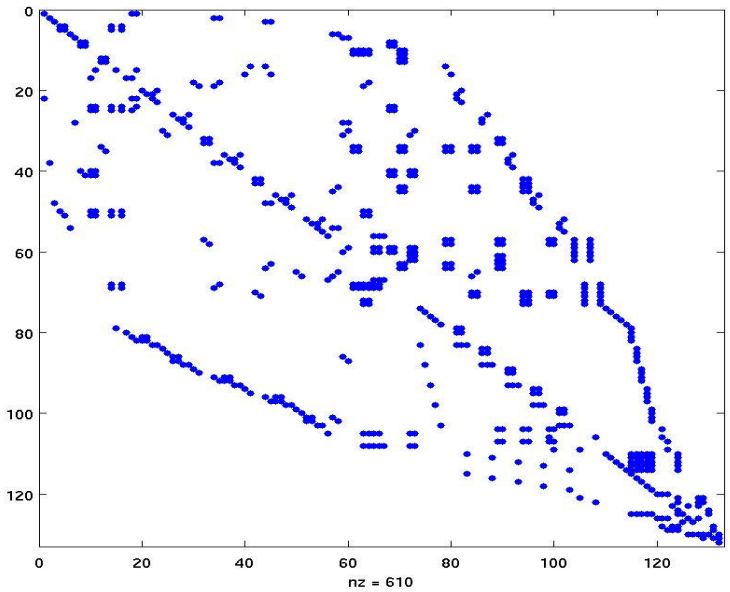

Fig. 22 RCM Reordered non zero element distribution for the matrix in Fig. 21

The Figure below show the symamd reordered non zero element distribution for the matrix in Fig. 21

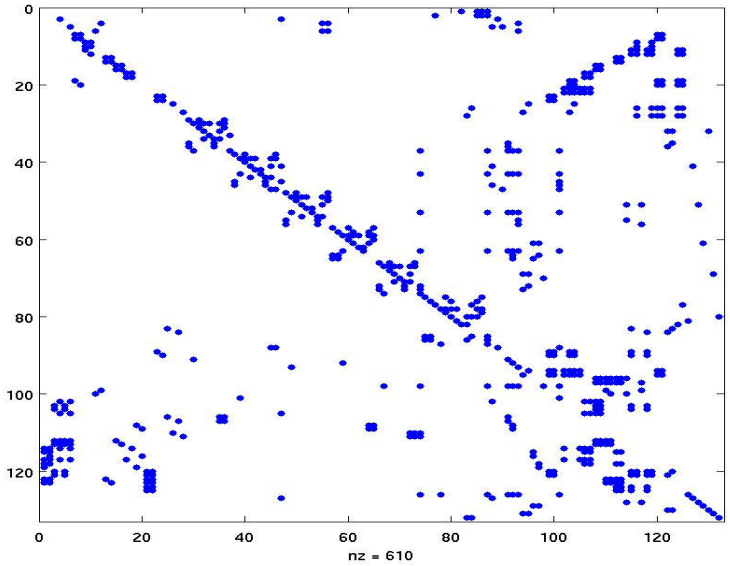

Fig. 23 Symamd Reordered non zero element distribution for the matrix in Fig. 21

Table 22 shows the performance comparison of the computational time in seconds for the three different iterative solvers namely GMRESR, BiCGStab, QMR for the six generator test system. All the three methods are preconditioned versions , with ILU as the preconditioners. In all the three cases the solvers failed for drop tolerance greater than 0.05. The drop

tolerance of 0 indicates complete LU factorization. This suggests strongly how the ILU preconditioners are very ineffective for unsymmetrical matrices as in power system time domain solution. From Table 22 it is clear that the GMRESR with drop tolerance 0.05 gives the best performance among the iterative solvers compared here. Another important observation is that the computational time actually increases for QMR and BiCGStab for drop tolerance 0.05 as compared to drop tolerance 0. This suggests how the LU factors obtained from ILU actually worsen the convergence and it takes more iteration and hence more time for convergence. Another important observation is that the reuse of the LU factors which are already approximate worsened the convergence. For the rest part only comparison with the ILU preconditioned GMRESR with drop tolerance 0.05 is given.

Table 22 Comparison of ILU preconditioned different iterative solvers

Contingency no.	Gmresr_droptol_0 (Secs)	Gmresr_droptol_0.05 (Secs)	qmr_droptol_0 (Secs)	qmr_droptol_0.05 (Secs)	Bicgstab_droptol_0 (Secs)	Bicgstab_droptol_0.05 (Secs)
1	276.85	250.20	256.15	264.69	268.31	262.10
2	195.59	187.29	192.45	190.65	203.44	245.38
3	227.78	206.40	212.37	243.50	220.07	366.11
4	200.61	187.04	193.53	206.91	195.89	213.79
5	283.85	261.7	282.23	383.51	276.83	703.82
6	212.89	207.01	218.77	232.92	225.73	285.38
7	306.25	248.33	265.24	325.21	253.46	471.04
8	257.31	238.47	256.51	310.61	257.05	326.22

Table 23 shows the comparison of the computational time of the multifrontal preconditioned GMRESR solver with the modified multifrontal solver, other direct sparse solvers, and ILU preconditioned GMRESR solver for the six generator test system. Column 5 ,6 and 7 refer to the time taken by the multifrontal preconditioned GMRESR solver when the LU factors were rebuilt depending on the number of iterations it took for the solution to converge in the previous and the current iteration . The number of iteration in column 5, 6, and 7 are 1, 3 and 5 respectively.

Table 23 Comparison of multifrontal preconditioned GMRESR solver with other solvers: 6 generator system

Contingency no.	Gmresr_droptol_0.05 (Secs)	Sparse solvers (Secs)	Modified Multifrontal (Secs)	Multi-GMRESR ITR - 1 (Secs)	Multi-GMRESR ITR - 3 (Secs)	Multi-GMRESR ITR - 5 (Secs)
1	250.20	250.2	33.119	41.14	40.88	44.76
2	187.29	189.3	24.897	33.19	32.29	34.99
3	206.40	210.96	25.780	27.66	29.71	32.69
4	187.04	205.53	24.978	29.89	33.23	34.22
5	261.70	258.19	34.030	43.75	43.75	49.96
6	207.02	209.63	27.210	34.17	35.26	42.66
7	248.33	249.36	32.314	39.46	40.49	43.82
8	238.48	257.85	32.573	43.33	47.10	56.25

Table 24 shows the speed up comparison of the multifrontal preconditioned GMRESR solver with the modified multifrontal solver, other direct sparse solvers, and ILU preconditioned GMRESR solver for the six generator test system. We can see that the developed iterative solver is five to seven times faster than all other ILU preconditioned iterative solvers and other direct sparse solvers. Also the modified multifrontal methods are 1.2 to 1.4 times faster than the multifrontal GMRESR iterative solver.

Table 24 Speed up comparison of multifrontal preconditioned GMRESR solver with other solvers: 6 generator system

Contingency no.	Gmresr_droptol_0.05 / Multi-GMRESR ITR - 3	Sparse solvers/ Multi-GMRESR ITR - 3	Multi-GMRESR ITR – 3/ Modified Multifrontal
1	6.120	6.120	1.234
2	5.798	5.861	1.297
3	6.947	7.101	1.152
4	5.627	6.183	1.330
5	5.981	5.901	1.285
6	5.870	5.944	1.296
7	6.133	6.158	1.253
8	5.063	5.474	1.446

Table 25 shows the comparison of the computational time of the multifrontal preconditioned GMRESR solver with the modified multifrontal solver, other direct sparse solvers, and ILU preconditioned GMRESR solver for the thirty two generator test system.

Table 25 Comparison of multifrontal preconditioned GMRESR solver with other solvers: 32 generator test System

Contingency no.	Gmresr_droptol_0.05 (Secs)	Sparse solvers (Secs)	Modified Multifrontal (Secs)	Multi-GMRESR ITR - 1 (Secs)	Multi-GMRESR ITR - 3 (Secs)	Multi-GMRESR ITR - 5 (Secs)
1	1078.55	944.25	32.928	60.18	64.37	63.03
2	1412.42	1165.93	44.781	73.97	92.26	87.57
3	986.96	828.69	29.252	56.20	56.27	49.33
4	1287.51	928.56	38.524	79.95	76.28	68.51

Table 26 shows the speed up comparison of the multifrontal preconditioned GMRESR solver with the modified multifrontal solver, other direct sparse solvers, and ILU preconditioned GMRESR solver for the thirty two generator test system. We can see that the developed iterative solver is 13.5 to 20 times faster than all other ILU preconditioned iterative solvers and other direct sparse solvers. Also the modified multifrontal methods are 1.6 to 1.8 times faster than the multifrontal GMRESR iterative solver.

Table 26 Speed up comparison of multifrontal preconditioned GMRESR solver with other solvers: 32 generator test system

Contingency no.	Gmresr_droptol_0.05 / Multi-GMRESR ITR - 3	Sparse solvers/ Multi-GMRESR ITR - 3	Multi-GMRESR ITR – 3/ Modified Multifrontal
1	17.921	15.690	1.827
2	19.094	15.761	1.651
3	20.005	16.797	1.686
4	18.793	13.553	1.778

From the above results and analysis it is clear that with proper design of the preconditioner and proper intelligence for its reuse great computational efficiency can be achieved compared to the existing direct and the iterative solvers. We also see that the developed iterative solvers can be highly competitive with the direct solvers in terms of robustness and speed. Also the speed up increases non linearly with the increase in size of the system. We expect that with further improvement in the preconditioner and increase in size of the system iterative solvers would outperform the modified multifrontal solvers also.

CHAPTER 5 MODELING AND PROTECTION

This chapter describes the modeling of the power system components and generator protection adopted for this research. At the outset the chapter describes the component modeling and the formulation of the differential algebraic equations governing the system. Following this the results of an in depth study of cascading events over the past 40 years focusing on generator protection under abnormal conditions are synoptically presented, highlighting the importance of generation protection during the unfolding of such uncontrolled high consequence scenarios. After the historical perspective a detailed description of generator protection modeling used in this research is given. The next section presents the fundamental concepts for island detection and subsequent simulation on each islands formed as a result of the cascading phenomena. The chapter is followed by the results and discussion of the implementation of the above described component modeling, generator protection and island detection and simulation on a test system.

5.1 Component Modeling and Formulation of Dynamic Algebraic Equations

5.1.1 Exciter Model

In this research a simple PI controller is used for generator terminal-voltage control. The block diagram of the exciter is shown below in Fig. 24.

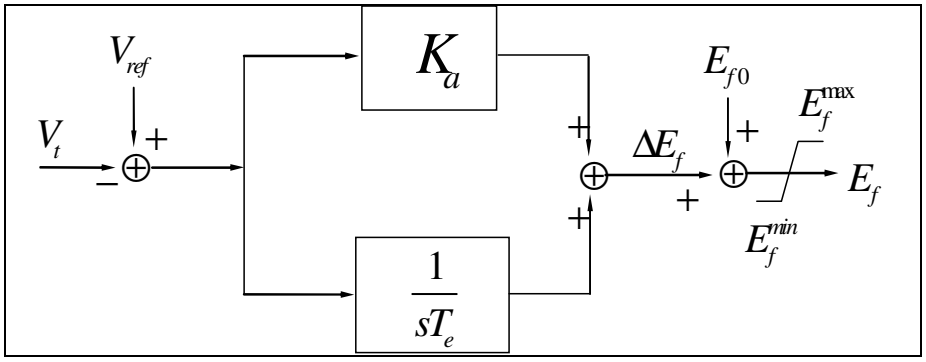

Fig. 24: Block diagram of exciter

5.1.2 Governor Model

The governors are all modeled as a speed integrator with droop ratio *R* as in Fig. 25. T_{CH} is the time constant for hydro-mechanically server, which is modeled as an inertia link. The output of the governor is *Y*, which is the mechanical power input to electric machine. L^g_{ref} is the output of Automatic Generation Control (AGC), which is illustrated in Fig. 26. It is actually the summation of the gate reference $L^g_{ref\,0}$ and the AGC adjustment signal. Here it is assumed that every generator participates in the global frequency adjustment.

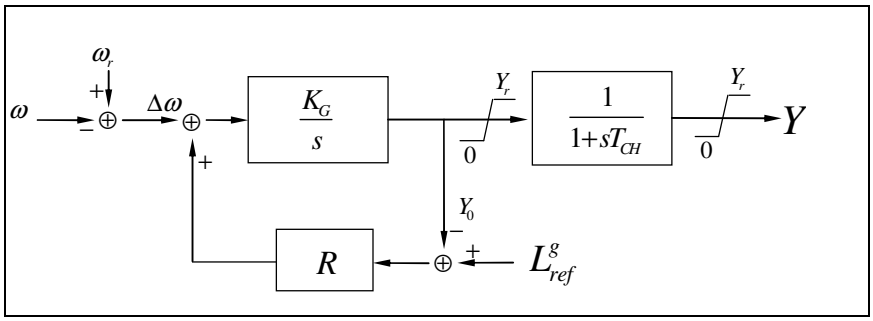

Fig. 25: Governor

5.1.3 AGC Model

Fig. 26 illustrates the AGC model used in this research. The aim of the AGC is to regulate the system frequency to the reference frequency ω_g^{ref}. Any deviation from this value will be sensed by the AGC. The inverse of the time constant in each of the integrators in Fig. 26 is proportional to the size of the unit, for which the output signal is intended. This underlying philosophy is that a larger generator contributes more to regulate the frequency than a smaller generator.

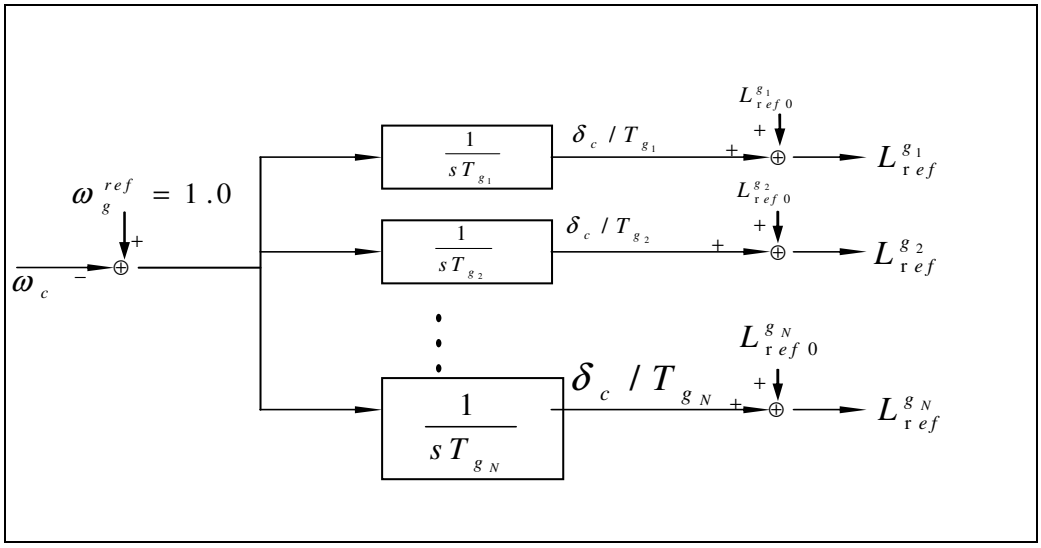

Fig. 26: Block diagram of Automatic Generation Controller (AGC)

5.1.4 Over-excitation Limiter Model

A summed-type over-excitation limiter (OEL) model shown in Fig. 27 is used in this research. The regulating part of the OEL is a pure integrator. It simulates the heat build-up in the exciter. A wind-up limiter is added to the integrator to limit the output of OEL to exciter. The direct output of OEL is not limited because it is a reflection of winding temperature rather than a concrete element that has a physical limit.

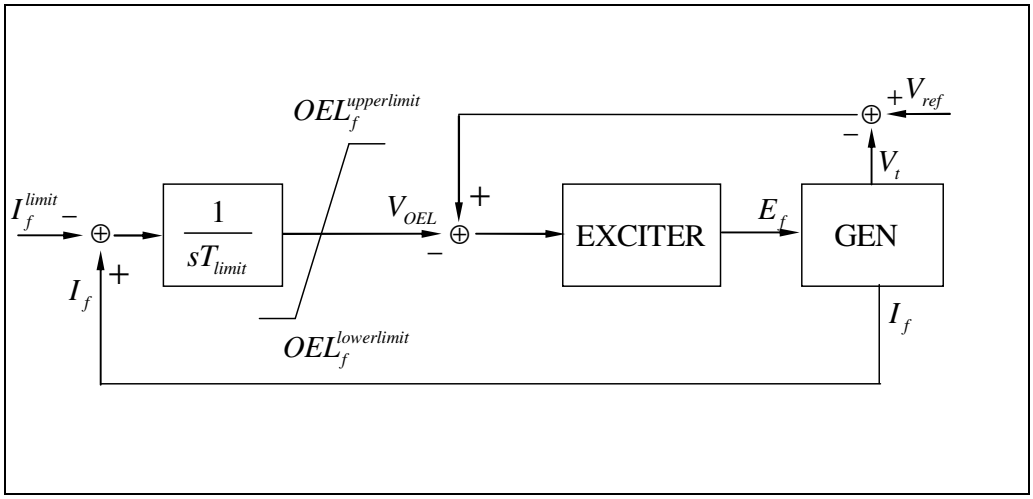

Fig. 27: Over-exciter limiter

5.1.5 Load Model

The loads are modeled as constant active and reactive power injection.

5.1.6 Formulation of Dynamic Algebraic Equations

The equations developed are for all the generations including the exciter, the governor and the AGC models. The two axis model for the generator is used in the present study. For generators, the meanings of the notation are the same as in [25]. The notation for exciter, governor, and the AGC are same as shown in Fig. 24-Fig. 27. The limiter for each variable is implemented as logic in program and is not shown in the above equations.

The set of differential equations are as the same as discussed in equations (47)-(58).

The loads in our test system are modeled as constant active and reactive power injection.

A general power system dynamic algebraic equation (DAE) groups for equations in (47) through (58) are summarized in (59) and (60).

5.2 Generator Protection

5.2.1 Importance of Generator Protection

Power systems are constantly subjected to the transient disturbances due to system component faults, switching of major loads, occasional lightening flashover, intentional sabotage, human errors and unintentional protective relay operation and so on. During this transient period from one steady state to the next the performance of the generator excitation system and the turbine control system play an important role in ensuring system stability. However, the coordination between these and the other control mechanisms with system protection is of prime importance to avert a cascading event [143]. Of particular importance in this long term simulation study is the role of generator protection especially under abnormal conditions. Along with coordinating with the system to avoid misoperation, the protective relays must protect the generating plant damage which would otherwise seriously hamper restoration and cause huge economic loss.

In many of the past blackouts the operation of the generator protective relays stands out as one of the very critical events in the sequence of events leading to those catastrophic scenarios. Many times the unexpected relay operation has been due to the lack of coordination between the control and protection function of the generator with that of the system [144]. This research effort reports conclusively the importance of generator protection modeling in dynamic simulation studies to trace the system trajectory following a transient disturbance to the system. This study is also important in planning out control strategies to interrupt the unfolding of a cascading event.

5.3 Historical Evidence/Perspective

This section presents a historical perspective, over the past 40 years, of the role of generator protection under abnormal conditions in the unfolding of the cascading events. The purpose of this section is not to describe any of these catastrophic events in detail which would be voluminous, rather in this section an attempt is made to report the critical protective relay operations for generator protection leading to these blackouts. The purpose of this study is to substantiate the importance of generator protection modeling in the dynamic simulation study of the power system.

5.3.1 Northeast Blackout November 9-10, 1965

This information was obtained from [144, 145, 146, 147, 148, 149]. An out of step condition developed due to continued acceleration of The PASNY and Ontario Hydro generators at Niagara Falls, and caused two 345 kV lines between Rochester and Syracuse to be opened by distance relay action; all parallel underlying lower voltage lines were also tripped. Four seconds after the initial line trip, five out of the sixteen PASNY-Massena generators tripped and the system islanded into 5 areas as shown in Fig. 28.

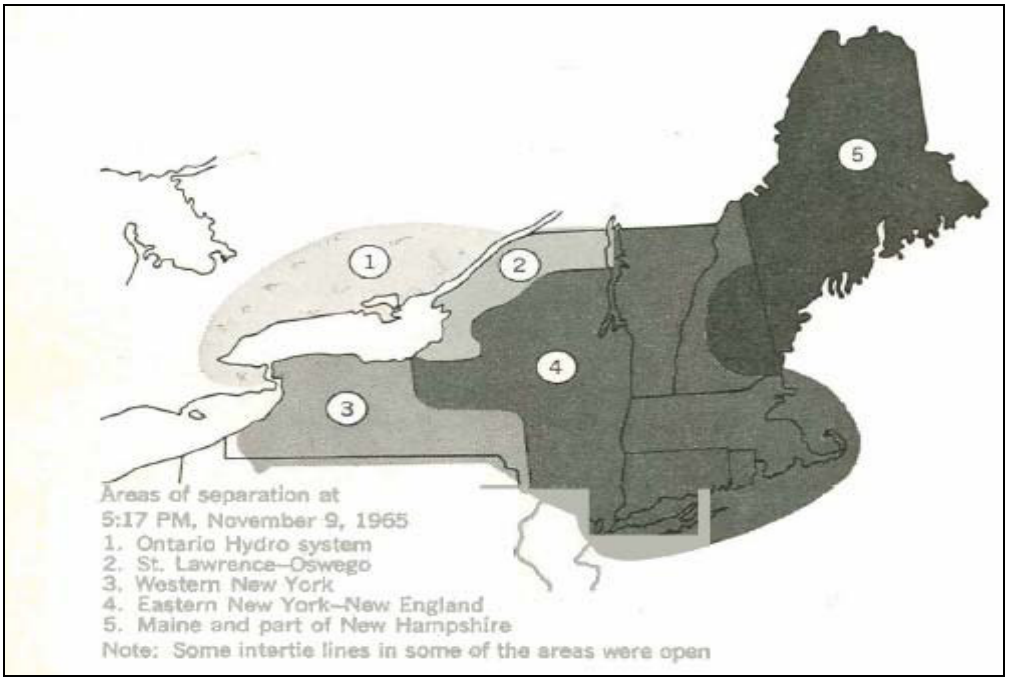

Fig. 28: System islanding into 5 areas [144]

In area 3 an *overfrequency* condition developed due to large generation excess and thus all steam power plants were tripped by *overspeed protection*. This was followed in quick succession by simultaneous tripping of 10 generators at Beck due to excessive governor operation and tripping five PASNY-Niagara pumping-generating units by *overspeed* protection. Thus an underfrequency condition ensued and the whole area blacked out. Similarly in area 4 there was complete blackout since all the generators tripped within 11 minutes due to *undervoltage* and *underfrequency protection*.

5.3.2 June 5, 1967, PJM Disturbance

About 26 generators were automatically tripped during this disturbance—12 by loss-of-field relaying, six due to abnormal current or voltage, four by turbine protection, and four by other protective devices [143].

5.3.3 North American Northeast Blackouts of 1977

This information was obtained from [144, 150, 151, 152]. After a sequence of line trips and a generator trip, the loss of a generator, Ravenswood #3 unit, due to the *loss of field* relay operation was very critical because it was responding to sharp voltage fluctuations

accompanying load shedding. This caused sharp frequency drop up to 54 Hz and Arthur Kills #3 unit tripped due to *underfrequency protection*. This was followed by immediate tripping of remaining generators in the islanded Con Edison system.

5.3.4 French Blackout December 19, 1978

The sequential tripping of a 400 kV line and three 225 kV lines due to overcurrent protection followed by the tripping of a hydro unit of Revin power plant due to generator *overcurrent protection* led to this blackout [143].

5.3.5 Tennessee Disturbance August 22, 1987

Voltage controlled/restrained overcurrent and distance relays on generators tripped [143]. This started a cascading effect that eventually tripped all source lines into TVA's South Jackson, Milan, and Covington substations [153].

5.3.6 The Tokyo Blackout 1987

After the initial tripping of lines and transformers due to improper operation of zone 4 impedance relay, the loss of the load caused a frequency spike and due to overfrequency generator protection the units Kashima #6 and Kawasaki #6 tripped and Kashima #4 was manually stopped [143, 153].

5.3.7 PECO Disturbance February 21, 1995

During the second fault, the Limerick 1 and 2 generators were tripped by ground overcurrent relays connected to their step-up transformers [143].

5.3.8 Western System July 2, 1996

This information was obtained from [4, 144, 154, 155]. At 1:25 P.M. on July 2, 1996, a huge disturbance occurred in WSCC system. A short circuit occurred on a 345 kV line between the Jim Bridger plant near Rock Springs and it was tripped successfully. This disturbance caused a parallel line to be tripped also. An SPS scheme was initiated after the tripping of the two lines, which shut down two generating units at the Jim Bridger plant. About 24 seconds after the fault, the outage cascaded through tripping of small generators

near Boise plus tripping of the 230 kV line from Western Montana to SE Idaho. . The *undervoltage* and *inter-area oscillation* problem developed quickly throughout the system. This was further aggravated by false *tripping* of 3 units at McNary. Within a few seconds, five islands were formed and as a result. 2,500MW power was lost and 1,500,000 customers were affected.

5.3.9 Western System August 10, 1996

This information was obtained from [4, 156, 157]. Due to poor design of *overexcitation limiters* many generators tripped at inappropriate time. The most critical event was sequential tripping of 13 McNary generators due to the *generator field current protection* scheme which operated to trip the generators instead of limiting the field current. In the southern islands, many generators tripped undesirably following underfrequency load shedding. A total of 175 generating units were tripped and 5,700,000 customers were interrupted.

5.3.10 Chilean Blackout May 1997

The main cause identified for the voltage collapse in the Chilean Interconnection System was the overexcitation limits in the generating units at Colbun-Pehuenche [143].

5.3.11 North American Northeast Blackouts of August 14, 2003

Eastlake 5 unit tripped due to *overexcitation protection*. Machines in Detroit pulled out of step and lost synchronism. Among other factors overreaching impedance relays (zone 2 and zone 3) and a lack of coordination between *generation protection* and transmission protection systems led to this widespread blackout [158].

5.3.12 Blackout in Southern Sweden and Eastern Denmark – September 23, 2003

This information was obtained from [159, 160, 161]. A nuclear plant at Oskarshamn tripped at 12:30 due to technical problems and the north south flow on the west side increased. Coincidently the switching device at Horred substation broke apart with another nuclear plant and two important north-south connections lost. Due to loss of transmission path to the west coast the east side became overloaded. Thus within seconds, the

underfrequency and *undervoltage* generator and other grid protections reacted and resulted in a complete voltage collapse.

5.3.13 Italian Blackout September 28, 2003

One of the main lessons learnt after this severe disturbance was that a thorough and accurate testing of protecting devices and governors should be performed during the commissioning of the power system [162, 163, 164, 165].

5.3.14 Greece July 12, 2004

The critical event occurred at 12:37 when Unit 3 of Aliveri power station serving the weak area of Central Greece tripped *automatically* [166]. At 12:38 the remaining unit in Aliveri was *manually* tripped. At 12:39 voltage instability leading to collapse happened and the system was split in two by line protection devices and disconnected the generation from the separated Southern part. Thus the blackout spread into the area of Athens and Peloponnesus.

5.3.15 Australian Blackout Friday August 13, 2004

The initiating event was an internal fault in a transformer which triggered the tripping of three generators due to *generator differential protection* [144,167]. Another independent generator tripped due to premature *negative phase sequence protection* as a result of a faulty timer circuit. Due to sudden generation loss the frequency dropped and Underfrequency load shedding along with generator trippings due to *underfrequency protection* and *automatic voltage regulator protection* followed.

5.3.16 Central-South System Collapse of the Peninsular Malaysia Grid System January 13, 2005

After the initial circuit trippings, the North East and the Central South sub system were left interconnected only through the four transformers at Port Klang [144]. The sub systems began to pull apart as the generators in the North East went *out of step* with those in the Central South sub system. Soon they separated with each sub system having load and generation imbalances. In the Central sub system the frequency spiraled down due to

generation deficiency and all the generators tripped. However it was not due to underfrequency protection. The system frequency fluctuations disrupted the fuel to air ratio of premix burners, resulting in a very lean mix of fuel and air that caused flame instability. Along with this there were other factors involved and finally the *turbine protections* acted to trip the turbines due to high vibration in the combustion chamber. The major disturbances in 1996, 1998, 2001 and 2005 on the TNB grid were due to either inadvertent tripping of the gas turbine based plants or undesirable performance of the gas turbine based units.

5.3.17 Blackout in the Swiss Railway Electricity Supply System June 22, 2005

After the initial event the SBB system was split into two parts, the Southern and the Northern [144]. The southern part had an excess of 200MW which led to frequency increase and thus the *overfrequency protection* tripped most of the generators were tripped within eight seconds and the whole area was blacked out. On the contrary the northern part was generation deficient and to maintain the stability the generation from Châtelard, Vernayaz and Etzel power plants and the import from Germany increased. However shortly after this the generators were tripped due to *overload* and the tie line from Germany was opened causing complete system shutdown.

5.3.18 UCTE Major Disturbance of 4 November, 2006

In the Western Subsystem load generation imbalance led to frequency decline to 49 Hz and *underfrequency* tripping of pump storage hydro units and large portion of wind and cogeneration units [144]. The North East Subsystem had huge excess of generation up to 10 GW and the frequency initially increased to 51.4 Hz. To the advantage, wind generations tripped due to *overfrequency protection* and the frequency recovered. But unfortunately soon some of the wind generators automatically reconnected as the frequency recovered, and the frequency once again began to increase.

5.4 Generator Protection Types and Strategies

In this research the main concern is the generator protective relay operation under severe disturbance conditions. In the previous section on the synoptic study of the past blackouts,

the specific generator protections that operated and which were critical events in the unfolding of the cascading were identified in italics. Of all them we would focus on a subset which is most important and frequent in such critical scenarios. They are enumerated below and are followed by a detailed discussion of each of them. In this study the generator protection studied are as follows:

- Overexcitation
- Overcurrent
- Overvoltage
- Undervoltage
- Overfrequency
- Underfrequency
- Out of Step

In summary the generator protection must be coordinated with the allowed voltage and frequency regulating ranges. Thus the generator voltage protection is set outside a threshold of about ±10% of nominal voltage and the frequency related protection generally operates within ±5% of the nominal speed. The overcurrent protection is delayed with respect to the automatic voltage regulator and governor dynamics. Most of materials discussed below on the different generator protection under abnormal conditions come from references [143, 168, 169, 170, 171, 172, 173, 174, 175, 176, 177, 178, 179].

5.4.1 Overexcitation (Volt per Hertz protection) Device 24

Generators and transformers require an internal magnetic field to operate. The core of a transformer and the stator of a generator are designed to provide the magnetic flux necessary for rated load. Deviations in frequency, power factor and voltages outside the intended limits of generator and transformer operation cause thermal stress and insulation degradation. An overexcitation condition occurs when the generator or the transformer equipment is operated such that flux levels exceed the design values. These design limits are specified in terms of the ratio of the voltage to frequency (V/Hz) applied at the terminals of the equipment.

The core area and the magnetic properties of the core material define the excitation capability of a generator or transformer. The core is designed to support a flux density necessary for full load operation and to dissipate the heat associated with that excitation level.

Standards ANSI/IEEE C50.13 (generators); C57.12 (transformers); IEEE Std C50.12, 4.1.5; IEEE C50.13, 4.17; IEEE Std 67 do not specify V/Hz limits for transformer or generators directly, but the voltage limits specified for this equipment at rated frequency imply continuous V/Hz limits. For instance the standards require a generator to be capable of operation at rated kVA, frequency and power factor with terminal voltage variations of ± 5%. Continuous operating capabilities are indicated below:

- Generators: 1.05 p.u. (generator base);
- Transformers: 1.05 p.u. on transformer base at full load, 0.8 pf or 1.1 p.u. at no load at the secondary terminals of the transformer.

Transformers and generators can withstand overexcitation for a short time. Maximum allowable component temperature and the rate of temperature rise in these components determine the limits. However the limiting component vary with design, and this has prevented the standardization of on overexcitation withstand characteristic and it must be obtained from individual manufacturers.

1) Overexcitation and Overvoltage

A generator operating at no load with rated voltage and frequency would have one per unit flux and is said to be operating at one per unit excitation. Overexcitation would result from high voltage at rated frequency and from rated voltage with low frequency. Overexcitation condition is not the same as overvoltage condition where the dielectric breakdown is the concern. Overexcitation can occur without notice being a function of voltage and frequency. Generators can be subjected to repeated overexcitation by inappropriate operating practices or operator error without a disruption to operations. The resulting thermal degradation of insulating material is cumulative. The transformer or generator that survives a serious overexcitation event or many small events may fail as a result of a moderate event or during normal service.

2) Causes of overexcitation

It usually occurs during periods of reduced frequency operation such as start up or shutdown under automatic voltage regulator control. CTGs with converter starting may be subjected to very low frequencies (such as 2 Hz) during starting. Another classic V/Hz damage scenario is the failure of the field breaker to open for shutdown. Failure within voltage regulator and associated circuits can cause damaging overexcitation to the synchronized generator and connected transformer. The loss of generator voltage signal to the regulator is an example.

Load rejection with the automatic voltage regulator in service and a capacitive load can cause overexcitation. The capacitive load could be shunt capacitor used for voltage control or VAR support or it could be the charging current for a high voltage transmission line. The V/Hz may exceed 125%.

Overexcitation Due to Overvoltage: When a power system island is formed during a major system disturbance, it may have excessive VARS in relationship to VAR load. These VAR sources are shunt capacitors, as well as VARS produced by generators within the island. Sudden power system disturbances can also unload transmission lines whose shunt capacitance can contribute to high VAR levels within the island. Ideally, control actions, such as tripping of shunt capacitor banks within the island, will reduce system voltage to within generator and transformer continuous capabilities. At power plants, automatic generator excitation control will reduce VAR output to control voltage within the island. If required, generators can operate underexcited and absorb VARS. The amount of VARS that the generator can absorb is limited by the generator underexcited capability, which is limited by stator end iron heating. Other considerations, such as steady-state stability limits and loss of excitation protection can also limit under excited generator operation. The minimum excitation limiter in the voltage regulator limits the VAR intake level. This is a settable control within the generator voltage regulator that needs to be properly adjusted, to coordinate with generator capability and steady state stability limitations. If during a major system disturbance, the generator excitation control is in manual, none of the generator control actions described above will take place and the generator VAR output will not be reduced to lower system voltage. If a significant number of generators within an island formed during a major disturbance are operating with their voltage regulator control in

manual, it will greatly exacerbate high voltage problems with the island. If high voltage during a major system disturbance is not reduced to within generator and transformer capabilities, protection is provided to trip generators and their associated transformers.

Overexcitation Due to Underfrequency: A volts per hertz overexcitation condition can also occur due to low system frequency resulting from a major system disturbance. This, however, is a less likely cause than high voltage. Its trip time is usually much slower than under frequency relaying.

3) Damage

When a transformer or a generator is operating within rated parameters, the flux in the core will be below the saturation flux density and it will confine itself to the core since the core permeability will be much higher than that of adjacent structures. Core heating will also be within design limits. Flux produced in excess of design limits will saturate the core and will spill into the surrounding air space and stray flux would be induced into non-laminated metallic structures around the core which are not designed to carry flux. Damage to a laminated core due to increased losses requires extreme overexcitation for a significant time. However eddy currents induced in non-laminated structures can cause severe component damage and quick thermal runaway.

In a generator the most damaging spill flux will appear at the ends of the stator core. Also, the excessive induced currents within the stator laminations can create voltage gradients between core laminations sufficient to break down the inter-laminar insulation. If it occurs the core will be permanently damaged, rendering it incapable of carrying even normal flux without arcing, increased heating and further deterioration. Stator core restacking is a very expensive procedure. Field current in the generator can also become excessive.

4) Protection

Protection for a generator or generator and connected transformer against overexcitation can be provided in several forms such as V/Hz relaying at the generator terminals, by V/Hz limiting circuitry within the automatic voltage regulator, or by relay sensing machine field current or voltage.

Field Monitoring Relays: Relays within the excitation system can provide limited overexcitation protection by monitoring field current or voltage. This relaying would be set

slightly above the field current or field voltage necessary to produce rated generator output voltage at no load. Tripping would be through a timer with a few second delay. This relaying would be in service only when the generator is offline to provide overexcitation protection during startup and shutdown.

V/Hz Limiter: V/Hz limiter circuitry is within the automatic voltage regulator. It senses voltage and frequency at generator terminals and adjusts the generator field as required to prevent operation above a preset V/Hz value. Many limiter designs exist and it may be in service at all times or it may be in service only when the generator is offline. It functions only in the automatic control mode. Care should be taken while setting the limiter so that the short time overexcitation capability of the generator can be utilized during system disturbances. When the excitation control is out of service then V/Hz relaying is used to protect the station transformers and the generator.

V/Hz Relay Application (Device 24): If the prime mover and associated mechanical systems are capable of withstanding a load rejection, the V/Hz relaying should trip the field and generator breakers. The prime mover need not be tripped. This will facilitate a rapid restart of the unit after the cause of the overexcitation is cleared. If the mechanical system cannot withstand the load rejection associated with the generator trip, a prime mover trip must be initiated. V/Hz relaying for the protection of the generator is applied at the generator terminals. They have either the definite time or inverse time characteristic. Either characteristic must be set to initiate tripping before damage occurs at the maximum level of overexcitation anticipated. The inverse time characteristic is preferred to allow maximum utilization of the short time capability of the generator. The definite time characteristic overprotects at low levels of overexcitation, thus jeopardizing unit availability during system disturbances.

Practical Consideration: The reset is intended to mimic the thermal characteristic of the protected generator or transformer. Assume that a given overexcitation condition will damage equipment in 60 seconds and therefore V/Hz relay is set to operate in 50 seconds. But the V/Hz limit violation is removed after 40 seconds and reappears after 10 seconds. If the relay is reset after the initial violation recedes, then upon recurrence of the event the equipment will be subjected to the overexcitation condition for full 50 seconds before

tripping. This means the equipment is exposed for 90 seconds. This would cause damage to the equipment. Also the heat generated in the protected equipment will not dissipate in short time between events. Therefore the memory feature is required for the relay to reset at a rate comparable to the cooling rate of the protected equipment.

5) Settings

The system operating voltage range extends to the continuous V/Hz capability of generators and transformers. Thus the setting must be done in a way to guarantee that overexcitation protection will not actuate when the system is operating at the maximum continuous V/Hz capability of the equipment. To accomplish this, the settings must be above the applicable limit with sufficient margin to allow for relay and potential transformer errors. The setting should also include an appropriate safety margin. The resulting V/Hz settings can be substantially above the continuous V/Hz capability.

The delay for the overexcitation protection should allow for the maximum utilization of the short time capability of the protected equipment. Overexcitation can occur during a system disturbance because of field forcing, reduced system frequency or both. In this situation the output of every generator is very critical to system recovery. Protective relays that do not optimize the equipment capability reduce the reliability of the entire power system. The setting for the generator is straightforward. The V/Hz limit at the generator terminal is 105% regardless of the load condition. The initiation setting for the pickup of the relay should be set above 105%+margin (device error + PT error + safety margin). Short-time overexcitation withstand curves provided by manufacturers are often based on actual core limits. When such curves are applied at the equipment terminals, they represent a no load condition. The application of such curves under load may be optimistic. When using short time curves, the applicable conditions for the curves must be known.

Time delay settings: The V/Hz relay must be set with sufficient time delay to override system fault voltage transients and to allow the voltage regulator to restore normal voltage following load rejection. These minimum delay conditions are normally met when the delay is set to maximize utilization of the short time overexcitation capability of the equipment. However the determination of anticipated maximum excitation level would require a dynamic study involving the generator, voltage regulator and governor, saturation

characteristics of the generator and transmission parameters. In practice the maximum V/Hz condition at the generator terminals can be estimated from the generator's open circuit saturation curve. Generally the shape of the curve is such that the saturation of the stator will limit the terminal voltage to less than about 1.25 pu. Therefore at 1.25 pu the limiter if installed should act to reduce the excitation before relaying initiates a generator trip, otherwise the relay must initiate a trip before the short time withstand of the generator or connected transformer.

5.4.2 Overcurrent

The continuous output capability of a generator is expressed in kilovolt-amperes (kVA) available at the terminals at a specified frequency, voltage, and power factor. For hydrogen-cooled generators, the output rating is usually given at the maximum and several lesser hydrogen pressures. For CTGs, this capability is given at an inlet air temperature in the range of –20° C to 50° C. In general, generators may operate successfully at rated kVA, frequency, and power factor for a voltage variation of 5% above or below rated voltage.

Under emergency conditions, it is permissible to exceed the continuous output capability for a short time. In accordance with IEEE Std. C50.13, the armature winding short time thermal capability is given in Table 27.

Table 27: Overcurrent relay settings

Time (seconds)	10	30	60	120
Armature current (percent)	218	150	127	115

where 100% current is the rated current of the machine at maximum hydrogen pressure. In some instances, generator overload protection may be provided through the use of a torque controlled overcurrent relay that is coordinated with the IEEE C50.13 short time capability curve. This relay consists of an instantaneous overcurrent (IOC) unit and a time-overcurrent unit having an extremely inverse characteristic. The instantaneous unit is set to pick up at 115% of full-load current and is used to torque control the time-overcurrent unit. The instantaneous unit dropout should be 95% or higher of pickup setting.

The time-overcurrent unit is set to pick up at 75% to 100% of full-load current, and a time setting is chosen so that the relay operating time is 7.0 s at 218% of full-load current.

With this approach, the relay is prevented from tripping for overloads below 115% of full-load current and yet provides tripping in a prescribed time for overloads above 115% of full-load current. The overcurrent relay settings should be provided to transmission system protection personnel for coordination purposes. An overload alarm may be desirable to give the operator an opportunity to reduce load in an orderly manner. This alarm should not give nuisance alarms for external faults and should coordinate with the generator overload protection if this protection is provided.

For air-cooled generators that may operate in a wide range of ambient temperatures, it is necessary to coordinate the IEEE C50.13 thermal capability and the relay setting with the increased capability of the turbine and the generator at reduced ambient temperature. Conversely, it may be difficult to protect the generator for its reduced capability when the ambient temperature is high.

5.4.3 Overvoltage

Voltage regulators control the generator excitation levels to ensure the terminal voltage is maintained at a level that is within the rated operating range of the generator. Voltages outside that range could result in damage to the generator or unacceptable power system conditions. Voltages may exceed rated levels during system disturbances, while the generator excitation system is limited by its internal controllers, or is operating in a manual control mode. Abnormal voltage protection for generators must coordinate with any external control systems regulating the system voltage that would help to restore normal voltage levels at the generator terminals.

Abnormally high voltages could cause excessive dielectric stress on the generator or unit transformer insulating materials and result in insulation failure. As discussed earlier overexcitation and overvoltage are related but not the same. Overvoltage condition may occur without necessarily exceeding the flux limits. For example in hydrogenerators an overspeed of 200% or more can occur upon load rejection leading to serious overvoltage condition especially if they are operating in manual excitation control mode.

Overvoltage protection is sometimes provided to protect the generator from excessive dielectric stress. In addition to coordinating with external system voltage control devices,

generator overvoltage protection must also coordinate with internal excitation system voltage controllers. Such coordination is not difficult as long as the protection is set to pick up at a higher level than the maximum setting on the generator voltage reference control and the setting of the excitation system volts per hertz controller at a fundamental frequency (if this auxiliary control device is provided). Coordination with exciter controls for temporary excursions above the maximum controlled voltage level is easily achieved with even small time delays on the protection, because the control devices are normally quite fast (exerting control within less than 1 s).

A major cause of overvoltage is sudden loss of load. Power equipment involving iron (rotating generators, transformers) operate close to the knee of their saturation curves. Thus small overvoltages result in large increases in exciting current and cause major damage. Typical permissible overvoltage at no load is given in Table 28

Table 28: Typical Overvoltage limits

Generator	
105%	Continuous
110%	30 minutes
115%	5 minutes
125%	2 minutes

Instantaneous overvoltage setting should be about 106%-110% of rated voltage to ensure prompt removal.

5.4.4 Undervoltage

Undervoltage conditions are not usually harmful to generators themselves, so direct undervoltage protection is not normally provided for them. However sustained operation of a generator with terminal voltage lower than 95% of its rated voltage may cause reduction in stability limits, import of excessive reactive power from the grid to which it is connected and can lead to malfunctioning of voltage sensitive devices and equipments. Also, overheating due to extended operation at low voltages may damage the auxiliary motors for turbine generator sets. Auxiliary supplies are therefore sometimes monitored by undervoltage relays that may trip the generator off line to protect the motors.

Auxiliary undervoltage tripping is usually applied at nuclear generating stations, where the protection of safety related auxiliary equipment is of paramount importance. The undervoltage relays are typically set close to 0.9 p.u. of normal operating voltage, with time delay to prevent tripping during successful clearing of external faults. However, this setting can cause tripping during system disturbances involving sustained undervoltage conditions.

5.4.5 Overfrequency

Off nominal frequency operation is a result of load generation mismatch. Turbine operation capabilities at abnormal frequency are usually more restrictive than generators and transformers. Operation of a turbine between 59.5 and 60.5 Hz (in a 60-Hz system) is considered within the unrestricted time operating frequency limits, whereas the operation above 60.5 Hz and below 59.5 Hz is regions of restricted time operating frequency limits. Continuous operation in this region under generator-loaded condition is not recommended.

Overfrequency is usually the result of a sudden reduction in load or unit full load rejection and, therefore, corresponds to light-load or no-load operation of a generator. Overfrequency operation is less of a concern than underfrequency operation. This is because normal frequency can be quickly restored by reduction in generation by operator or governor control action. Overfrequency increases ventilation and therefore the load carrying capability is increased without the danger of overheating. Also the flux density required for a given terminal voltage is reduced.

As an example overfrequency operation or overspeed operation is a concern for a hydro turbine. A hydro turbine typically has a huge mass and high kinetic energy of water in the penstock. A sudden loss of load on it accelerates the turbine- generator mass and results in an overspeed of up to 150%. On a hydro turbine, the input energy is a large mass of water traveling at significant speed. A rapid closure of the gate would result in water hammer with a pressure spike that would damage the penstock. Consequently, the minimum and maximum design pressures for the penstock limit the rate of gate movement. However, if a failure occurs within the gate or governor system, the hydro unit could attain a speed of 200% rated, incurring major damage.

5.4.6 Underfrequency

Frequency decay is a generally a result of a system disturbance caused by the loss of a large generation resulting in system separation and overloading. The generators may be subjected to prolonged periods of underfrequency operation which pose a serious threat to the turbines and other auxiliaries along with the generator. Underfrequency operation reduces ventilation, increases overheating and reduces the load carrying capability of the generators.

The generators can operate up to 0.95 pu rated speed for prolonged periods without overexcitation if the output is reduced proportional to speed at rated terminal voltage. From 0.95 pu to 0.90 rated speed, both output voltage and current should be reduced in proportion to speed, thus reducing output capability by the square of the speed reduction [177].

The standards do not specify generator capability at reduced frequencies, but this information can be made available from the generator manufacturer. The reduction in output capability coupled with possible overloading of the generator during a system disturbance may result in thermal damage to the generator if its short time thermal capability is exceeded.

1) Underfrequency Turbine Capability

Generally the turbines are considered to be more restrictive than the generators they drive at reduced frequencies because of possible mechanical resonances in the many stages of turbine blades. These limitations usually apply to steam turbine generators. Combustion turbine generators (CTGs) in general have greater tolerance than steam units for underfrequency operation.

Combustion turbine generators: They can usually operate down to 57 or 58 Hz for extended periods of time. The specific underfrequency limit should however be consulted from the manufacturer for each CTG. However, CTGs are frequently limited by combustion instability and/or sharply reduced turbine output as frequency drops due to reduced airflow through the turbine. Loss of air flow will result in immediate unit trip following the detection of a change in axial rotor position, shaft and/or bearing vibration, loss of flame in the combustor(s), or excess temperature of the turbine. One manufacturer estimated a 17% loss in output at 55 Hz. In general, there are no restrictions on hydrogenerators. Combustion turbines (particularly

under 200MW) have limited number of blade sizes and, therefore, have fewer resonant frequencies.

Steam turbine generators: Of all turbines steam turbines are most adversely affected by underfrequency operation. Damage due to blade resonance is of primary concern in the turbine blade design. Resonance occurs when the frequency of the vibratory stimuli and the natural frequency of a blade coincides or are close to each other. The steam flow path is not homogeneous due to physical irregularities in the flow path and this produces cyclical force to the blades. At resonance the cyclical forces increases the stress and the damage to the blades is accumulated and may appear as a crack of some parts in the assembly. Although these cracks especially in tie wire and blade cover may not be catastrophic in these areas but they can alter the blade tuning such that resonance could occur near rated speed.

Every turbine blade has numerous natural resonance modes, namely tangential, axial, and torsional. Each mode has a natural frequency that varies with the physical dimensions of the blade. Short blades in the high-pressure and intermediate pressure stages of the turbine can be designed to withstand a resonant condition. However the longer turbine blades associated with the low pressure turbine are prone to damage by prolonged abnormal frequency operation. These blades are protected by tuning their natural resonant frequencies away from rated speed. These blades generally determine the turbine's vulnerability to under frequency operation.

Standards do not specify short time limits for over-or underfrequency operation. The manufacturer of the specific turbine must provide this data. Reference [178] lists the following limitations for one manufacture's turbines as:

- 1% change (59.4–60.6 Hz), no adverse effect on blade life
- 2% change (58.8–61.2 Hz), potential damage in about 90 minutes
- 3% change (58.2–61.8 Hz), potential damage in about 10–15 minutes
- 4% change (57.6–62.4 Hz), potential damage in about 1 minute

Reference [179] states that with a 5% frequency deviation, damage could occur within a few seconds. These withstand times are not typical. Limits vary dramatically among manufacturers, as can be seen in Fig. 29, which includes limitation curves from four manufacturers.

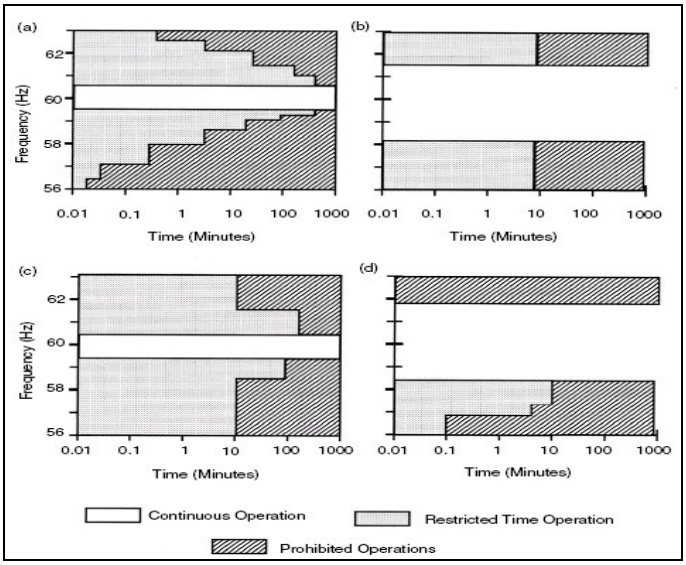

Fig. 29: Steam Turbine Partial or Full-Load Operating Limitations During Abnormal Frequency [176]

Time spent in a given frequency band and hence the fatigue damage is cumulative and is independent of the time accumulated in any other band. For each incident, the first ten cycles in a given frequency band are not accumulated since some time is required for mechanical resonance to be established in the turbine blades. The fatigue life is used up during abnormal underfrequency operation and a series of such events influence the total fatigue life, as the first underfrequency event will weaken the turbine blades and reduce the number of cycles to failure for subsequent events.

2) Settings

The settings should be such as to coordinate with the automatic load shedding on the system and at the same time provides protection for each band of the manufacturer's withstand characteristics. It is also important to take into account the past history of the turbine with respect to the accumulated vibratory stresses in each band of underfrequency operation.

The first line of action against the underfrequency protection is automatic load shedding. This is continued until there is no mismatch between the load and the generation. It is designed based on the frequency decay and the rate of frequency decay. It is generally employed in steps. However due to the extreme complexity of the power system it is extremely difficult to reach an exact match between load and generation especially during

cascading events when several islands are formed with different load and generation mismatch. Moreover this island formation may be different can conceived in the planning stage for the automatic load shedding. Finally the frequency decay is also oscillatory and non homogeneous. Thus second line of defense in the form of backup protection is essential and is discussed in the following paragraph.

The backup protection employs a multilevel underfrequency tripping scheme. A separate time delayed underfrequency function is required for each band on the manufacturer's limit curve. The scheme for timers used in this research is one of cumulative timers to store a history of the operating time in each protective band in a nonvolatile memory. This scheme takes full advantage of the underfrequency capability of the prime mover and is only available in microprocessor relays. The timers set near the maximum allowable time for the band they protect. This strategy aims at maximizing the availability of large units during system disturbances, thus enhancing the power system's ability to ride through such disturbances. Fig. 30 shows a six-level accumulated time scheme. Underfrequency trip settings are slightly above the start of each band, and timers are set slightly below the total allowable time for each band. When the cumulative operating time in a band for all previous underfrequency events plus the current event equals that band timer setting, the scheme will operate to trip the generator. The operation of this scheme indicates that the blades associated with the actuated band are at the end of their useful life. At a minimum, a complete inspection of the blades is indicated.

The first line of defense is preferred as long as the disturbance can be successfully handled by it.

The commonly used timer schemes do not have memory. They measure the duration of current frequency operation and then resets to zero. Also they keep on accumulating the time as long as the frequency remains below their actuation limit. This does not correspond to the actual behavior of the turbine. Hence it is a compromise protection scheme.

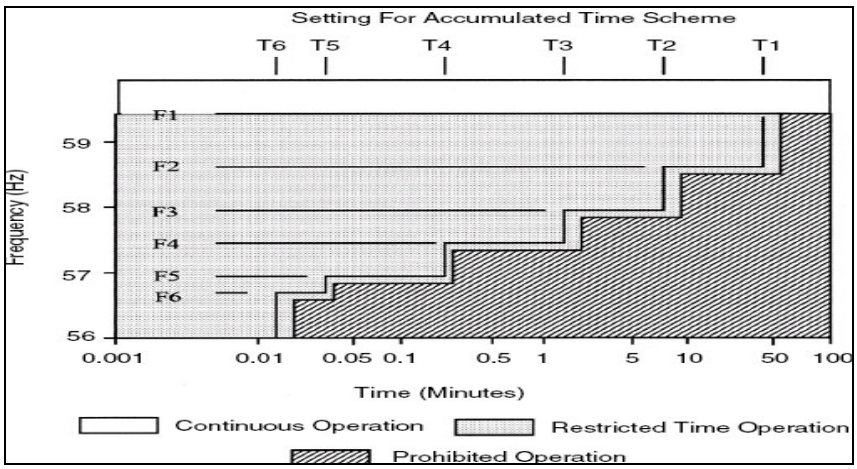

Fig. 30: Time accumulation based Timers [170]

5.4.7 Out of Step

The discussion on out of step is taken mainly from references [143] and [170]. Prior to the 1960s, electrical centers were normally found on the transmission system and out-of step protection was provided by line relaying without the need for trip generation. Over the years, the transmission system became stronger. Generator and GSU transformer impedances have increased because the improved cooling technology provided greater MVA capacity from physically smaller units. As a result, the electrical centers on many systems have moved into the GSU transformer and the generator itself, significantly increasing the stresses on both the components. These swings would not be detected by network protection, thus the need for out-of-step protection at the generator.

Out-of-step protection may also be required at the generator if the electrical center is located beyond the GSU on the transmission system, but the transmission relaying is slow or incapable of detecting the out-of-step condition. Also, the overcurrent relays used for generator protection do not provide reliable loss of synchronism detection. Although currents may be high enough to actuate an overcurrent relay, tripping will depend on the duration of the excess current, which is determined by the slip frequency. The operating time of an overcurrent relay will normally exceed the duration of the current pulse each slip cycle. If the condition persisted for many slip cycles, an electromechanical overcurrent relay might “ratchet” closed and trip the generator. Solid-state and microprocessor relays with fast reset characteristics will not ratchet.

Differential relays will not detect an out-of-step condition because the infeed and outfeed currents within the differential zone are equal. Following a system disturbance, the generator rotor angle will oscillate as the generator attempts to find a new steady-state operating point. These rotor oscillations produce variations of stator voltage and current. The quotient of these varying quantities represents the dynamic system impedance during the transient as viewed from the generator terminal. The dynamic impedance is also referred to as the "swing impedance" or just "swing." Distance relays applied at the generator as system backup protection will detect a swing if the swing impedance passes through the trip characteristic. The relay time delay and the speed at which the apparent system impedance crosses the relay characteristic will determine if tripping is initiated. Normally, the delay required for coordination with network relaying will prevent these schemes from operating during out-of-step events. Loss-of-field protection is an impedance-based relay scheme applied at the generator terminals to detect the failure of the generator field. Fig. 31 shows the trip characteristic for one popular LOF configuration. The trip characteristic is set with a time delay. Because this scheme measures the impedance looking into the generator, it cannot detect swings that pass through the GSU transformer.

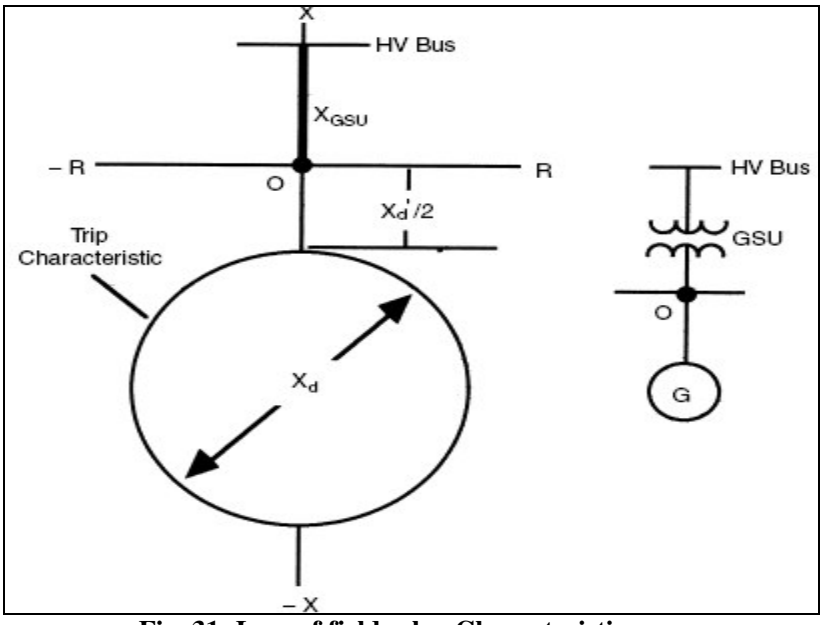

Fig. 31: Loss of field relay Characteristics

The offset of the characteristic also precludes detection of swings within the generator near the terminals. The trip characteristic will operate for slow-moving swings that linger within its characteristic in excess of the trip delay setting, typically 0.5 sec to 1.0 sec. The bottom line is that the loss-of-field protection may operate for specific out-of-step conditions, but cannot provide standalone out-of-step protection.

Over the years, specialized detection schemes have been developed. Early out-of-step protection schemes counted the current pulsation each time a generator pole slipped (passed through 180 degree separation with system voltage). Tripping was initiated after a preset number of counts. Now it is recognized that the system impedance viewed from the generator terminals provides a method for the rapid detection of a loss of synchronism. Consequently, out-of-step detection schemes employ impedance-sensing elements and specialized logic to distinguish between a fault condition and a loss of synchronism. In order to apply this type of protection, it is necessary to understand how system impedance varies during a loss of synchronism.

When a generator loses synchronism, the resulting high peak currents and off-frequency operation can cause winding stresses, high rotor iron currents, pulsating torques, and mechanical resonances that are potentially damaging to the machine. To minimize damage, the generator should be tripped without delay, preferably on the first slip cycle. During an out-of-step condition, the apparent impedance, as viewed from the generator terminals, will vary as a function of system and generator voltages and the angular separation between them. The impedance locus will depend on the excitation system, machine loading, and initiating disturbance.

Normally, system transient studies should be performed to determine the system impedance swing against time for different scenarios. The relays are set so that they will not trip for any stable swing but will trip if the swing is unstable. The swing is more likely to be unstable when the generator is operating at unity or leading power factor with the automatic voltage regulator out of service. For unstable swings, the impedance loci for each generator should be determined with system configurations that give maximum and minimum system impedances and with voltage regulators in and out of service. With different generator loading conditions and system configurations, the transient response of the machines is

determined for different fault conditions. Generally, systems are required to withstand close in three-phase fault on the high side of the step-up transformer and breaker failure conditions. Even with fast relaying and breaker operating times, this condition may sometimes result in generator loss of synchronism. Out-of-step protection on a generator is required when relatively a large generator can go unstable for reasonable system contingencies and the swing goes through the generator/transformer zone. Many new generating plants are combined cycle, with a combination of gas turbines and a steam turbine at the same location. The latter will normally be lower inertia and will tend to go out of step before the higher inertia units. Out-of-step protection applied on the steam unit can lead to faster recognition of out-of-step conditions and it is possible that, in some cases, tripping of the steam unit quickly will result in the gas turbines staying in synchronization with the system. It has also been suggested that a back-up distance relay, set to trip if the primary breaker does not clear the critical fault, can be used in some conditions to trip the steam turbine and keep the gas turbines on line.

While planning studies can identify what setting to apply to out-of-step relays, it should be recognized that these studies are usually based on limited anticipated scenarios (e.g., three phase faults, breaker failure, specific system configurations, and loading, etc.). Severe system disturbances often involve multiple events with depressed system voltages, switching events, and system oscillations. In addition, under abnormal system conditions, such as underfrequency, the relay characteristics may vary from ideal. Under these circumstances, application of an out-of-step relay may cause the impedance to enter the relay tripping characteristic for some situations where the machine is not necessarily out of step, thus causing nuisance tripping and possibly worsening overall system conditions. Detailed studies of performance under severe multiple contingencies must balance the risk of undesirable tripping against the risk of damage to the machine. The tripping mode recommended (breaker trip, assuming the unit can respond to full load rejection) does allow the machine to be quickly reconnected. Reference [170] provides a detailed discussion on the swing characteristics and the settings consideration for the relay.

5.5 Automatic Island Detection and Simulation

A depth first search (DFS) based algorithm is developed to simulate the cascading scenarios in power system including generator protection. DFS is a graph, tree or tree structure search algorithm which starts at one root and explores as far as possible along each branch before backtracking as in breadth first search algorithm. Then the search backtracks, returning to the most recent node it hadn't finished exploring. Extremes are searched first. DFS tends to require less memory, as only nodes on the "current" path need to be stored. Time complexity of both algorithms are proportional to the number of vertices plus the number of edges in the graphs they traverse (O(|V| + |E|)). DFS can be asily implemented using the *recursion* methodology.

The figure shown below Fig. 32 is a representative structure of the cascading phenomena starting at root node A and progressing on any of the three branches initially, which can further branch depending on the trajectory of the system. DFS is ideally suited for simulating the cascading phenomena in power system.

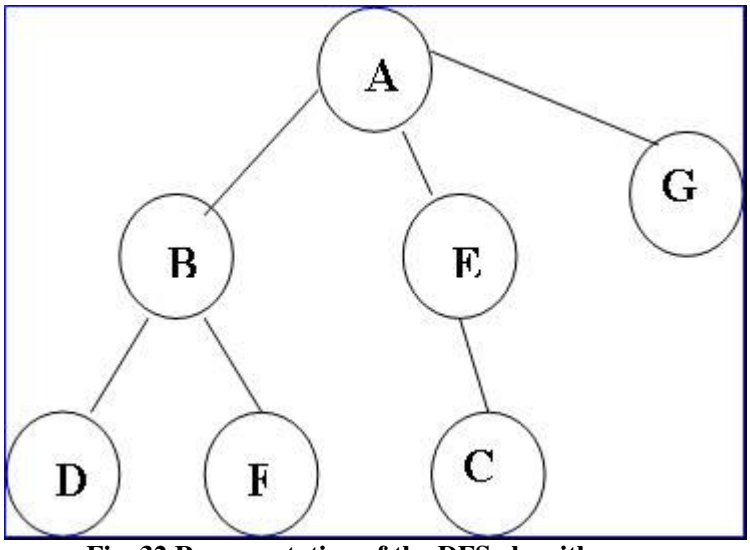

Fig. 32 Representation of the DFS algorithm

A depth-first search starting at A, assuming that the left edges in the shown graph are chosen before right edges, and assuming the search remembers previously-visited nodes and will not repeat them (since this is a small graph), will visit the nodes in the following order: A, B, D, F, E, C, G.

Figure shown below Fig. 33 is the typical scenario of a system undergoing cascading and leading to the formation of multiple islands some of which are stable and others are unstable and collapse completely. The developed DFS based algorithm keeps track of the different islands and performs simulation recursively. The islands formations are detected by a graph search algorithm based on breadth first search and kept track of for performing simulation by DFS.

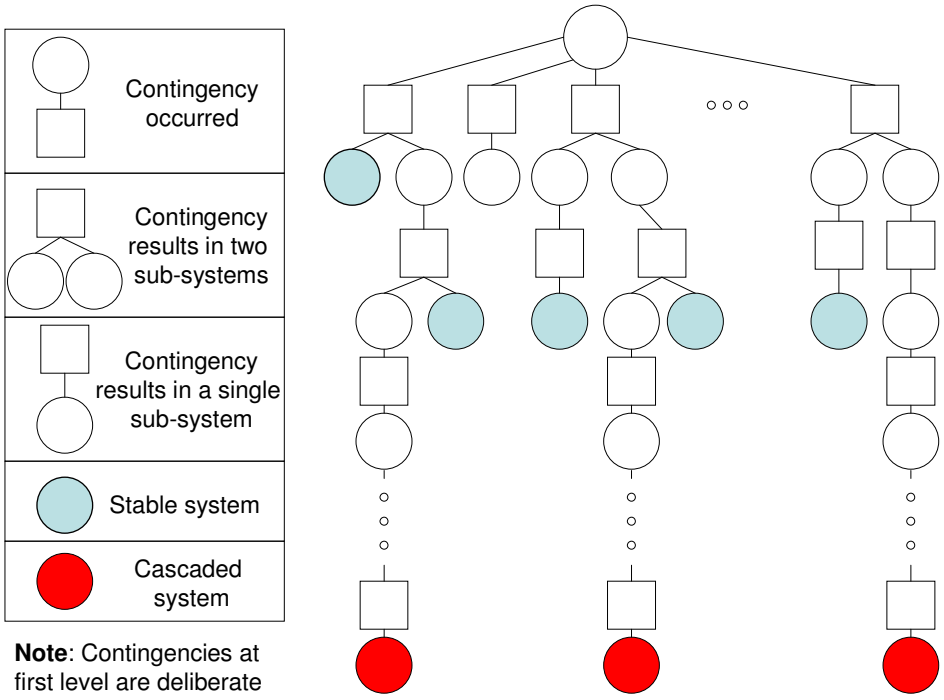

Fig. 33 A typical cascading scenario

CHAPTER 6 RESULTS AND DISCUSSION

6.1 Validation of the Dynamic Simulation Tool

Our dynamic simulation engine is tested on the Ontario Hydro 4 bus test system (see Appendix A for details of the system). Since the program builds network model directly from EMS's one-line substation in addition to an initial converged power flow case, 18 breakers were added to the test system so that all the lines, generators, load and shunt can be isolated by opening the associated breakers. Other parameters of the system stay unchanged.

Before fault, the statuses of generators are listed in Table 29. These initial generator parameters are sufficient to decide all other variables like bus voltages and line flows. The exciter model used is a standard ETMSP Type 30 as shown in Fig. 34. The scenario simulated is a 3-phase ground fault at bus 5. The fault was cleared by itself after 0.01 second without any breaker operation. The ETMSP application is used as a benchmark to our program.

Table 29: Initial status of generator for Ontario test system

No	V-abs	V-angle	P	Q
1	1.03	2.928	790	77.57608
2	1.01	-7.906	790	188.01250
3	1.03	0.6634	690	69.85064
4	1.01	-8.78658	740	85.26508

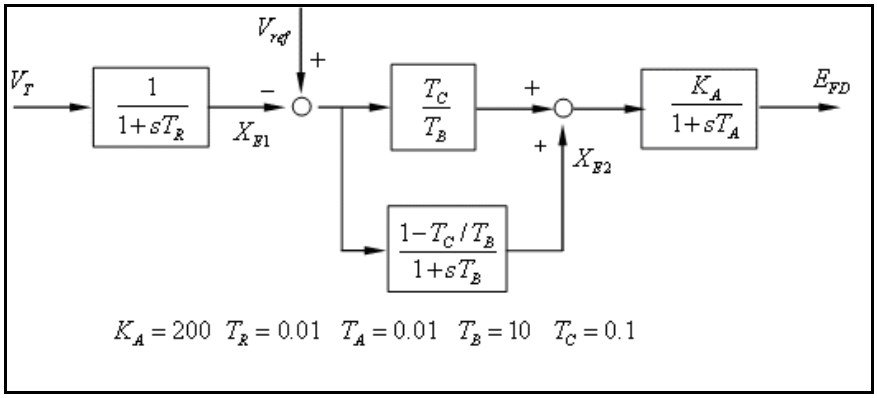

Fig. 34: ETMSP type 30 exciter for Ontario hydro 4-generator

The simulation results from the ETMSP application and our dynamic simulation engine are presented in Fig. 35 and Fig. 36 respectively. The two figures are almost identical. The minimal differences are probably introduced by different algorithm the two programs use. The ETMSP application uses fixed step Runge-Kutta algorithm for integration while our simulator uses step-variable implicit integration algorithm.

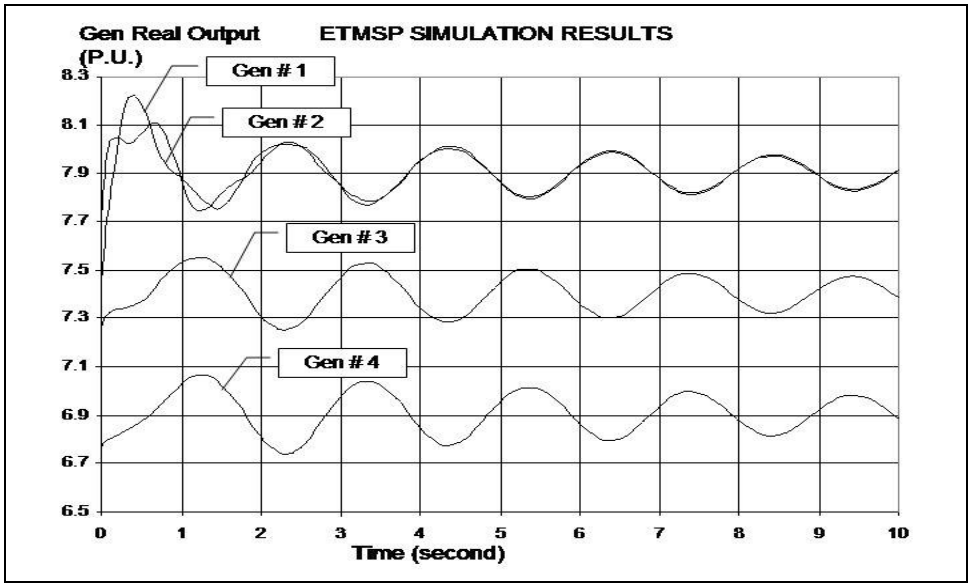

Fig. 35: Response of generator after a temporary fault at bus section 5 (ETMSP)

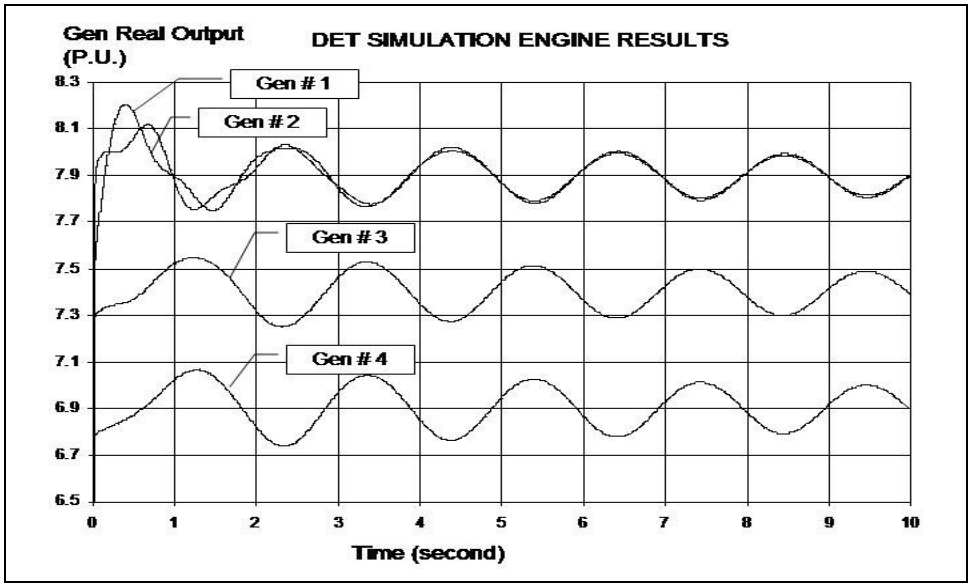

Fig. 36: Response of a generator after a temporary fault at bus section 5 (Developed Simulator)

6.2 Decision Event Tree Generation

The test simulation uses the current system topology to generate an extended contingency list as the first tier of event nodes. An iterative programming technique and an LP optimizer are then employed to predict and track system response to corrective actions or no action on the part of the operator, for each contingency as illustrated in Fig. 37. The branches B1, B3, and B5 represent the initial contingency, the system reconfiguration, and the emergency load shedding respectively, The branches B2 and B4 represent the "do-nothing" decision. The nodes (S_i's) in Fig. 37 represent the status/trajectory of the system after/before the actions (B_i's) are applied to the system.

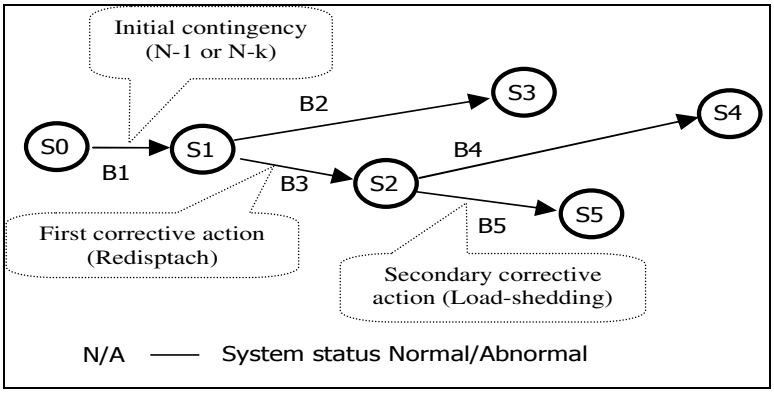

Fig. 37: Dynamic event tree template for the test system

6.2.1 Test Scenario

We studied the possible cascading for a one-hour time interval during which the load ramped 20% from 900 seconds to 2700 seconds as shown in Fig. 38 for a scenario where the system is in a weakened condition due to the outage of a tie line. Line loadings are monitored, and the most effective redispatch & load curtailment actions are identified for overloaded lines.

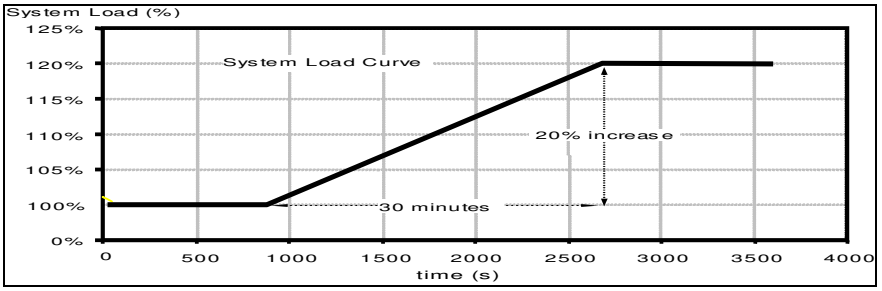

Fig. 38: System load ramp curve

6.2.2 Contingency Event Branch

We generated a comprehensive list of initiating contingencies including the functional group tripping contingencies, stuck breaker contingencies and the inadvertent tripping contingencies for the selected scenario. Since both the long-term and transient dynamic simulation are done in one application, we assume faults are cleared without any delay. This was done as a result of a programming limitation. However, this assumption does not seriously compromise our analysis since a close examination of all the NERC's record [20] of major power system disturbances reveals that an initiating fault never causes the immediate collapse of system; rather it is always a fault followed by an outage that causes a serious problem.

6.2.3 Decision Event Branch Set and Decision Identification

The decision set is the combination of all the redispatch of all the available generators and, if necessary, load curtailment (Appendix H). We assume any of the available generators can generate between zero MW to its maximum output. We use linear programming optimization to find the initiating redispatch and/or load curtailment to back off any line loading that exceeds a specified threshold. The formulation for this approach is provided in Appendix H. It is solved within the time domain simulation process only whenever it is necessary, i.e., when the flow on a line exceeds a defined percent its emergency loading. After we find the primary redispatch, we set the governor setting of each generator according to the redispatch and simulate the response of system to check if the redispatch is effective. Since the system total load increases between 900s and 2700s, decisions that are effective for now may fail after loading increases to certain level. In that case, we apply the secondary decision straightforward: direct load shedding, i.e. shed any increased load(s) that cause new problem. Also decisions taken without consideration of the generator protection modeling differ drastically from the decisions taken with the generator protection taken into consideration. These considerations are further illustrated through examples in the next section.

6.3 Results Analysis

6.3.1 Without Generation Protection

In this section we present the simulation results without the generator protection in the simulator. The result of the simulation engine computations for this scenario is a large repository of information that includes contingency specification, the response curves of all key variables for those contingencies and necessary actions. Of the 322 contingencies we analyzed, 10 resulted in fast (within 1 minute) instability and 312 of them resulted in stable, but unacceptable performance. Our implementation of the simulator does not generate a corrective action for cases resulting in instability within 1 minute since this is not enough time to implement operator-initiated actions. Of the other 312 contingencies, all of them resulted in overloading problems that were corrected by proper generator and load reconfiguration as identified by our optimization approach. Fig. 39 illustrates a representative initiating contingency of the loss of a generator (G-102) in the upper area, which serves as B1, the initial contingency in the template in Fig. 37. We see that line L118 is the most loaded line for the entire system. Fig. 40 shows the time domain simulation results of the flow on Line L118 with and without the first and second actions (B3 and B5 in Fig. 37) applied. The effectiveness of the first redispatch only holds until time 1100s. After that, load increase causes the flow on that line to exceed 100% again. To prevent further loading, an emergency load-shedding scheme is identified and executed to prevent circuit loadings from exceeding their ratings. The initiating contingency and system trajectory with and without actions, as shown in Fig. 40, are mapped to the branches and nodes shown in Fig. 37.

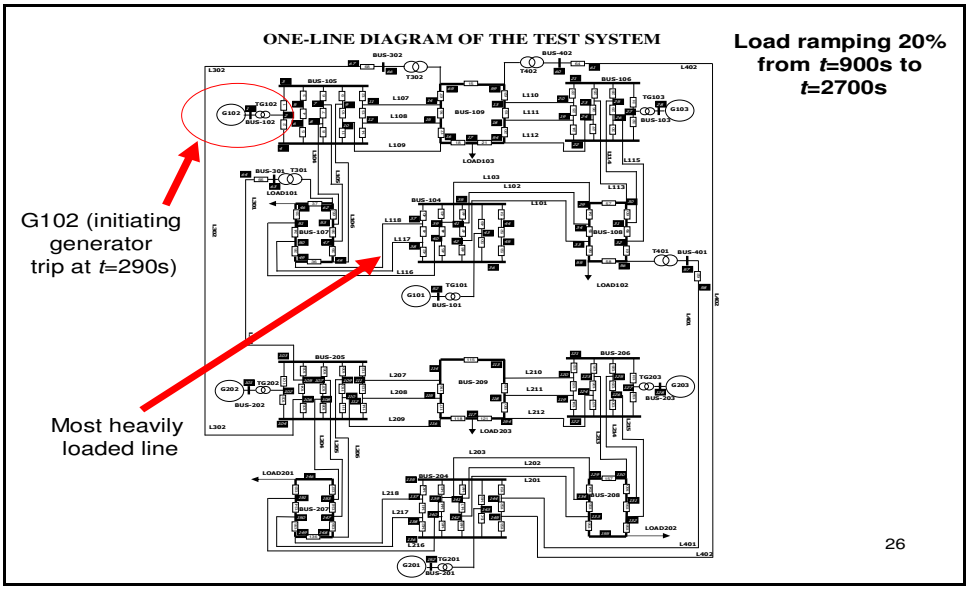

Fig. 39: Branch loading after loss of the largest generator

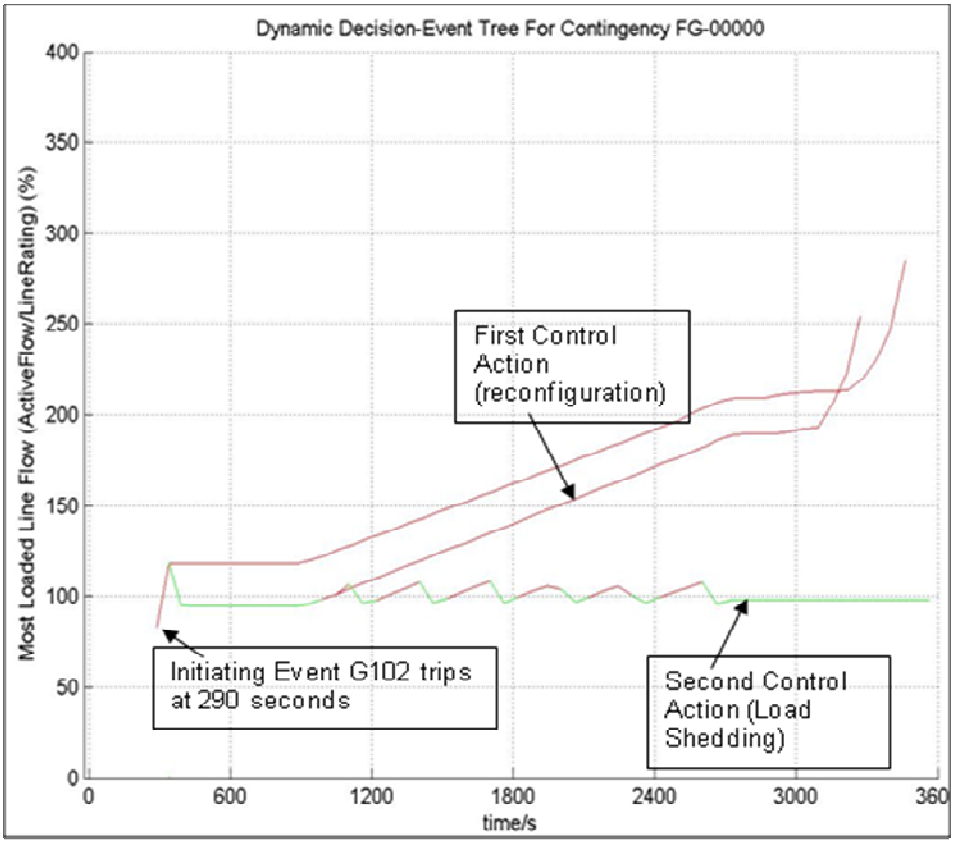

Fig. 40: Line flow response after the loss of the generator G102 (most severely overloaded circuit)

Since our engine has the capability of slow dynamic simulation, we can also observe the voltage variation in the test system. We find that, even through the engine for the test system is designed to solve the overload problems only, the action taken by the engine solves the voltage problems as well. Fig 41 shows the voltage of the most severely depressed bus following the same contingency. The voltage collapses after 3200 seconds) if the operator does not take any action. Following the system reconfiguration (a redispatch) the system behaves well until 3400 seconds, where a low voltage problem shows up. If the secondary action is applied, the system will avoid both the overloading and the voltage problems.

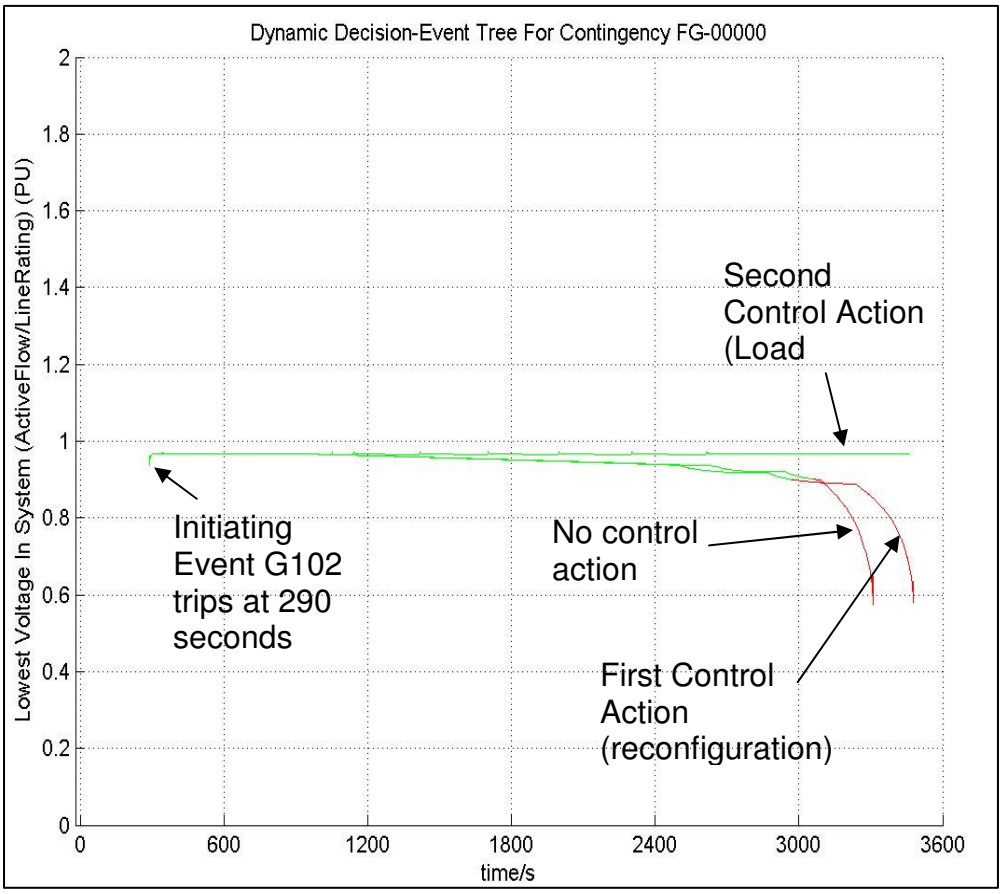

Fig. 41: Voltage response after the loss of G102

6.3.2 With Generation Protection

6.3.2.1 A cascading scenario

In this section we present the simulation results with the generator protection embedded into the simulator. A Depth First Search (DFS) based algorithm is implemented to continue

simulation on each island formed as a result of a contingency or a sequence of contingencies and being detected by a graph search algorithm based on breadth first search. The DFS algorithm is employed to simulate cascading under stressed condition of 20% load ramping from 900 seconds to 2700 seconds. The results presented are for the test system in Appendix D. Fig. 42 below shows the sequence of events that led to cascading when the system was under very stressed condition of heavy loading and one of relays, namely the overexcitation relay of the generator which was protecting the generator G101 was set lower than its actual setting, a classic case of setting errors. Therefore when there was a fault in line L215 at t= 300 seconds the generator G101 tripped and further stressed the system and thus causing the other generators to be overexcited and a sequence of events happened due to proper generator protection and generators G102 and G201 tripped in the next 15 minutes leading a major load generation imbalance and the system collapsed. Fig. 43 below shows the simulation result for the described cascading scenario. It shows the most loaded line flow on the system with and without the generator flow. In Fig. 43, the first line from below show the most loaded line flow without generator protection and we identify the point at which generator G101 would trip if the generator protection were in service. The next line simulates the flow with generator G101 tripped and identifies the point at which the next generator would trip if the relay is functional. This is simulated in the next line where the next generator G102 is tripped at t= 925.37s and identifies the next generator trip at t = 1260.17s where the generator G202 trips and blacks out the system. Fig. 44 shows the lowest system voltage for the same cascading scenario and it corresponds to the maximum line flow graph in Fig. 43 with respect to the sequence of events.

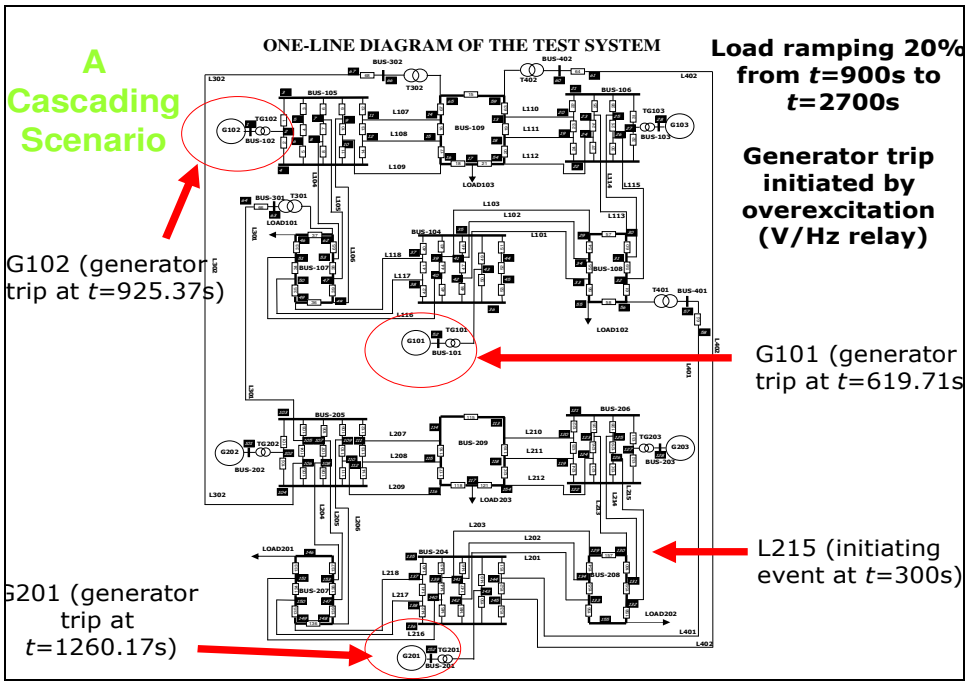

Fig. 42: Sequence of events leading to cascading

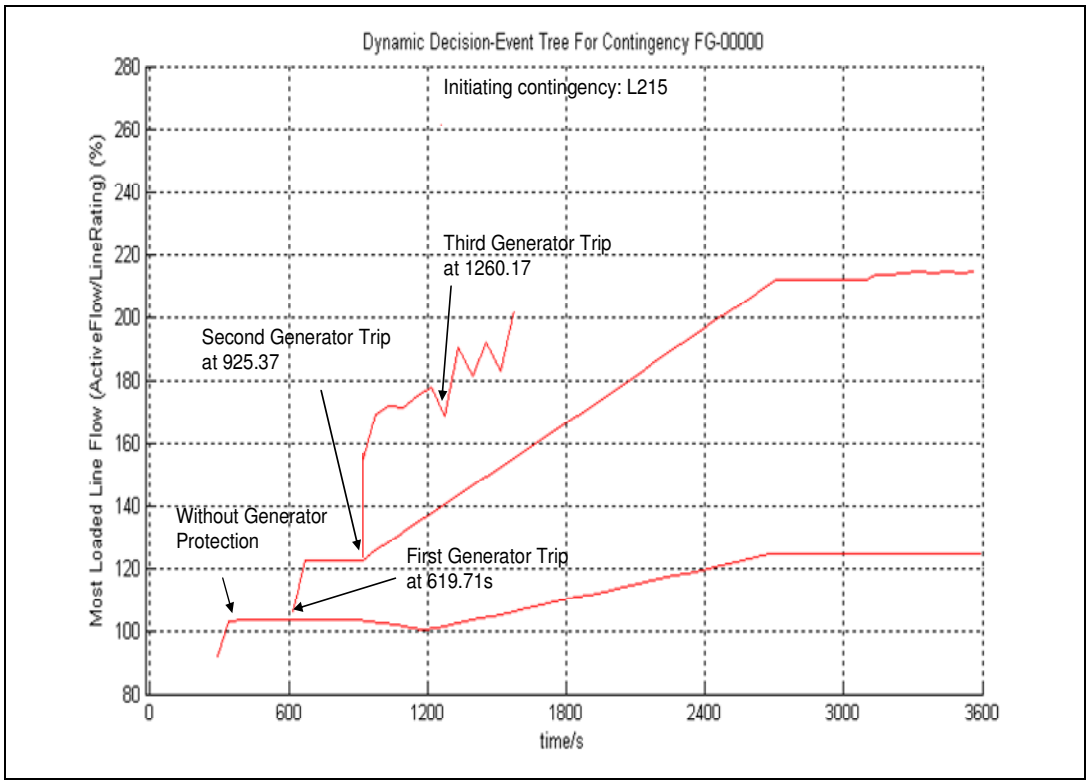

Fig. 43: Maximum line flow in a cascading scenario

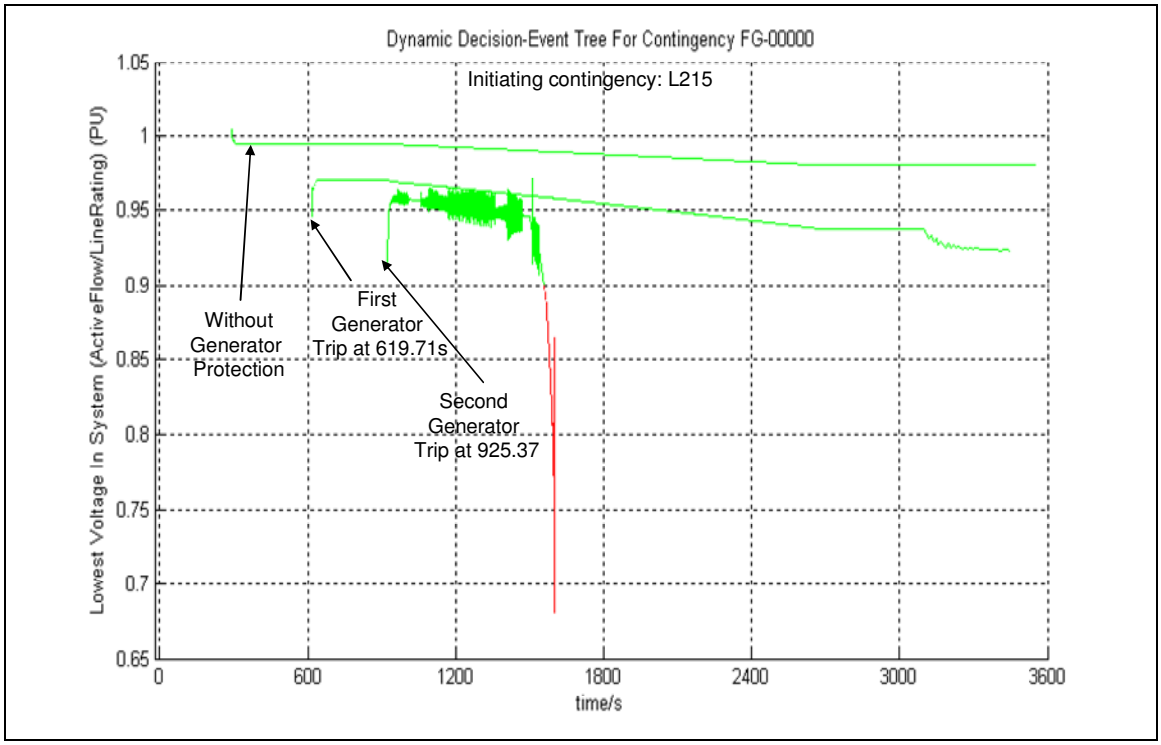

Fig. 44: Lowest voltage in the system for a cascading scenario

6.3.2.2 An islanding scenario

Fig. 45 shows a different system scenario with the sequence of events that led to islanding with the same initiating event as in Fig. 42, *i.e.*, L215. In this case also, the system response was simulated under stress condition of heavy loading, and the relay setting of generator G101 set below the calculated value. After the initiating event, the four tie-lines L301, L302, L401, and L402 tripped very quick succession (assumed simultaneously) due to heavy loading and sagging into the tress followed by the generator G101 trip, and separating the system into two islands - with the top island having 2 generators and load with deficient generation and frequency excursion, and the bottom island with 3 generators and load with excess generation. There developed an underfrequency situation on the top island and overfrequency situation in the bottom island. The top island collapsed immediately due to successive protection actuated generator trips within a few seconds. In the bottom island, the generator G201 tripped at t=945.27s, and subsequently, the system recovered by balancing the generation and load through governor and other control mechanisms, and was stabilized.

Fig. 46 shows the two islands formed after initiating event followed by the tie-line trips. Fig. 47 show the maximum loaded line flow for the above scenario.

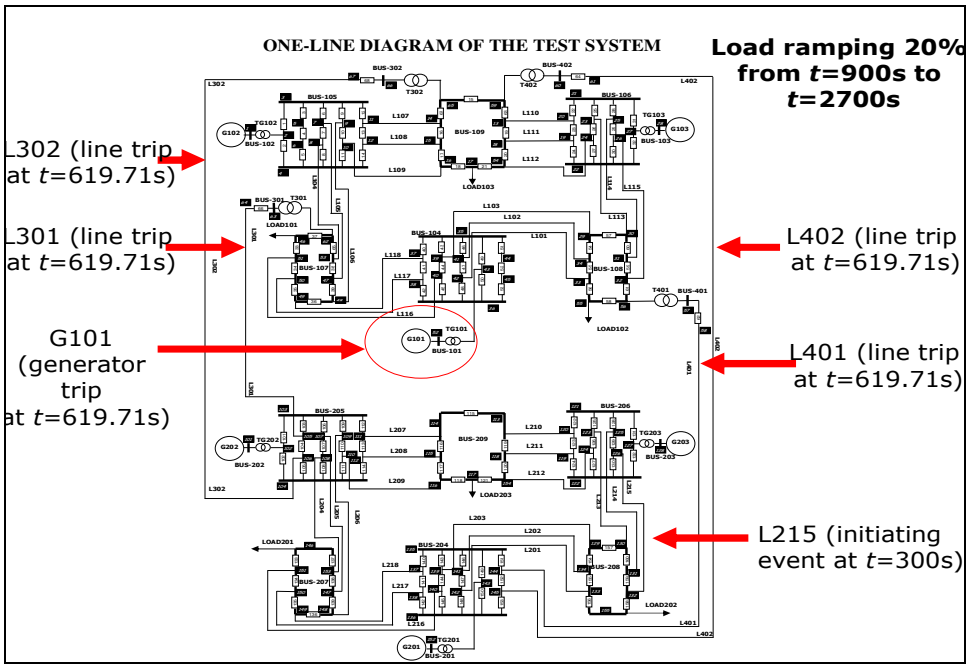

Fig. 45: Sequence of events leading to islanding

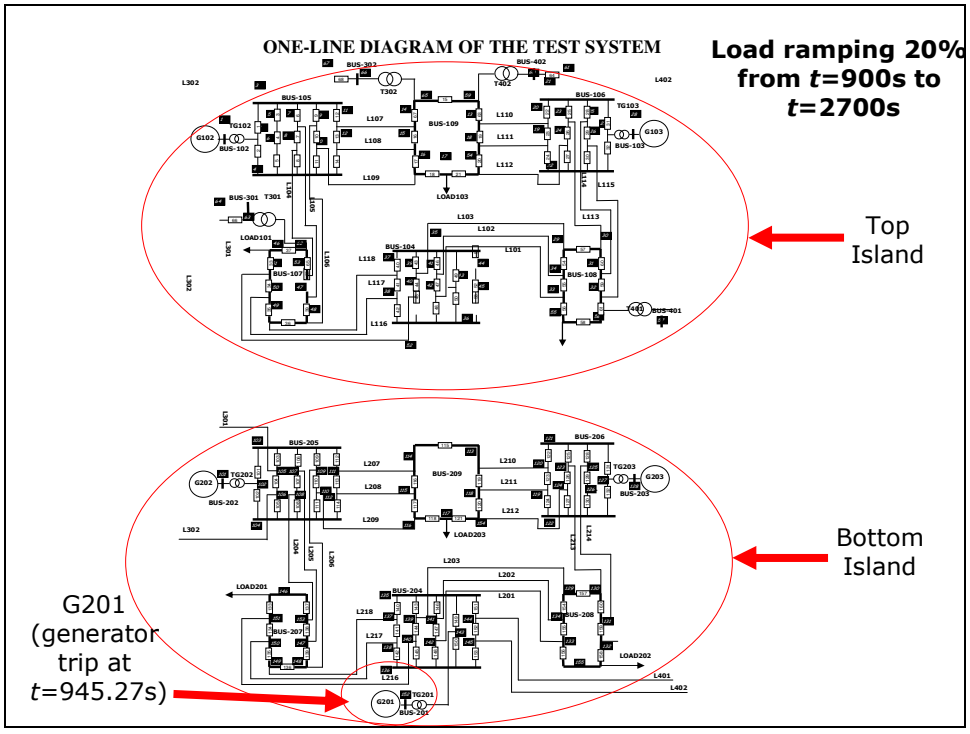

Fig. 46: The two islands resulting from the sequence of events in Fig. 45

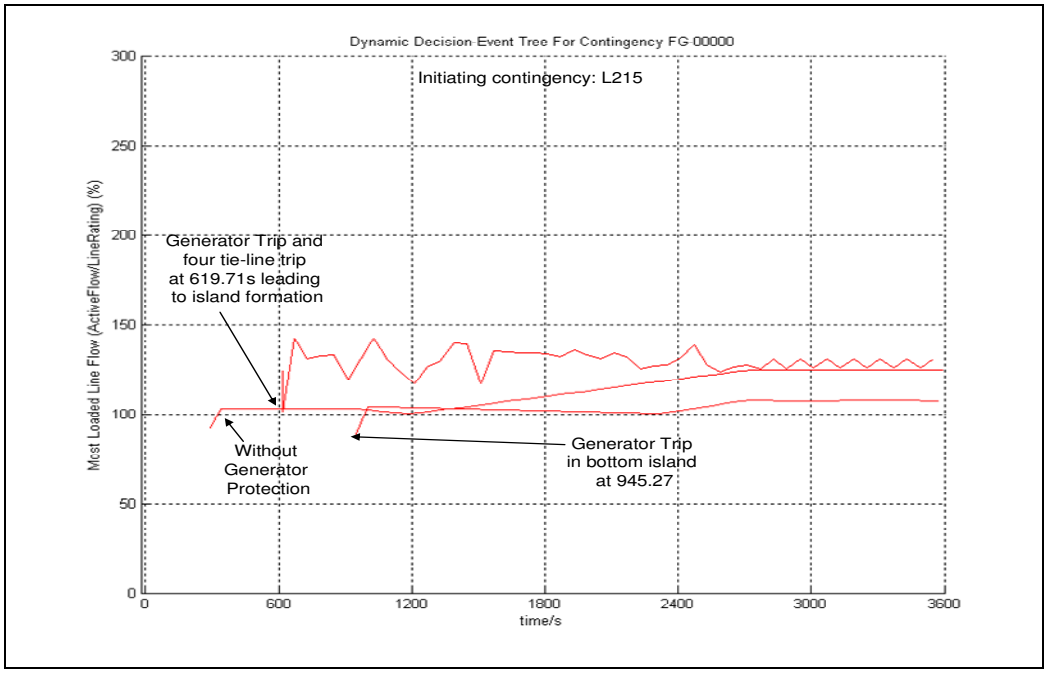

Fig. 47: Maximum line flow in an islanded scenario

In both the scenarios described above - one leading to cascading, and the other leading to islanding, we observe that after the initiating event, there is a period of slow progression of trip events, which is followed by a fast succession of events, leading to high consequence events – like total system blackout, or unstable island formation, which ultimately culminates in cascading. This gives a chance to the operator to take corrective actions during the slow progression period to avoid the disaster, if he is aware of the complex unfolding of the future events.

6.3.2.3 Some more illustrative examples

The example below shows the difference in the simulation plots with and without considering generator protection in the dynamic simulation of the power system to provide decision support for the operators to take corrective action. Fig. 48 and Fig. 49 shows the simulation plot for an initial line contingency (L110) at 300 seconds. The most overloaded line in the system is the line L112 as a result of the L110 trip. We can see from Fig. 48 that with generator protection in place there would be a protection actuated generator trip at 627.9 seconds which would in reality overload the lines to a much higher than 100% ,as is the case

without generator protection being simulated and is represented by the blue line in the figure below.

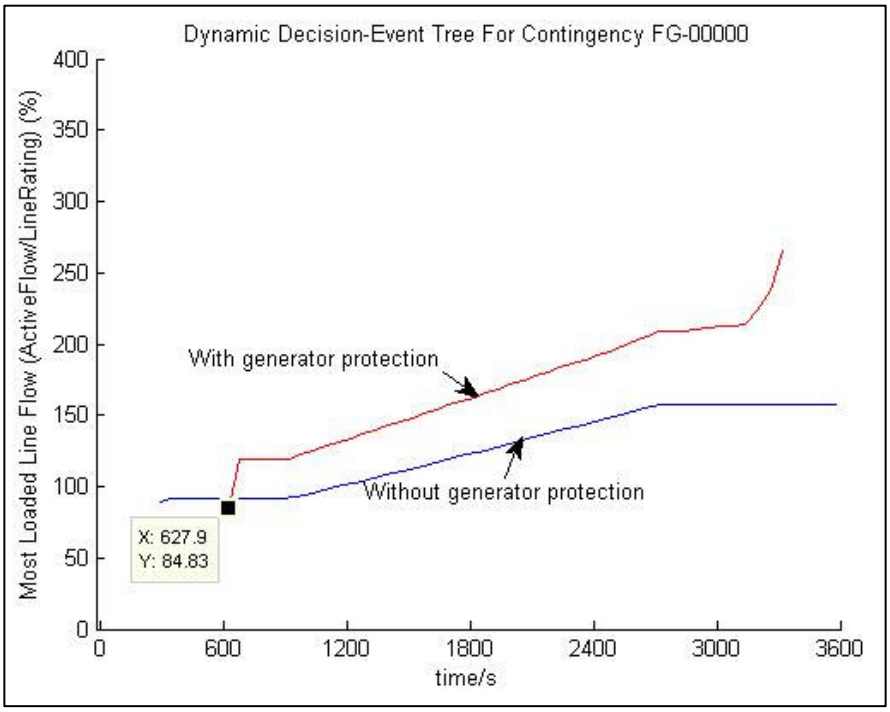

Fig. 48 Circuit loading with and without generator protection

Similarly we can see in Fig. 49 that the system is apparently voltage stable when the generator protection is not included in the simulation modeling, whereas the system actually has a long term voltage collapse which becomes evident when generator protection is also modeled in the simulation.

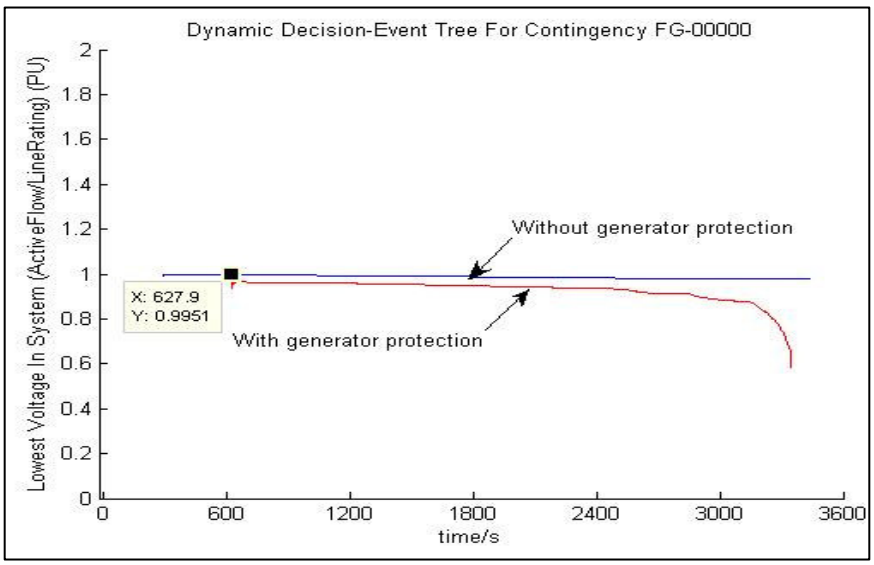

Fig. 49 Voltage response of system with and without generator protection

In the next example shown in Fig. 50, the initiating event is a generator trip. In this case as well, the system is highly stressed, and the simulation results indicate that it would lead to cascading. However, if proper control actions are taken at the right time, the long term stability of the system can be ensured. Fig. 51 shows the simulation results with the corrective actions taken by the operator at t=595.142 and t=1004.60. The first corrective action taken at t=595.142 brings the maximum line flow within the desired limits, and the system becomes stable after the initiating event and the transients. However, due to load ramping, the system again violates the operational constraints at a later time, as can be seen in Fig. 51. The second control action initiated at t=1004.60, which involves multiple load shedding events at different points of time ensures system stability. Fig. 52 shows the lowest system voltage before and after the control actions following the initiating event.

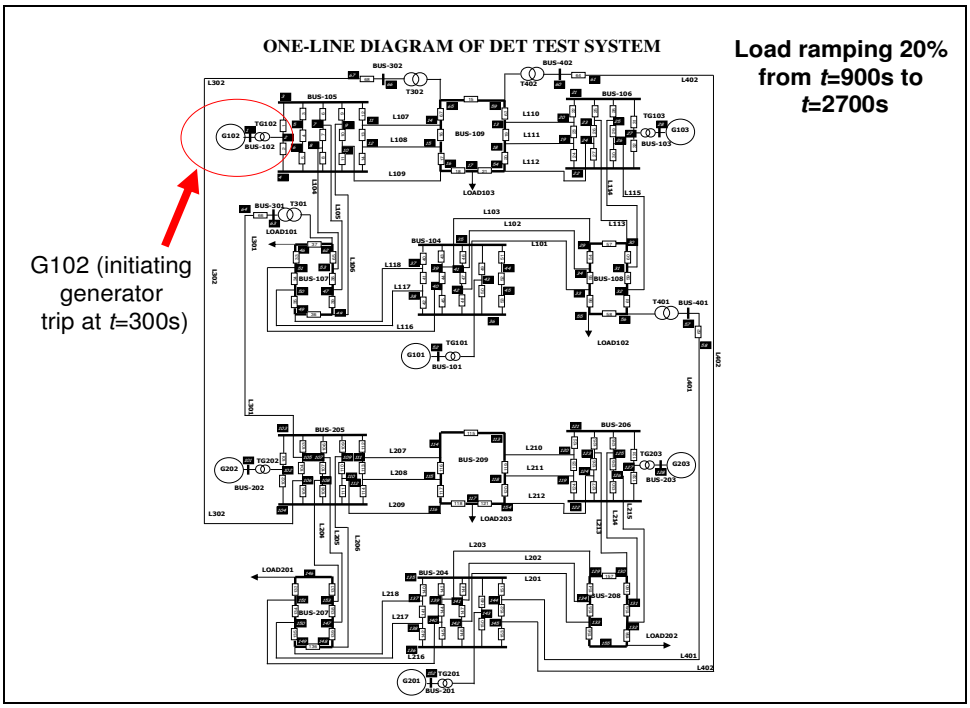

Fig. 50: A scenario with the initiating contingency as generator trip

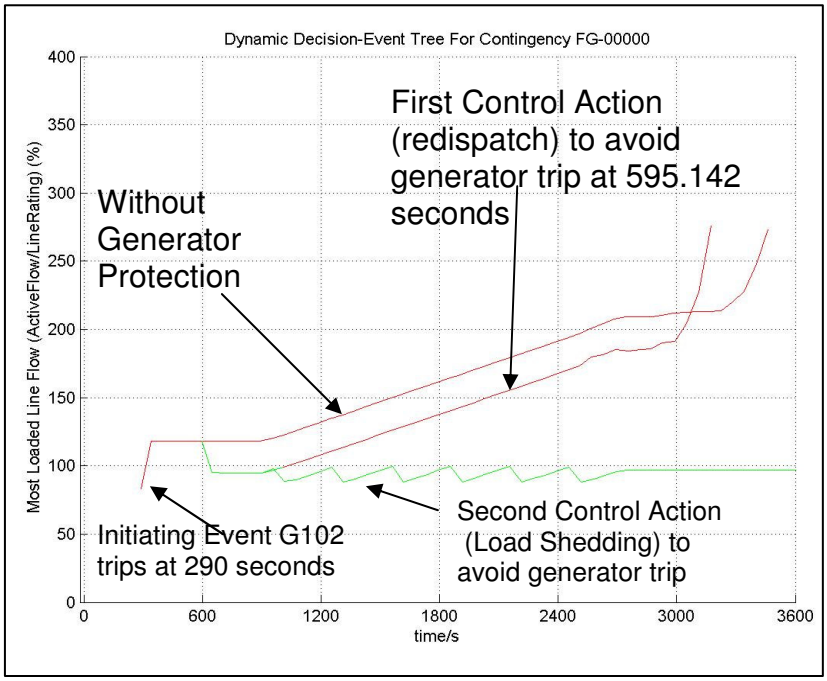

Fig. 51: Maximum line flow with corrective actions to prevent generator trip and relieve line overloading

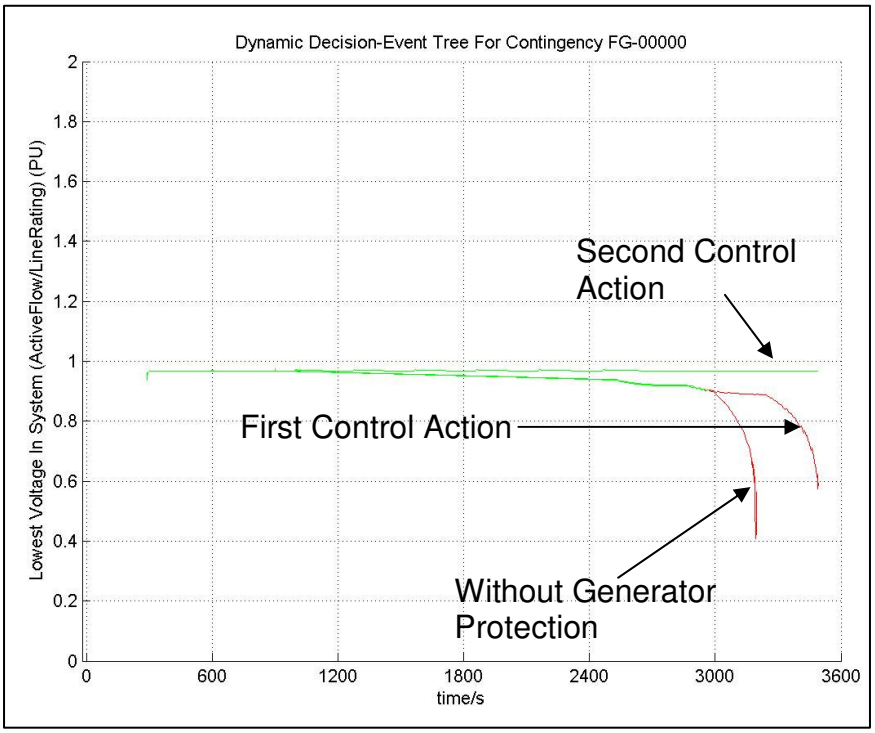

Fig. 52: Lowest voltage in the system with corrective actions to prevent generator trip and relieve line overloading

CHAPTER 7 CONCLUSION

In this research we have made significant contributions *"to provide operators with a **very fast** (online) computational capability to **predict system response** and **identify corrective actions** through **analytical modeling** and **fast numerical simulation** studies for **low probability**, **high-consequence** catastrophic events (**blackouts**) by exploiting the state of the art in software"*.

Around the world, most of the control centers still perform static or steady state contingency analysis and very few companies and/or control centers have on-line transient instability analysis for detection of early-swing problems. ***We are not aware of any company/control center that has implemented long-term simulation capability for on-line purposes.*** Nonetheless the long-term dynamic simulation of a power system is of interest and extremely valuable because it provides ability for the evaluation and analysis of multi element events (N-*k*) which may lead to cascading outages. Such information is not available today in control centers with dynamic simulation tools.

However, in order for such simulation to be of practical utility in an operational context, it must be able to perform simulations very fast. This is one of the principal goals of this research that we have addressed by making algorithmic improvements to power system time domain simulation methods.

There is still quite a distance to cover in terms of implementing full functional capability into the developed simulator apart from technical issues before it can be sitting in one of the modern control centers seamlessly integrated with the EMS. However the roadmap to take it onsite is clear. The simulator needs to be tested with large systems which would require the system model from the EMS with associated dynamic data and development of an interface with the software with its associated data format. More complete and rigorous component and protection modeling including power electronic devices and controllers, more intensive failure detection with a larger array of intelligent and optimal corrective actions including adaptive system separation schemes need to be implemented in the proposed simulator for it to be put in place and used by the operators. It can be further enhanced with visual and sonic translations of its output to make it easier for the operators to appreciate its value in dealing

with the impending situations. Companies like Entergy have already shown interest in trying out some of our ideas and do field trials as a second phase of this research which strongly indicates the relevance of the current research and its scope as a useful addition to an EMS.

An important factor in any technology being implemented in real life is the adaptive considerations of the operators to changes. This would require a comprehensive effort in training in these tools to build confidence in the individuals responsible for decision making. This becomes easier to achieve when the impact that such a technology would have in operation if it were in place, is clear. It motivates operators to learn with enthusiasm. So, in essence, education in its importance, impact and efficiency is imperative for it to be widely accepted in future.

On line dynamic simulation of power systems will have significant impact on their future design and operation. The contrast of its presence to its absence is too stark. It will enhance power system security and reliability and hence customer satisfaction and utility profits, and will promote secure power grid expansion. Specifically the research addressed herein will have great impacts in reducing the severity and frequency of cascading events. As we pointed out previously the blackouts greater than thousand megawatts are doubling every decade. This decade is not yet over and with ever increasing complexity in grid operations the danger of such events is more imminent in the absence of such a cascading event tracking and avoidance decision support tool. This research can be seen as an enabling technology towards a secure and reliable power grid.

This research has attempted to utilize the state of the art research in numerical algorithms and it is customized for power system applications to gain great computational efficiency. We are not aware of such applications from the literature.

Blackouts typically result from low probability events. Corrective control is the operational solution to blackouts. It is event-based with actions determined on-line via anticipatory computing as decision support for the operator. This research establishes the need of such an on-line tracking and blackout avoidance decision support tool for the operators.

The research objectives are achieved through contributions in six major areas as described below:

Blackout analysis	An in depth study of blackouts in last four decades is done and blackout attributes and characteristics are developed; from which simulator attributes are derived.
Low probability high consequence event	Proposed a systematic approach to strategically select N-k inadvertent tripping contingencies using system real-time topology information and calculate event probability as well. The algorithm is verified against test systems.
Analytical modeling	Accurately models generation protection systems and establishes its importance in simulating cascading events. Failure detection through activation of protection and conditions of overload, underfrequency and undervoltage conditions exceeding tolerable thresholds.
Islanding	Development and implementation of recursive algorithms based on depth first search for simulation on different islands formed as a result of cascading sequence of events or as a result or corrective action. Ability to handle any number of islands formed.
Numerical algorithms-Direct methods	The simulator is computationally enhanced via implementation of intelligent Jacobian updating and implementation of advanced sparsity based multifrontal linear solvers for dynamic simulation. Multifrontal methods have inherent parallel hierarchy and divide the task into number of subtasks to achieve high computational gain. The algorithms are customized for power system through intelligent symbolic and numeric factorization to gain speed up. Other sparse solvers available in Matlab are implemented and compared with developed multifrontal methods.
Numerical algorithms-Iterative methods	A new class of preconditioners based on multifrontal solvers is developed for iterative solvers like GMRESR, BiCGStab, and QMR to achieve high computational gain. The ILU preconditioner based iterative methods are implemented and compared with multifrontal preconditioner based iterative method called GMRESR.

CHAPTER 8 FUTURE RECOMMENDATIONS BASED ON DISCUSSION WITH THE INDUSTRY

This research lays the foundation for operational defense to cascading events through very fast anticipatory computing of the evolution of the system trajectory and its response and identifying intelligent and optimal corrective solutions. This can be achieved in an online environment with significant improvements and implementation of both the state of the art software and hardware technology in power system dynamic simulation. This research has made some significant contributions towards that end and opened up many future directions for research to make it feasible and more computationally efficient for its deployment in an online environment.

There is a lot of scope for research in the area of modeling improvements in terms of development of efficient algorithms to reduce the stiffness of the DAE of the power system to gain computational efficiency. This can also be viewed in terms of model reduction strategies.

In terms of numerical algorithms employed in power system, there is scope for algorithmic developments in integration schemes and solvers for linear system of equations. Development of algorithms for adaptive time stepping and adaptive integration schemes to simulate multi scale and multi component power system can be an active area of research. Effectively combining the direct methods with the iterative methods can result in huge computational saving as shown in this research.

Field trials and testing with larger real system can be taken up to enhance the robustness and its applicability. This would require system model from the EMS with associated dynamic data and development of an interface with the software with its associated data format.

Further recommendations for future research are implementation of Out-of-Step (OST) Relaying schemes across interregional cutplanes (the California- Oregon flow, or the east-of-river flow into southern California.) [180, 181] and implementation of well designed controlled system separation schemes, using special protection systems and/or OST and power swing blocking (PSB) functions as they provide a safety net to lessen the consequences of major system disturbances.

APPENDIX A: RARE EVENT APPROXIMATION

Suppose $p_1, p_2, \ldots, p_n$ are the individual probabilities of a group of independent events $E_1, E_2, \ldots E_3$. The probability of a compound event, i.e., a combination of events $E_1, E_2, \ldots, E_n$, can always be expressed as a polynomial of $p_1, p_2, \ldots, p_n$. For example, the probability of the event $(E_1 \cap E_2) \cup E_3$ is $p_3+p_1p_2-p_1p_2p_3$ Further suppose that $p_1, p_2, \ldots, p_n$ are all of approximately the same order of magnitude, then the order of magnitude of each product term in the polynomial will depend on how many terms are in the product. We call the number of terms in the product the *probability order*. Thus, the probability of $(E_1 \cap E_2) \cup E_3$ is composed of three different terms p_3 (probability *order 1*), p_1p_2 (probability *order 2*), and $p_1p_2p_3$ (probability *order 3*). ***In many decision problems, knowledge of the "probability orders" of the significant events is sufficient to distinguish between alternatives.***

The basic idea of rare event approximation is that, if the individual probabilities of a group of independent events are very small, we can always simplify the calculation by omitting the higher order terms of the polynomial without much loss of precision [18]. In the given example, if we knew that p_1, p_2, and p_3 were very small, then the probability of $(E1 \cap E2) \cup E3$ could be approximated as $p_3+p_1p_2$, or even as p_3.

Often, the failure probability of an individual component is very small for a well-managed system such as a power system. The fault probability of a power system component is usually at the magnitude of 10^{-6} per hour (or <1% per year) [182]. Suppose the fault probability of a line is p_1 per hour and the failure probability of a breaker is p_2/hour. Obviously, they are not exclusive events. The probability of a fault (p_1), breaker in a failed state (p_2), or both can be expressed as $p_1+p_2-p_1p_2$, assuming the two events are independent. Considering the small nature of p_1 and p_2, if we ignore the probability component of simultaneous occurrence of the two events, the error is only about 10^{-12}.

The implication is that when dealing with rare events, the probability of a compound event is dominated by the lowest *order* terms, and thus the probability *order* is a reasonable measure of event's probability. Based on this idea, we focus on the high order events with higher probability first, then lower probability, since, as the order of contingency increases, the probability of its occurrence decreases sharply to infinitesimal. A complete discussion of rare event systems can be found in [18].

APPENDIX B: PSEUDO CODE FOR GRAPH SEARCH ALGORITHM FOR FUNCTIONAL GROUP DECOMPOSITION

This is a Breath-first search algorithm.

1. *Beginning of decomposition;*
2. *Label all components (bus section, non switching components (lines, capacitors, generators, transformers etc),switching components (switches, breakers etc) as unvisited;*
3. *Arbitrarily choose one unvisited vertex (bus section) as a starting component;*
4. *Initialize functional group and bus indices;*
5. *Establish a new empty functional group object without any component in it;*
6. *Add the chosen bus section to the functional group object as its first component;*
7. *Starting from this vertex, merge the functional group's immediate neighboring components (lines, capacitors, generators, transformers and other non switching components) into the group and label them as visited;*
8. *The step 2 continues until the group expands to its border, where the bordering components are all switching components (breakers and open switches);*
9. *If all components in the power system are visited, stop searching and go to the last step; else choose another unvisited bus section and return to step 2 all over again;*
10. *End of decomposition.*

APPENDIX C: PSEUDO CODE FOR GRAPH SEARCH ALGORITHM FOR INADVERTENT TRIPPING CONTINGENCY

1. *Graph Search Algorithm outlined in Appendix B finds all the Functional Group;*
2. *For each Functional Group we find the interfacing elements (breakers and switches) and the components in the Functional Group ;*
3. *For a failure/fault in the Functional Group extract the interfacing elements and the Functional Group connected to them (step 2);*
4. *Check if any of the Functional Groups extracted above have components other than a Bus section; then the one with component/components other than only Bus section can suffer inadvertent tripping;*
5. *If the Functional Groups connected the to faulted/failed Functional Group contain only Bus section as their components then we go for second tier of search;*
   a) *Identify the interfacing circuit breaker and Functional Group that connect the Bus section and take the union to form the set of Functional Groups excluding the failed/faulted Functional Group;*
   b) *If only one of the remaining Functional Groups has a component other than Bus section then only that Functional Group can trip (SB-TB) and stop.*
   c) *Else if there are more than one Functional Group with component other than Bus section then go for the third tier of search;*
6. *End of decomposition*

APPENDIX D: ONE-LINE DIAGRAM OF TEST SYSTEM

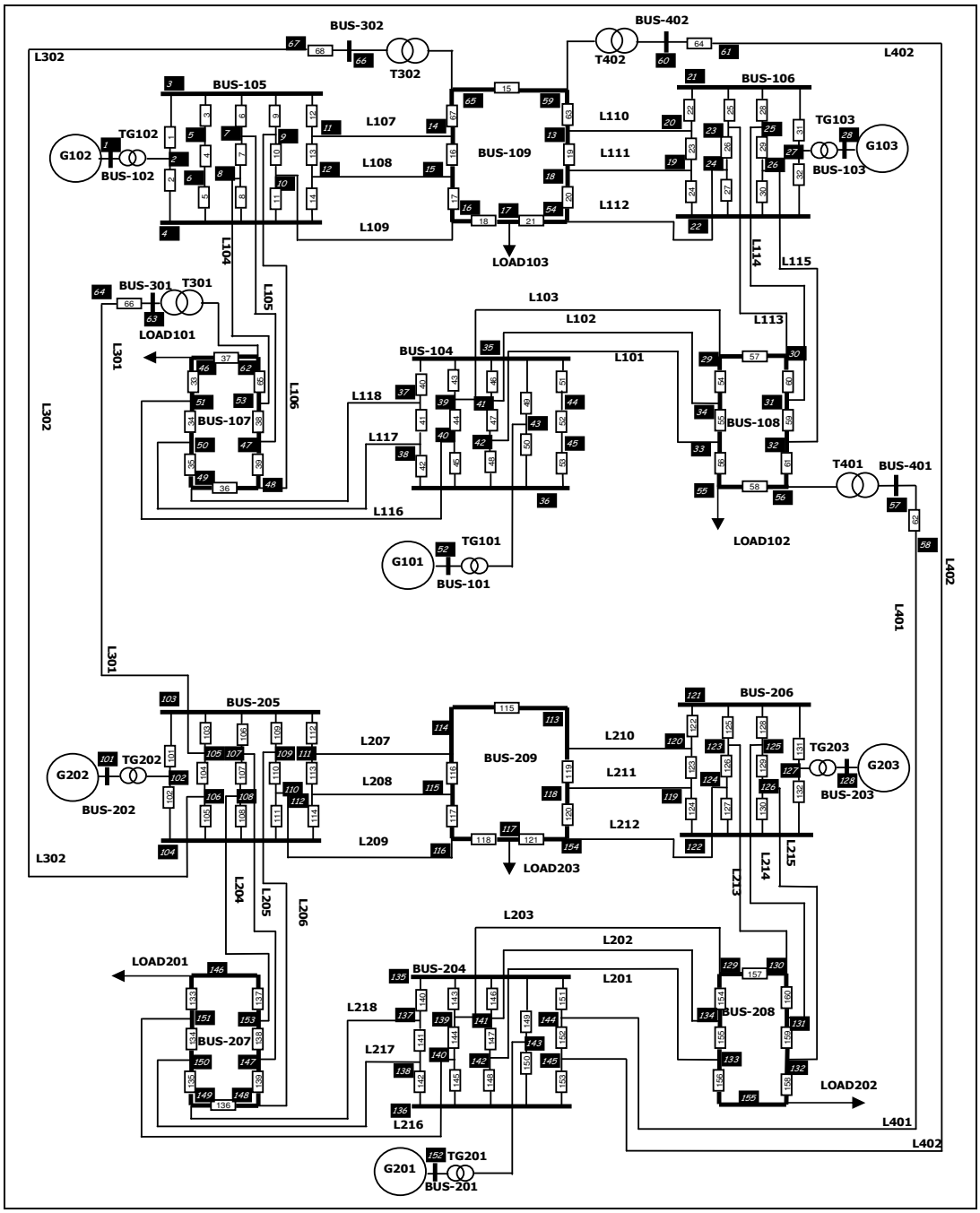

Fig. 53: One line diagram of a test system

APPENDIX E: TEST SYSTEM DATA

Table 30: The bus-breaker connection data

fb	to	name	No	fb	to	name	No	fb	to	name	No	fb	to	name
2	3	BUS-7	33	46	51	BUS-5	67	18	65	BUS-8	131	127	121	BUS-9
2	4	BUS-7	34	51	50	BUS-5	68	66	67	BUS-8	132	122	127	BUS-9
5	3	BUS-7	35	50	49	BUS-5	101	102	103	BUS-7	133	146	151	BUS-5
5	6	BUS-7	36	49	48	BUS-5	102	102	104	BUS-7	134	151	150	BUS-5
6	4	BUS-7	37	46	62	BUS-5	103	105	103	BUS-7	135	150	149	BUS-5
7	3	BUS-7	38	53	47	BUS-5	104	105	106	BUS-7	136	149	148	BUS-5
8	7	BUS-7	39	47	48	BUS-5	105	106	104	BUS-7	137	146	153	BUS-5
8	4	BUS-7	40	37	35	BUS-4	106	107	103	BUS-7	138	153	147	BUS-5
9	3	BUS-7	41	37	38	BUS-4	107	108	107	BUS-7	139	147	148	BUS-5
9	10	BUS-7	42	38	36	BUS-4	108	108	104	BUS-7	140	137	135	BUS-4
10	4	BUS-7	43	39	35	BUS-4	109	109	103	BUS-7	141	137	138	BUS-4
3	11	BUS-7	44	39	40	BUS-4	110	109	110	BUS-7	142	138	136	BUS-4
11	12	BUS-7	45	40	36	BUS-4	111	110	104	BUS-7	143	139	135	BUS-4
12	4	BUS-7	46	41	35	BUS-4	112	103	111	BUS-7	144	139	140	BUS-4
13	14	BUS-8	47	42	41	BUS-4	113	111	112	BUS-7	145	140	136	BUS-4
14	15	BUS-8	48	42	36	BUS-4	114	112	104	BUS-7	146	141	135	BUS-4
15	16	BUS-8	49	43	35	BUS-4	115	113	114	BUS-8	147	142	141	BUS-4
16	17	BUS-8	50	43	36	BUS-4	116	114	115	BUS-8	148	142	136	BUS-4
13	18	BUS-8	51	44	35	BUS-4	117	115	116	BUS-8	149	143	135	BUS-4
65	54	BUS-8	52	45	44	BUS-4	118	116	117	BUS-8	150	143	136	BUS-4
17	54	BUS-8	53	45	36	BUS-4	119	113	118	BUS-8	151	144	135	BUS-4
20	21	BUS-9	54	34	29	BUS-6	120	118	154	BUS-8	152	145	144	BUS-4
20	19	BUS-9	55	34	33	BUS-6	121	117	154	BUS-8	153	145	136	BUS-4
19	22	BUS-9	56	33	55	BUS-6	122	120	121	BUS-9	154	134	129	BUS-6
21	23	BUS-9	57	29	30	BUS-6	123	120	119	BUS-9	155	134	133	BUS-6
23	24	BUS-9	58	55	56	BUS-6	124	119	122	BUS-9	156	133	155	BUS-6
24	22	BUS-9	59	31	32	BUS-6	125	121	123	BUS-9	157	129	130	BUS-6
25	21	BUS-9	60	30	31	BUS-6	126	123	124	BUS-9	158	155	132	BUS-6
25	26	BUS-9	61	56	32	BUS-6	127	124	122	BUS-9	159	131	132	BUS-6
26	22	BUS-9	62	57	58	BUS-6	128	125	121	BUS-9	160	130	131	BUS-6
27	21	BUS-9	65	53	62	BUS-5	129	125	126	BUS-9	-	-	-	-
22	27	BUS-9	66	63	64	BUS-5	130	126	122	BUS-9	-	-	-	-

Table 31: Line data for the test system

NAME	F-BUS	T-BUS
L1	42	33
L2	41	34
L3	39	29
L4	53	8
L5	47	7
L6	48	9
L7	11	14
L8	12	15
L9	10	16
L10	13	20
L11	18	19
L12	54	24
L13	30	23
L14	31	25
L15	32	26
L16	40	51
L17	38	50
L18	37	49
L101	142	133
L102	141	134
L103	139	129
L104	153	108
L105	147	107
L106	148	109
L107	111	114
L108	112	115
L109	110	116
L110	113	120
L111	118	119
L112	154	124
L113	130	123
L114	131	125
L115	132	126
L116	140	151
L117	138	150
L118	137	149
L301	105	64
L302	106	67
L401	144	58

APPENDIX F: IEEE-RTS 24 BUS TEST SYSTEM

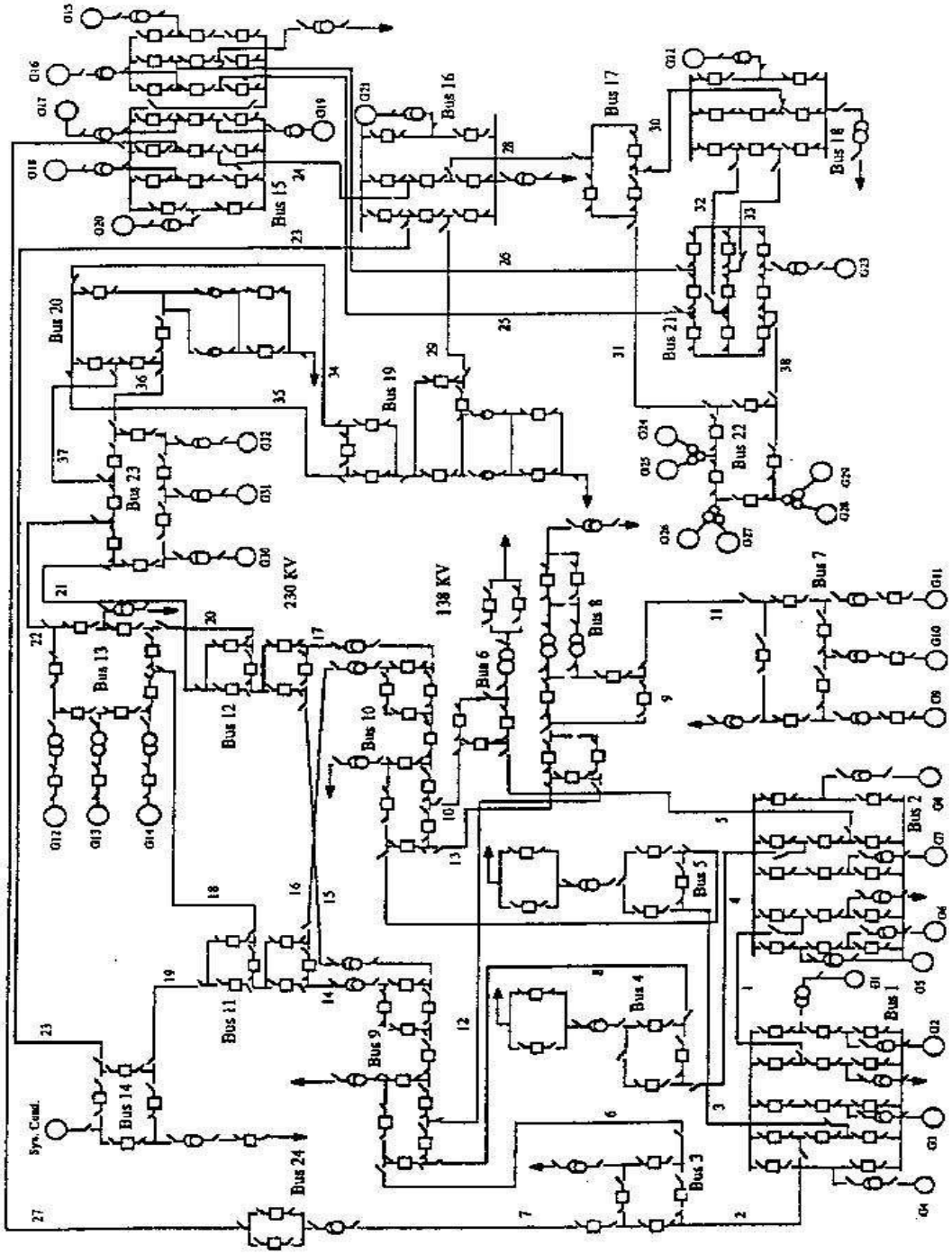

Fig. 54: IEEE RTS-24 bus test system substation diagram

APPENDIX G: PRECONDITIONED GMRESR ALGORITHM

In the preconditioned GMRESR algorithm, x_0 is the initial guess, m is the number of inner GMRES iterations, *tol* is the tolerance limit, r is the residual vector, u is an auxiliary vector, c is also an auxiliary vector satisfying the orthogonality conditions $\left(r_{k+1} \perp c_k \text{ and } c_i \perp c_j \text{ for } i \neq j\right)$, and α is an auxiliary scalar.

(1) Select x_0, m, *tol*;

$r_0 = b - Ax_0, k = -1;$

$r_0 = M^{-1} r_0$, (M is the preconditioner obtained from direct solver)

(2) do until $\|r_{k+1}\|_2 > tol$

$k = k + 1;$

$w_k = M^{-1} r_k;$

Solve $Au_k^{(0)} = w_k$ (use m iterative steps of GMRES);

$c_k^{(0)} = Au_k^{(0)};$

for $i = \max\left(0, k - j\right), ..., k - 1$

$\alpha_i = c_i^T c_k^{(i)};$

$c_k^{(i+1)} = c_k^{(i)} - \alpha_i c_i;$

$u_k^{(i+1)} = u_k^{(i)} - \alpha_i c_i;$

$c_k = c_k^{(k)} \Big/ \left\| c_k^{(k)} \right\|_2 ; u_k = u_k^{(k)} \Big/ \left\| c_k^{(k)} \right\|_2 ;$

$x_{k+1} = x_k + u_k c_k^T r_k;$

$r_{k+1} = r_k - c_k c_k^T r_k;$

APPENDIX H: OPTIMIZATION CODE FOR REDISPATCH AND LOAD SHEDDING (FROM [4])

Since branch loading is a slow process and each line usually has its emergency rating in addition to its normal rating to allow overloading for a short time period, a system operator has the time needed to perform redispatch so that the power flow of related line is adjusted to its nominal limit. Load-shedding happens only if it is impossible to bring the power flow in each line back to its long-term rating using some other means. In order to simulate the action of system operator, we use the following linear program problem to model what a system operator will do to avoid overloading.

Objective:

$$Max \sum_{i\in\{1,\ \ldots\ N\}} \alpha_i \times P_{D_i} \qquad \text{H.1}$$

Constraint:

$P_{D_i}^{\max} \geq P_{D_i} \geq 0, \quad i \in \{1,\ \ldots N_D\},$ The served load at bus i should be less than the total demand $P^{\max}$ at bus i;

$P_{G_i}^{\max} \geq P_{G_i} \geq 0, \quad i \in \{1,\ \ldots N\}$, Each generator generates between $0MW$ to $P_{\max}$;

$\gamma_i P_{B_i}^{\max} \geq P_{B_i} \geq -\gamma_i P_{B_i}^{\max}, \quad i \in \{1,\ \ldots N_B\}$, The power flow in each branch (line or transformer) is limited by its rating

$B^{'} \times \theta = P^{inject} = (P_G - P_D)$, DC power flow equations;

$(D_B \times A)\ \times \theta - P_B = 0$, Branch flow equations;

where

N_D is the total number of load buses;

N_B is the total number of branches;

N_G is the total number of generating buses;

P_{D_i} is the load demand at bus i;

α_i is the price factor to shed one unit MW load at bus i;

L_i is the total load (MW) served at bus i;

P_{G_i} is the real power generation at bus i;

$P_{G_i}^{\max}$ is the maximum real power generation at bus i, it is the summation of rating of all generators connected to bus i;

P_{B_i} is the real power flow in branch i;

$P_{B_i}^{\max}$ is the short term rating (MVA) of branch i;

γ_i is the constant factor to account for the power factor of the power flow in branch i and $1 \geq \gamma_i \geq 0$;

$B^{'}$ is the $N \times N$ B-matrix used in DC power flow and N is the number of buses;

A is the $M \times N$ adjacency (or incidence) matrix

D_B is the $M \times M$ diagonal matrix where the i^{th} diagonal element is the admittance of the i^{th} branch.

θ is the $N \times 1$ vector representing the voltage angles in radius at each bus;

P^{inject} is the $N \times 1$ vector representing the net power injection for each bus, and its element P_i can be calculated by $P_i = P_{g_i} - L_i$.

Not all the buses are both generator bus and load bus. It is observed that some buses are load bus only, some others are generation bus only, and some others may have no load or generator connected to them. If bus i has no generator connected to it, then we let $P_{G_i}^{\max}$ to be zero so that inequality $P_{G_i}^{\max} \geq P_{G_i} \geq 0$ will force the generation at bus i to be zero. We do the same thing for those buses without load connected to them.

In order to solve the above linear programming problem, we need to standardize the above inequalities and equalities so that we can use the standard LP subroutine in Matlab. We will change the object function and the constraint to the following standard format:

Objective:

$$\max f^T \cdot x \qquad \text{H.2}$$

Constraints:

$$A_{eq} \cdot x = b_{eq} \qquad \text{H.3}$$

$$lb \le x \le ub \qquad \text{H.4}$$

We define

$$P_G = \begin{pmatrix} P_{G_1} \\ P_{G_2} \\ \vdots \\ P_{G_{N_G}} \end{pmatrix}_{(N\times 1)} ; \quad P_D = \begin{pmatrix} P_{D_1} \\ P_{D_2} \\ \vdots \\ P_{D_N} \end{pmatrix}_{(N\times 1)} ; \quad P_B = \begin{pmatrix} P_{B_1} \\ P_{B_2} \\ \vdots \\ P_{B_M} \end{pmatrix}_{(M\times 1)} ; \quad \theta = \begin{pmatrix} \theta_1 \\ \theta_2 \\ \vdots \\ \theta_N \end{pmatrix}_{(N\times 1)} \qquad \text{H.5}$$

$$P_G^{\max} = \begin{pmatrix} P_{G_1}^{\max} \\ P_{G_2}^{\max} \\ \vdots \\ P_{G_N}^{\max} \end{pmatrix}_{(N\times 1)} ; \quad P_D^{\max} = \begin{pmatrix} P_{D_1}^{\max} \\ P_{D_2}^{\max} \\ \vdots \\ P_{D_N}^{\max} \end{pmatrix}_{(N\times 1)} ; \quad P_B^{\max} = \begin{pmatrix} \gamma_1 P_{B_1}^{\max} \\ \gamma_2 P_{B_2}^{\max} \\ \vdots \\ \gamma_M P_{B_M}^{\max} \end{pmatrix}_{(M\times 1)} ; \quad \theta^{\max} = \begin{pmatrix} \pi \\ \pi \\ \vdots \\ \pi \end{pmatrix}_{(N\times 1)} \qquad \text{H.6}$$

$$P_G^{\min} = \begin{pmatrix} 0 \\ 0 \\ \vdots \\ 0 \end{pmatrix}_{(N\times 1)} ; \quad P_D^{\min} = \begin{pmatrix} 0 \\ 0 \\ \vdots \\ 0 \end{pmatrix}_{(N\times 1)} ; \quad P_B^{\min} = \begin{pmatrix} -\gamma_1 P_{B_1}^{\max} \\ -\gamma_2 P_{B_2}^{\max} \\ \vdots \\ -\gamma_M P_{B_M}^{\max} \end{pmatrix}_{(M\times 1)} ; \quad \theta^{\min} = \begin{pmatrix} -\pi \\ -\pi \\ \vdots \\ -\pi \end{pmatrix}_{(N\times 1)} \qquad \text{H.7}$$

$$\alpha_G = \begin{pmatrix} 0 \\ 0 \\ \vdots \\ 0 \end{pmatrix}_{(N\times 1)} ; \quad \alpha_D = \begin{pmatrix} \alpha_1 \\ \alpha_2 \\ \vdots \\ \alpha_N \end{pmatrix}_{(N\times 1)} ; \quad \alpha_B = \begin{pmatrix} 0 \\ 0 \\ \vdots \\ 0 \end{pmatrix}_{(M\times 1)} ; \quad \alpha_\theta = \begin{pmatrix} 0 \\ 0 \\ \vdots \\ 0 \end{pmatrix}_{(N\times 1)} \qquad \text{H.8}$$

$$x = \begin{pmatrix} P_G^{\mathrm{T}} & \mathrm{P_D^T} & P_B^T & \theta^T \end{pmatrix}^{\mathrm{T}} \qquad \text{H.9}$$

$$f = \begin{pmatrix} \alpha_G^T & \alpha_D^T & \alpha_B^T & \alpha_\theta^T \end{pmatrix} \qquad \text{H.10}$$

$$\text{where } A_{eq} = \begin{pmatrix} 0 & 0 & I_{M\times M} & -D_{M\times M}\times A_{M\times N} \\ I_{N\times N} & -I_{N\times N} & 0 & -B'_{N\times N} \end{pmatrix}_{(M+N)\times(N+N+M+N)} \quad \text{H.11}$$

where the submatrix A, D and B inside A_{eq} are what we have defined at the beginning of this section, and I is the identity matrix. A_{eq}, ub and lb are defined as follows

$$B_{eq} = \begin{pmatrix} 0 \\ \vdots \\ 0 \end{pmatrix}_{(M+N)\times 1} \qquad ub = \begin{pmatrix} P_G^{\max} \\ P_D^{\max} \\ P_B^{\max} \\ \theta^{\max} \end{pmatrix} \qquad lb = \begin{pmatrix} P_G^{\min} \\ P_D^{\min} \\ -P_B^{\max} \\ \theta^{\min} \end{pmatrix} \quad \text{H.12}$$

After solving the LP to obtain a feasible solution for x, we get a new system profile that has no overloading problem. The total forced load shedding can be obtained through the following formula:

$$\sum_{i\in\{1,2,\cdots,N\}} (P_{D_i}^{\max} - P_{D_i}) \quad \text{H.13}$$

We use a simple example to show our method. The following diagram shows a 2-generator 3-bus system taken from [7]. For this system, we assume each load is of the same importance such that the cost to shed 1.0 p.u. of load is uniformly one. The fact device can adjust the flow on each line so that power flow factor for each line is 0.8, i.e. $\gamma_i = 0.8$ for $i = 1,\ 2,\ 3$. Since we need the adjacency matrix of the graphic representation of this system, which model the topology of the power system as a directed graph, we label each line with an arrow showing the reference direction of the active power flow in the line. There is not generator at BUS-2 and there is no load at BUS-1 and BUS-3. The constraints in the LP problem formulation will force the generation at BUS-2 and the load at BUS-1 and BUS-3 to be zero.

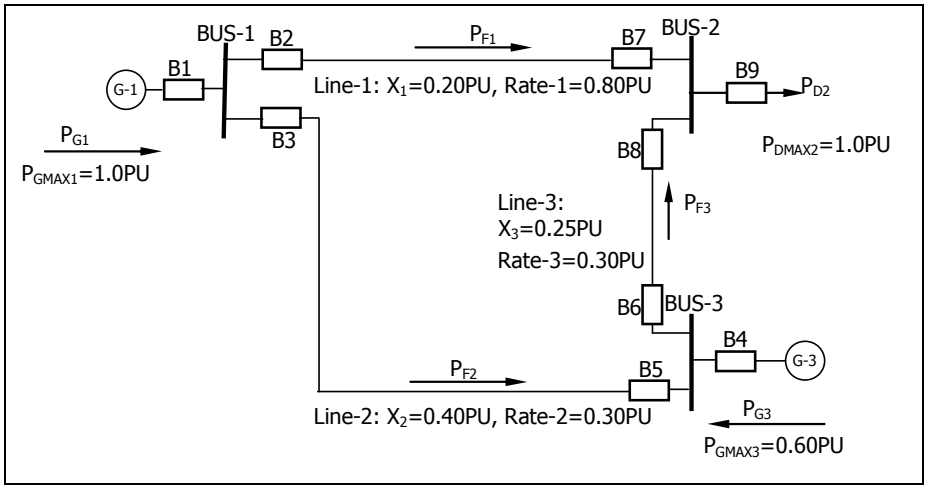

Fig. 55: Example system for linear programming illustration

Objective:

$$\max f^T \cdot x =$$
$$(0,\ 0,\ 0,\ 1,\ 1,\ 1,\ 0,\ 0,\ 0,\ 0,\ 0,\ 0)\times \qquad \text{H.14}$$
$$(P_{G_1},\ P_{G_2},\ P_{G_3},\ P_{D_1},\ P_{D_2},\ P_{D_3},\ P_{B_1},\ P_{B_2},\ P_{B_3},\ \theta_1,\ \theta_2,\ \theta_3,)^T$$

Constraints:

$$\begin{pmatrix} 0 & 0 & 0 & 0 & 0 & 0 & 1 & 0 & 0 & 5.0 & -5.0 & 0 \\ 0 & 0 & 0 & 0 & 0 & 0 & 0 & 1 & 0 & 2.5 & 0 & -2.5 \\ 0 & 0 & 0 & 0 & 0 & 0 & 0 & 0 & 1 & 0 & -4.0 & 4.0 \\ 1 & 0 & 0 & -1 & 0 & 0 & 0 & 0 & 0 & 7.5 & -5.0 & -2.5 \\ 0 & 1 & 0 & 0 & -1 & 0 & 0 & 0 & 0 & -5.0 & 9.0 & -4.0 \\ 0 & 0 & 1 & 0 & 0 & -1 & 0 & 0 & 0 & -2.5 & -4.0 & 6.5 \end{pmatrix} \times \begin{pmatrix} P_{G1} \\ P_{G2} \\ P_{G3} \\ P_{D1} \\ P_{D2} \\ P_{D3} \\ P_{B1} \\ P_{B2} \\ P_{B3} \\ \theta_1 \\ \theta_2 \\ \theta_3 \end{pmatrix} = 0 \qquad \text{H.15}$$

$$\begin{pmatrix} 0 \\ 0 \\ 0 \\ 0 \\ 0 \\ 0 \\ -0.8\times 0.80 \\ -0.8\times 0.30 \\ -0.8\times 0.30 \\ -\pi \\ -\pi \\ -\pi \end{pmatrix} \leq \begin{pmatrix} P_{G1} \\ P_{G2} \\ P_{G3} \\ P_{D1} \\ P_{D2} \\ P_{D3} \\ P_{B1} \\ P_{B2} \\ P_{B3} \\ \theta_1 \\ \theta_2 \\ \theta_3 \end{pmatrix} \leq \begin{pmatrix} 1.0 \\ 0 \\ 0.6 \\ 0 \\ 1.0 \\ 0 \\ 0.8\times 0.80 \\ 0.8\times 0.30 \\ 0.8\times 0.30 \\ \pi \\ \pi \\ \pi \end{pmatrix} \quad \text{H.16}$$

The solution for the above linear programming problem is listed in Table 32

Table 32: Solution for the sample LP problem in Fig. 55

P_{G1}	P_{G2}	P_{G3}	P_{D1}	P_{D2}	P_{D3}	P_{B1}	P_{B2}	P_{B3}	θ_1	θ_2	θ_3
0.81	0	0.07	0	0.88	0	0.64	0.17	0.24	-0.065	0.063	0.0027

Substitute the solution of the parameters in Table 32, we find the max load the system can serve is 88 MW (0.88 p.u.).

ACKNOWLEDGMENTS

I would like to express my sincere gratitude to Dr. James D. McCalley, my major professor and advisor, for his constant support and guidance throughout the course of this study. One specific thing that I really appreciate in him is his open mindedness and he is always ready to hear out his student's ideas. He gives so many opportunities to explore new research directions and ready to extend his support. He is very meticulous in going through the student's work, papers and gives very relevant inputs. Particularly I have benefitted a lot from his inputs and suggestions. He is very eager for the welfare of the student.

I am also grateful to Dr. Ajjarapu for the seminars that he organized. They greatly helped me in getting a broader outlook. My sincere thanks are due to all my committee members for their insightful comments. They always spared time for me to discuss whenever I needed their help. I would also like to acknowledge the facilities that the department provided in terms of the computer facilities, CSG, labs, supercomputer, and a unique group of faculties in different research areas and in so many other ways. I also appreciate the department chair for his wonderful leadership to the department and taking it forward. I would like to gratefully thank all the friends and colleagues at Iowa State whose friendships helped me in a number of ways and made this stay very comfortable.

I cannot sufficiently express my heartfelt gratitude with words for my eternal teacher, Dr. P. V. Krishnan and his wife. Dr. Krishnan's perfect example in character and in his work has inspired me very deeply and completely changed my life. He gave me a vision in life to live by principles and always aspire for the ultimate good for all living entities, free from any tendency for exploitation for personal name, fame etc. By his own example he has taught us

how to become completely selfless and use all the resources (including our PhD) at our disposal for the genuine progress and upliftment of the society. He and his wife have sacrificed their entire life to create a class of genuine intellectuals who would be emblems of perfect character and qualities and would give true leadership to the society. Anyone who comes in contact with them even for once experiences unprecedented love and care and a change of heart by their association. I hope I can live up to their teachings in my life.

I am also extremely grateful to my father, brother and all other members of my family for sacrificing their personal comforts and allowing me to come to US to pursue my degree in very difficult circumstances. Their support has been unfailing, without which I would not have been able to do this work. Special love to my brother, Harsha, whose support and sacrifices are known only to me. I am also very grateful to my wife for her support during its completion. I am also genuinely touched by the love and help of my very dear friends especially Ankit, Dr. Kasthurirangan, Amit, Abhisek, Dr. Lakshminarasimhan, Dr. Siva Kumar, Venkat, Tanay and Chetan. Ankit helped me a lot with his brilliance in computers and Dr. Rangan's friendship was very vital for psychological support. I am also very grateful to all the trees who sacrificed their lives for the numerous papers that I printed during the course of this PhD.

Part of this work was sponsored by PSerc S-26 and I am grateful for their support.

LIST OF PUBLICATIONS

Journals:

1. Multifrontal Solver for Online Power System Time Domain Simulation: under review IEEE Transactions on Power Systems. (Chapter 3)
2. Probability Estimation of High Risk N-k Inadvertent Contingencies for Online Security Assessment: under review IEEE Transactions on Power Systems. (Chapter 2)
3. A class of new preconditioners for iterative solution of power system time domain simulation: to be submitted to IEEE Transactions on Power Systems. (Chapter 4)
4. Importance of Generator Protection Modeling for On-line Cascading Event Tracking and Avoidance Decision Support Tool: to be submitted to IEEE Transactions on Power Systems. (Chapter 5 and 6)
5. DFS based algorithm for simulating cascading: in preparation (Chapter 5 and 6)
6. A study of Blackouts in past 40 years: in preparation (Chapter 1)

REFERENCES

[1] N.B. Bhatt, " August 14, 2003 U.S. – Canada blackout," presented at the IEEE PES General meeting, Denver, CO, 2004

[2] W.R. Lachs - "Controlling Grid Integrity After Power System Emergencies," IEEE Transactions in Power Systems PWRS No.17 No.2 May 2002

[3] W.R. Lachs – "A New Horizon for System Protection Schemes," IEEE Transactions in Power Systems PWRS No.18 No. 1 – February 2003 pp.334-338

[4] Qiming Chen, "The probability, identification and prevention of rare events in power system," PhD Thesis, ECE, Iowa State University, 2004

[5] J. McCalley, "Transmission Security: Rules, Risks, and Blackouts," Midwest ISO's System Operator Training Short Course, April 24-28, 2006.

[6] P. Jian, J. McCalley, "On-line analysis of high-order contingencies," in Proc. North Amer. Power Symp., Oct. 15-16, 2001, pp. 297-302.

[7] Allen J. Wood, Bruce F. Wollenberg, "Power generation, operation and control," John Wiley & Sons, Inc., 1996

[8] A. O. Ekwue, "A review of automatic contingency selection algorithms for online security analysis," The Third International Conference on Power System Monitoring and Control, pp 152-155, June 26-28, 1991

[9] R. N. Allan, A. N. Adraktas, "Terminal effects and protection system failures in composite system reliability evaluation," IEEE Transactions on Power Apparatus and Systems, Vol. PAS-101, No. 12, pp 4557-4562, Dec. 1982

[10] R. Billinton, T. K. P. Medicherla, "Station originated multiple outages in the reliability analysis of a composite and transmission system," IEEE Transactions on Power Apparatus and Systems, Vol. PAS-100, No. 8, pp 3870-3878, Dec. 1982

[11] R. Billinton, P. K. Vohra, Sudhir Kumar, "Effect of Station originated outages in a composite system – adequate evaluation of the IEEE reliability test system," IEEE Transactions on Power Apparatus and Systems, Vol. PAS-104, No. 10, pp 2649-2656, Oct. 1985

[12] A. G. Phadke, J.S. Thorp, "Expose hidden failures to prevent cascading outages in power

systems," IEEE Comput. Appl. Power, vol. 9, no. 3, pp. 20-23, Jul. 1996.

[13] D. C. Elizondo, J. de La Ree, A. G. Phadke, S. Horowitz, "Hidden failures in protection systems and their impact on wide area disturbances," in Proc. IEEE power Eng. Soc. Winter Meeting, vol. 2, 28 Feb. 2001, pp. 710-714

[14] Qiming Chen; James D. McCalley, "Identifying High-risk N-k Contingencies for On-line Security Assessment," *IEEE Transactions On Power Systems*, Volume 20, Issue 2, May 2005 Page(s):823 – 834

[15] McCalley, J.D.; Vittal, V.; Abi-Samra, N., "An overview of risk based security assessment," IEEE Power Engineering Society Summer Meeting, Vol. 1 ,pp 173-178, 1999

[16] Mohammad Modarres, Mark Kaminskiy, Vasiliy Krivtsov, "Reliability Engineering and Risk Analysis," Marcel Dekker, Inc., 1999

[17] Arnljot Hoyland, Marvin Rausand, "System Reliability Theory Models and Statistical Methods," John Wiley & Sons, Inc., 1994

[18] W.A. Thompson, Jr., "Point Process Models with Applications to Safety and Reliability," Chapman and Hall, 1988

[19] J. Lewis Blackburn, "Protective relaying, principles and applications," Marcel Dekker, Inc., 1987

[20] NERC (North American Reliability Council) Disturbance Analysis Working Group Database, "http://www.nerc.com/~dawg/database.html," 1984-2001 (Date accessed: September 1, 2005).

[21] Harary, F., Graph Theory. Reading, MA: Addison-Wesley, 1994

[22] IEEE Power System Relay Committee Working Group I17 Report, Transmission Relay System Performance Comparison

[23] Sanchez-Gasca, J.J.; D'Aquila, R.; Price, W.W.; Paserba, J.J.; "Variable time step, implicit integration for extended-term power system dynamic simulation," IEEE Conference Proceedings of Power Industry Computer Application Conference, pp 183-189, May 7-12, 1995

[24] Astic, J.Y.; Bihain, A.; Jerosolimski, M.; "The mixed Adams-BDF variable step size algorithm to simulate transient and long-term phenomena in power systems," IEEE

Transactions on Power Systems, Vol. 9, Issue 2, pp 929-935, May 1994

[25] Paul M. Anderson, A. A. Fouad, Power system control and stability, the Institute of Electrical and Electronic Engineers, Inc., 1994

[26] Brenan K.E., Campbell S.L.Petzold L.R, Numerical Solution of Initial-Value Problems in Differential- Algebraic Equations, SIAM,1996

[27] M. Berzins, R.M. Furzeland, "An Adaptive Theta Method for the Solution of Stiff and Non-Stiff Differential Equations," App. Num. Math., Vol. 9, pp 1.19, 1992.

[28] F.L. Alvarado, R.H. Lasseter, J.J. Sanchez, "Testing of Trapezoidal Integration with Damping for the Solution of Power Transient Problems," IEEE Trans. on Power App. and Syst., Vol. PAS-102, No. 12, pp. 3783-3790, 1983.

[29] T. Orfanogianni, R. Bacher. Using Automatic Code Differentiation in Power Flow Algorithms. IEEE Transactions on Power Systems, Vol. 14, No. 1, February 1999.

[30] J. Johnson, P. Vachranukunkiet, S. Tiwari, P. Nagvajara, C. Nwankpa, "Performance Analysis of Loadflow Computation Using FPGA," Proc. of 15th Power Systems Computation Conference 2005.

[31] Davis, T. A. and Duff, I. S, "A combined unifrontal/multifrontal method for unsymmetric sparse matrices," ACM Trans. Math. Software, Vol. 25, Issue 1, pp. 1–19, 1999.

[32] Davis, T. A., "Algorithm 832: UMFPACK - An unsymmetric-pattern multifrontal method," ACM Trans. Math. Software, Vol. 30, Issue 2, pp. 196-199, 2004.

[33] Davis, T. A. 'A column pre-ordering strategy for the unsymmetric-pattern multi-frontal method', ACM Trans. Math. Software, Vol. 30, Issue 2, pp. 165-195, 2004.

[34] Davis, T. A., Amestoy, P. R. and Duff, I. S. 'Algorithm 837: AMD, an approximate minimum degree ordering algorithm', ACM Trans. Math. Software, Vol. 30, Issue 3, pp. 381-388, 2004.

[35] Davis, T. A., Gilbert, J. R. and Larimore, E. 'Algorithm 836: COLAMD, an approximate column minimum degree ordering algorithm', ACM Trans. Math. Software, Vol. 30, Issue 3, pp. 377-380, 2004.

[36] Irons, B.M. 'A frontal solution scheme for finite element analysis', Numer. Meth. Engg, Vol. 2, pp. 5-32.1970.

[37] P. Hood. Frontal solution program for unsymmetric matrices. Int. J. Numer. Meth. Engng. 10, 379-400, 1976.

[38] I.S. Duff, MA32 - A package for solving sparse unsymmetric systems using the frontal method. Technical Report AERE R11009, Her Majesty's Stationery Office, London, 1981

[39] Dongarra J. J., J. Du Croz and S. Hammarling, A set of level 3 basic linear algebra subprograms. ACM -Trans. Math. Sofiw. 16, 1-17 (1990).

[40] K. V. Camarda, M. A. Stadtherr. Frontal solvers for process engineering: local row ordering strategies. Computers in Chemical Engineering, 22, 333-341, 1998.

[41] Zitney S. E., Sparse matrix methods for chemical process separation calculations on supercomputers. In Proceedings of Supercomputing '92, pp. 414-423, IEEE Computer Society Press, Los Alamitos, CA (1992).

[42] Zitney S. E. and M. A. Stadtherr, Frontal algorithms for equation-based chemical process flow sheeting on vector and parallel computers. -Computers Chem. Engng, 17, pp. 319-338, 1993.

[43] Zitney S. E: and fi. A. Stadtherr, Supercomputing strategies for the design and analysis of complex separation systems. Znd. Ennnn them. Res. 32. 604-612 1993.

[44] Zitney S. E., R. J. kmarger and P. Winter, The'impact.of supercomputing on dynamic simulation using the SPEEDUP system., Presented at AIChE National Meeting, New Orleans, March 1992.

[45] Zitney S. E., L. Brilll, L. Lang and R. Zeller, Plant wide dynamic simulation on supercomputers: modeling a Bayer distillation process. Presented at Foundations of Computer Aided Process Design, Snowmass Village, Colorado, July 1994.

[46] Zitney S. E., K. V. Camarda and M. A. Stadtherr, Impact of supercomputing in simulation and optimization of process operations. In Proc. Second Int. Conf. on Foundations of Computer-Aided Process Operations (Edited by Rippen D. W. T., J. C. Hale and J. F. Davis), pp. 463-468. CACHE Corp., Austin, TX (1994b)

[47] I. S. Duff. A review of frontal methods for solving linear systems. Computer Physics Communications 97, 45-52, 1996.

[48] I. S. Duff, J.A. Scott. A comparison of frontal software with other sparse direct solvers.

Technical Report RAL-TR-96-102 (Revised), Rutherford Appleton Laboratory, 1996a.

[49] I. S. Duff, J.A. Scott. The design of a new frontal code for solving sparse unsymmetric systems. ACM Trans. Mathematical Software, 22(1), 30-45, 1996b.

[50] I. S. Duff, J.A. Scott. MA42 - a new frontal code for solving sparse unsymmetric systems. Technical Report RAL-93-064, Rutherford Appleton Laboratory, 1993.

[51] I. S. Duff, J.K. Reid. The multifrontal solution of indefinite sparse symmetric linear systems. ACM Trans. Math. Softw. 9, 302-325, 1983.

[52] I. S. Duff, J.A. Scott. The use of multiple fronts in Gaussian elimination. in J. Lewis, ed., 'Proceedings of the Fifth SIAM Conference Applied Linear Algebra', pp. 567 571. SIAM, 1994b.

[53] I. S. Duff, J.K. Reid. The multifrontal solution of unsymmetric sets of linear systems. SIAM J. Sci. Stat. Comput. 5, 633-641, 1984.

[54] I. S. Duff, J.K. Reid. The design of MA48, a code for the direct solution of sparse unsymmetric linear systems of equations. ACM Trans. Mathematical Software, 22, 187-226, 1996.

[55] C. C. Ashcraft, R. Grimes. The influence of relaxed supernode partitions on the multifrontal method. ACM Trans. Math. Softw. 15, 4, 291-309, 1989.

[56] M. T. Heath, P. Raghavan. A Cartesian parallel nested dissection algorithm. SIAM J. Matrix Anal. Applic. 16, 1, 235-253, 1995.

[57] A. Gupta, F. Gustavson, M. Joshi, G. Karypis, V. Kumar. PSPASES: an efficient and parallel sparse direct solver. In Kluwer Intl. Series in Engineering and Science, T. Yang, Ed. Vol. 515. Kluwer, 1999.

[58] J. W. H. Liu. The multifrontal method for sparse matrix solution: Theory and practice. SIAM Rev. 34, 1, 82-109, 1992.

[59] I. S. Duff, J. K. Reid. MA27 - a set of Fortran subroutines for solving sparse symmetric sets of linear equations. Tech. Rep. AERE-R-10533, AERE Harwell Laboratory, United Kingdom Atomic Energy Authority, 1982.

[60] I. S. Duff. A new code for the solution of sparse symmetric definite and indefinite systems. Tech. Rep. TR-2002-024, Rutherford Appleton Laboratory, 2002.

[61] P. R. Amestoy, I. S. Duff. Vectorization of a multiprocessor multifrontal code. Intl. J.

Supercomputer Appl. 3, 3, 41–59, 1989.

[62] P. R. Amestoy, I. S. Duff, J.-Y. L'Excellent, J. Koster. A fully asynchronous multifrontal solver using distributed dynamic scheduling. SIAM J. Matrix Anal. Applic. 23, 1, 15–41, 2001a.

[63] I. S. Duff. The solution of nearly symmetric sparse linear systems. In Computing methods in applied sciences and engineering, VI, R. Glowinski and J.-L. Lions, Eds. North Holland, Amsterdam New York and London, 57–74, 1984.

[64] I. S. Duff, J. K. Reid. A note on the work involved in no-fill sparse matrix factorization. SIAM J. Num. Anal. 3, 37–40, 1983b.

[65] P. R. Amestoy, C. Puglisi. An unsymmetrized multifrontal LU factorization. SIAM J.Matrix Anal. Applic. 24, 553–569, 2002.

[66] T. A. Davis, I. S. Duff. An unsymmetric-pattern multifrontal method for sparse LU factorization. SIAM J. Matrix Anal. Applic. 18, 1, 140–158. 1997.

[67] A. Gupta. Improved symbolic and numerical factorization algorithms for unsymmetric sparse matrices. SIAM J. Matrix Anal. Applic. 24, 529–552, 2002.

[68] S. M. Hadfield. On the LU factorization of sequences of identically structured sparse matrices within a distributed memory environment. Ph.D. thesis, University of Florida, Gainesville, FL, 1994.

[69] S. M. Hadfield, T. A. Davis. The use of graph theory in a parallel multifrontal method for sequences of unsymmetric pattern sparse matrices. Cong. Numer. 108, 43–52, 1995.

[70] P. R. Amestoy, I. S. Duff, C. Puglisi. Multifrontal QR factorization in a multiprocessor environment. Numer. Linear Algebra Appl. 3, 4, 275–300, 1996a.

[71] P. Matstoms. Sparse QR factorization in MATLAB. ACM Trans. Math. Softw. 20, 1, 136–159, 1994.

[72] X. Li, Direct Solvers for Sparse Matrices, September 2006, http://crd.lbl.gov/~xiaoye/SuperLU/SparseDirectSurvey.pdf.

[73] Y. Chen, T. A. Davis, W. W. Hager, and S. Rajamanickam, Algorithm 8xx: CHOLMOD, supernodal sparse Cholesky factorization and update/downdate. Technical Report TR-2006-005, University of Florida, 2006. (http://www.cise.ufl.edu/research/sparse/cholmod/).

[74] I.S Duff and J. K. Reid. MA47, a Fortran code for direct solution of indefinite sparse symmetric linear systems. Technical Report RAL-95-001, Rutherford Appleton Laboratory, 1995

[75] F. Dobrian and A. Pothen. Oblio: a sparse direct solver library for serial and parallel computations. Technical report, Old Dominion University, 2000

[76] Kenneth Kundert. Sparse matrix techniques. In Albert Ruehli, editor, Circuit Analysis, Simulation and Design. North-Holland, 1986. (http://www.netlib.org/sparse)

[77] A. George and J. Liu. Computer Solution of Large Sparse Positive Definite Systems. Prentice-Hall Inc., Englewood Cliffs, New Jersey, 1981. (jageorge@sparse1.uwaterloo.ca).

[78] C. Ashcraft and R. Grimes. SPOOLES: An object-oriented sparse matrix library. In Proceedings of the Ninth SIAM Conference on Parallel Processing, 1999. (http://www.netlib.org/linalg/spooles).

[79] Esmond G. Ng and Barry W. Peyton. Block sparse Cholesky algorithms on advanced uniprocessor computers. SIAM J. Sci. Comput., 14(5):1034–1056, September 1993. (egng@lbl.gov).

[80] James W. Demmel, Stanley C. Eisenstat, John R. Gilbert, Xiaoye S. Li, and Joseph W. H. Liu. A supernodal approach to sparse partial pivoting. SIAM J. Matrix Anal. Appl., 20(3):720–755, 1999. (http://crd.lbl.gov/xiaoye/SuperLU).

[81] T. A. Davis. Algorithm 832: UMFPACK V4.3, an unsymmetric-pattern multifrontal method with a column pre-ordering strategy. ACM Trans. Mathematical Software, 30(2):196–199, June 2004. (http://www.cise.ufl.edu/research/sparse/umfpack/).

[82]J.S. Chai, N. Zhu, A. Bose and D.J. Tylavsky, 'Parallel Newton type methods for power system stability analysis using local and shared memory multiprocessors", IEEE Trans. Power Syst., Vol. 6, No. 4, pp. 1539-1545, November 1991.

[83] R. S. Varga, Matrix Iterative Analysis (Prentice–Hall, Englewood Cliffs, NJ, 1962).

[84] E. Wachspress, Iterative Solution of Elliptic Systems and Applications to the Neutron Diffusion Equations of Reactor Physics (Prentice–Hall, Englewood Cliffs, NJ, 1966).

[85] D. M. Young, Iterative Solution of Large Linear systems (Academic Press, New York, 1971).

[86] N¨oel M. Nachtigal, Satish C. Reddy, and Lloyd N. Trefethen. How fast are nonsymmetric matrix iterations? SIAM Journal on Matrix Analysis and Applications, 13 , pp 778–795, 1992.

[87] Pai M. A., Sauer P. W. and Kulkarni, "A Preconditioned iterative solver for dynamic simulation of power systems", In Proceedings of ISCAS 1995, pp. 1279-1282, 1995.

[88] Pai M. A. and Dag H., "Iterative Solver Techniques in Large Scale Power System Computation", In Proceedings of 36th Conference on Decision & Control, USA, pp 3861-3866, vol. 4, 1997.

[89]Yousef Saad and Martin H. Schultz. GMRES: A generalized minimal residual algorithm for solving nonsymmetric linear systems. SIAM Journal on Scientific and Statistical Computing, 7, pp 856–869, 1986.

[90] Ake Bj¨orck. Numerical Methods for Least Squares Problems. SIAM, Philadelphia, 1996.

[91]Roland W. Freund and N¨oel M. Nachtigal. QMR: A quasi-minimal residual method for non- Hermitian linear systems. Numerische Mathematik, 60, pp 315–339, 1991.

[92] Martin H. Gutknecht and Zdenˇek Strakoˇs. Accuracy of two three-term and three two-term recurrences for Krylov space solvers. SIAM Journal on Matrix Analysis and Applications, 22, pp 213–229, 2000.

[93] Martin H. Gutknecht. Variants of BiCGStab for matrices with complex spectrum. SIAM Journal on Scientific Computing, 14, pp 1020–1033, 1993.

[94] Gerard L. G. Sleijpen and Diederik R. Fokkema. BiCGStab(`) for linear equations involving unsymmetric matrices with complex spectrum. Electronic Transactions on Numerical Analysis, 1, pp 11–32, 1993.

[95] N¨oel M. Nachtigal. A look-ahead variant of the Lanczos algorithm and its application to the quasi-minimal residual method for non-Hermitian linear systems. PhD thesis, Massachussets Institute of Technology, Cambridge, Massachussets, 1991.

[96] Valeria Simoncini and Daniel B. Szyld. The effect of non-optimal bases on the convergence of Krylov subspace methods. Numerische Mathematik, 100, pp 711–733, 2005.

[97] Michael Eiermann, Oliver G. Ernst, and Olaf Schneider. Analysis of acceleration

strategies for restarted minimal residual methods. Journal of Computational and Applied Mathematics, 123, pp 261–292, 2000.

[98] Mark Embree. The tortoise and the hare restart GMRES. SIAM Review, 45, pp 259–266, 2003.

[99] Wayne D. Joubert. On the convergence behavior of the restarted GMRES algorithm for solving nonsymmetric linear systems. Numerical Linear Algebra with Applications, 1, pp 427–447, 1994.

[100] Valeria Simoncini. A new variant of restarted GMRES. Numerical Linear Algebra with Applications, 6, pp 61–77, 1999.

[101] L. N. Trefethen and D. Bau, III, *Numerical Linear Algebra,* SIAM, Philadelphia, PA, 1997.

[102] A. Greenbaum, V. Pt´ak, and Z. Strakoˇs, Any nonincreasing convergence curve is possible for GMRES, *SIAM J. Matrix Anal. Appl.* **17**, pp 465, 1996.

[103] Y. Saad, *Iterative Methods for Sparse Linear Systems,* PWS Publishing, Boston, 1996.

[104] S. L. Lee, *Krylov Methods for the Numerical Solution of Initial-Value Problems in Differential-Algebraic Equations*, Ph.D. thesis and Technical Report UIUCDS-R-93-1814 , Dept. Computer Science, Univ. Illinois at Urbana-Champaign, 1993.

[105] A. Greenbaum, *Iterative Methods for Solving Linear Systems,* SIAM, Philadelphia, PA, 1997.

[106] S. F. Ashby, P. N. Brown, M. R. Dorr, and A. C. Hindmarsh, A linear algebraic analysis of diffusion synthetic acceleration for the Boltzmann transport equation, *SIAM J. Numer. Anal.* **32**, pp 179, 1995.

[107] E.W. Larsen, Unconditionally stable diffusion-synthetic acceleration methods for the slab geometry discrete ordinates equations. Part I: Theory, *Nucl. Sci. Eng.* **82**, pp 47, 1982.

[108] D. R. McCoy and E.W. Larsen, Unconditionally stable diffusion-synthetic acceleration methods for the slab geometry discrete ordinates equations. Part II: Numerical results, *Nucl. Sci. Eng.* **82**, pp 64, 1982.

[109] J. S. Warsa, T. A. Wareing, and J. E. Morel, Solution of the discontinuous $P1$ equations in two-dimensional Cartesian geometry with two-level preconditioning, *SIAM J. Sci.*

Comput., in press.

[110] O. Axelsson and V. Eijkhout, Vectorizable preconditioners for elliptic difference equations in three space dimensions, *J. Comput. Appl. Math.* **27**, pp 299, 1991.

[111] I. S. Duff and G. Meurant, The effect of ordering on preconditioned conjugate gradients, *BIT* **29**, pp 635, 1989.

[112] M. Benzi, D. B. Szyld, and A. van Duin, Orderings for incomplete factorization preconditioning of nonsymmetric problems, *SIAM J. Sci. Comput.* **20**, pp 1652, 1999.

[113] E. Chow and Y. Saad, Experimental study of ILU preconditioners for indefinite matrices, *J. Comput. Appl. Math.* **86**, pp 387, 1997.

[114] M. Magolu monga Made, R. Beauwens, and G. Warz´ee, Preconditioning of discrete Helmholtz operators perturbed by a diagonal complex matrix, *Commun. Numer. Methods Eng.* **16**,pp 801, 2000.

[115] M. Magolu mongaMade and H. A. van der Vorst, Parallel incomplete factorizations with pseudooverlapping subdomains, *Parallel Comput.* **27**, pp 989, 2001.

[116] S. Le Borne, Ordering techniques for two- and three-dimensional convection-dominated elliptic boundary value problems, *Computing* **64**, pp 123, 2000.

[117] D. Hysom and A. Pothen, A scalable parallel algorithm for incomplete factor preconditioning, *SIAM J. Sci. Comput.* **22**, pp 2194, 2001.

[118] M. Heniche, Y. Secretan, and M. Leclerc, Efficient ILU preconditioning and inexact-Newton-GMRES to solve the 2D steady shallow water equations, *Commun. Numer. Methods Eng.* **17**, pp 69, 2001.

[119] H. C. Elman and M. P. Chernesky, Ordering effects on relaxation methods applied to the discrete one dimensional convection-diffusion equation, *SIAM J. Numer. Anal.* **30**, pp 1268, 1993.

[120] V. Eijkhout, Analysis of parallel incomplete point factorizations, *Linear Algebra Its Appl.* **154**, pp 723, 1991.

[121] L. C. Dutto, The effect of ordering on preconditioned GMRES algorithm, for solving the compressible Navier-Stokes equations, *Int. J. Numer. Methods Eng.* **36**, pp 457, 1993.

[122] I. S. Duff and J. Koster, The design and use of algorithms for permuting large entries to the diagonal of sparse matrices, *SIAM J. Matrix Anal. Appl.* **20**, pp 889, 1999.

[123] I. S. Duff and J. Koster, On algorithms for permuting large entries to the diagonal of a sparse matrix, *SIAM J. Matrix Anal. Appl.* **22**, pp 973, 2001.

[124] I. S. Duff and G. Meurant, The effect of ordering on preconditioned conjugate gradients, *BIT* **29**, pp 635, 1989.

[125] S. Doi, On parallelism and convergence of incomplete LU factorizations, *Appl. Numer. Math.* **7**, pp 417, 1991.

[126] S. Doi and T. Washio, Ordering strategies and related techniques to overcome the trade-off between parallelism and convergence in incomplete factorizations, *Parallel Comput.* **25**, pp 1995, 1999.

[127] E. F. D'Azevedo, P. A. Forsyth, and W.-P. Tang, Ordering methods for preconditioned conjugate gradient methods applied to unstructured grid problems, *SIAM J. Matrix Anal. Appl.* **13**, pp 944, 1992.

[128] A. George and J. W. Liu, Computer Solution of Large Sparse Positive Definite Systems, Prentice–Hall, Englewood Cliffs, NJ, 1981.

[129] E. Cuthill, Several strategies for reducing the bandwidth of matrices, in *Sparse Matrices and Their Applications*, p. 157, edited by D. J. Rose and R. A. Willoughby, Plenum, New York, 1972.

[130] S. W. Sloan, An algorithm for profile and wavefront reduction of sparse matrices, *Int. J. Numer. Methods Eng.* **23**, pp 239, 1986.

[131] N. E. Gibbs,W. G. Poole, Jr., and P. K. Stockmeyer, An algorithm for reducing the bandwidth and profile of a sparse matrix, *SIAM J. Numer. Anal.* **13**, pp 236, 1976.

[132] A. George and J. W. Liu, The evolution of the minimum degree algorithm, *SIAM Rev.* **31**, pp 1, 1989.

[133] J. W. H. Liu, Modification of the minimum degree algorithm by multiple elimination, *ACM Trans. Math. Software* **11**, pp 141, 1985.

[134] A. George, Nested dissection of a regular finite element mesh, SIAM J. Numer. Anal. 10, pp 345, 1973.

[135] R. J. Lipton, D. J. Rose, and R. E. Tarjan, Generalized nested dissection, *SIAM J. Numer. Anal.* **16**, pp 346, 1979.

[136] I. S. Duff and G. Meurant, The effect of ordering on preconditioned conjugate gradients,

BIT **29**, pp 635, 1989.

[137] G. A. Meurant, Computer Solution of Large Linear Systems, Studies in Mathematics and Its Applications, Vol. 28, North-Holland, Amsterdam, 1999.

[138] S. S. Clift andW.-P. Tang,Weighted graph based ordering techniques for preconditioned conjugate gradient methods, *BIT* **35**, pp 30, 1995.

[139] J. W. Watts, III, A conjugate gradient truncated direct method for the iterative solution of the reservoir simulation pressure equation, *Soc. Petrol. Eng. J.* **21**, pp 345, 1981.

[140] R. Bridson and W.-P. Tang, A structural diagnosis of some IC orderings, *SIAM J. Sci. Comput.* **22**, pp 1527, 2000.

[141] Y. Qu and J. Fish, Global-basis two-level method for indefinite systems. Part 2: Computational issues, *Int. J. Numer. Methods Eng.* **49**, pp 461, 2000.

[142] Vandervorst, H. A. and Vuik, C. (1994) 'GMRESR: A family of nested GMRES methods', *Numerical Linear Algebra with Applications*, Vol. 1, Issue 4, pp. 369-386.

[143] Patel et al. "Performance of generator protection during major system disturbances, IEEE Transactions on power delivery", Vol.19, Issue 4, October 2004.

[144] IEEE Task Force Report, Blackout Experiences and Lessons, Best Practices for System Dynamic Performance, and the Role of New Technologies, Final report May 2007

[145] G. S. Vassell, "Northeast Blackout of 1965," IEEE Power Engineering Review, Jan. 1991

[146] G. D. Friedlander, "The Northeast power failure – a blanket of darkness," IEEE Spectrum, Vol. 3, No. 2, Feb. 1966

[147] [Online]. Available http://blackout.gmu.edu/events/tl1965.html (Date accessed: December 30, 2005).

[148] [Online]. Available http://www.cmpco.com/about/system/blackout.html (Date accessed: December 30, 2005).

[149] [Online]. Available http://www.ceet.niu.edu/faculty/vanmeer/outage.htm (Date accessed: December 30, 2005).

[150] [Online]. Available http://www.answers.com/topic/new-york-city-blackout-of-1977 (Date accessed: December 30, 2005).

[151] Feinstein, Jack. "Learning from Experiences: Case Study 1, 1977 Con Edison

Blackout."

[152] Corwin, Jane L. and William T. Miles, "Impact Assessment of the 1977 New York City Blackout." Palo Alto: Systems Control Inc., Prepared for Lester H. Fink, Div. of Electric Energy Systems, U.S. Department of Energy, July 1978.

[153] A. Kurita, T. Sakurai, "The power system failure on July 23, 1987 in Tokyo," Proc. 27th conf. on Decision and Control, Austin, Texas, pp. 2093-2097, 1988.

[154] C.W.Taylor and D.C.Erickson, "Recording and analyzing the July 2 cascading outage," IEEE Comput. Appl. Power , vol 10, no. 4, pp. 40-44, Oct. 1997.

[155] The Electric Power Outages in the Western United States, July 2-3, 1996. Report to the President of the United States by the Secretary of Energy, August 2, 1996

[156] D. N. Kosterev, C. W. Taylor, and W. A. Mittelstadt, "Model Validation For The August 10, 1996 WSCC System Outage," IEEE Trans. Power Systems, vol. 14, no. 3, pp. 967-979, August 1999

[157] A Survey of the Implications to California of the August 10, 1996 Western States Power Outage. Report of the California Energy Commission, June 1997. Available on the Internet at http://www.energy.ca.gov/electricity/index.html#reliability

[158] U.S.-Canada Power System Outage Task Force, Final Report on the August 14, 2003 Blackout in the United States and Canada: Causes and Recommendations, April 2004.

[159] Office of Gas and Electricity Markets, Preliminary Report into the Recent Electricity Transmission Faults Affecting South London and East Birmingham, UK, September 2003.

[160] Elkraft System, Power failure in Eastern Denmark and Southern Sweden on 23 September 2003, Final report on the course of events, Nov. 2003.

[161] Svenska Kraftnat, The black-out in southern Sweden and eastern Denmark, 23 September, 2003 Preliminary report, Oct. 2003.

[162] Union for the Co-ordination of Transmission of Electricity, Interim Report of the Investigation Committee on the 28 September 2003 Blackout in Italy, UCTE Report, 27 October, 2003.

[163] AEEG and CRE: "Report on the events of September 28th, 2003 culminating in the separation of the Italian power system from the other UCTE networks", available at http://www.autorita.energia.it/docs/04/061-04all.pdf

[164] S. Corsi and C. Sabelli, "General Blackout in Italy: Sunday September 28, 2003, h. 03:28:00", Proceedings of IEEE-PES General Meeting, PSSS Panel on Recent blackouts, Denver 2004.

[165] A.Berizzi: "The Italian 2003 blackout". 2004 IEEE PES General Meeting, PSSS Panel on Recent Blackouts, Denver, June 2004.

[166] C. D. Vournas, V. C. Nikolaidis and A. Tassoulis, "Experience from the Athens Blackout of July12, 2004", IEEE Power Tech, St. Petersburg, June 2005.

[167] NEMMCO report "Power System Incident Report – Friday 13 August 2004", 28 January, 2005, http://www.nemmco.com.au/marketandsystemevents/232-0022.pdf

[168] IEEE Guide for AC Generator Protection, 1995, IEEE Standard C37.102-1995.

[169] IEEE Guide for AC Generator Protection, 1995, IEEE Standard C37.102-2006.

[170] D. Reimert, Protective Relaying for Power Generation Systems. Boca Raton: CRC Press, 2006.

[171] J.L. Blackburn, Protective Relaying Principles and Applications 2nd Edition New York Basel Marcel Dekker, Inc, 1998.

[172] P. Kundur, Power System Stability and Control. New York: McGraw-Hill, 1994.

[173] P. M. Anderson, Power System Protection, New York, IEEE Press/McGraw-Hill 1999.

[174] Requirements for Cylindrical Rotor Synchronous Generators, 1989 ANSI Std C50.13-1989

[175] Standard for Requirements for Salient-Pole Synchronous Generators and Generator/Motors for Hydraulic Turbine Applications, 1982. ANSI

[176] IEEE Guide for Abnormal Frequency Protection for Power Generating Plants, C37.106–1987, IEEE, New York, 1987.

[177] Crenshaw, M. L. and Temoshok, M., Protection of large steam turbine generators during abnormal operations, Pennsylvania Electric Association Relay Committee Meeting, October 21–22, 1971, Reading, PA.

[178] Baily, F. G., Bardwick, H. A., and Fenton, R. E. Operating and maintaining steam turbine generators–Operating at off-normal conditions, Power, August 1976, The McGraw-Hill Companies.

[179] Berdy, J., Brown, P. G., and Goff, L. E., Protection of Steam Turbine Generators

During Abnormal Frequency Conditions, General Electric Company, Schenectady, New York.

[180] Gerasimov, A., and Koshcheev, L., Main principles of automatic counter-emergency control in UPS of Russia, IEEE PowerTech Conference, St.Petersburg, Russia, 2005.

[181] Madani, V., Taylor, E., Erwin, D., Meklin, A., Adamiak, M, High-Speed Control Scheme to Prevent Instability of A Large Multi-Unit Power Plant, 60th Annual Conference for Protective Relay Engineers, pp. 271-282, 2007.

[182] Probabilistic Methods Work Group, WSCC Reliability Subcommittee, "Probabilistic based reliability criteria Phase 1: Event probability development and implementation plan", June 25, 1998.